Hydrogen and Syngas Production from Biodiesel Derived Crude Glycerol

By

Luke Grantham Silvey

Submitted to the graduate degree program in the Chemical and Petroleum Program, School of Engineering and the Graduate Faculty of the University of Kansas in partial fulfillment of the requirements for the degree of Master of Science.

_____

Chairperson Susan M. Williams, PhD

_____

Aaron M. Scurto, PhD

_____

Christopher Depcik , PhD

Date Defended: December 15, 2011

The Thesis Committee for Luke Grantham Silvey

certifies that this is the approved version of the following thesis:

Hydrogen and Syngas Production from Biodiesel Derived Crude Glycerol

_____

Chairperson Susan M. Williams, PhD

_____

Aaron M. Scurto, PhD

_____

Christopher Depcik, PhD

Date approved: January 30th, 2012

ABSTRACT

In the past decade, the production of biodiesel has increased dramatically. One of the major by-products of biodiesel production is crude glycerol, which is expensive to refine. As a result, the price of crude glycerol has plummeted to the point where biodiesel companies have to pay to dispose of it. This leads to an increased cost of biodiesel production. To make biodiesel production more cost-effective, it is vital that a use for this crude glycerol is found. One possible method is using steam reforming techniques to reform crude glycerol derived from biodiesel transesterification to produce hydrogen or synthesis gas. This gas can be converted to jet or diesel fuel by using Fischer-Tropsch principles or used in traditional hydrogen applications (e.g. fuel cells, renewable hydrogenation reactions, etc.).

In this study, the viability of using steam reforming techniques to convert crude glycerol into a hydrogen rich gas is addressed. To do this, the effects of the impurities in crude glycerol on catalyst life and activity were compared to pure glycerol reforming over two different steam reforming catalysts: Ni/MgO and Ni/γ-Al_2O_3 catalysts. Reactions over both catalysts showed that crude glycerol reforming can produce a product gas similar to the product gas produced by pure glycerol reforming. Unfortunately, the impurities found in the crude glycerol (e.g. unreacted triglycerides) limited catalyst life over time. They increase coke and tar formation and cause the reactor to plug after several hours. To solve this problem, a simple pre-wash of crude glycerol using acetic acid was performed. The acid-wash removed many of the impurities in the glycerol.

Acid-washed glycerol reforming over both catalysts showed dramatic improvements over crude glycerol reforming. Instead of having problems with reactor plugging, the reactions showed increased catalytic activity and little deactivation for 12 to 14 hours. Conversion of reactants to products was ~100% and the product gas had a hydrogen purity of 68-69%. Thermodynamic equilibrium predictions matched those provided by the experimental results.

The role of the different impurities found in crude glycerol was considered. Experimental and thermodynamic results show that the presence of methanol can aid in producing a product gas with a high hydrogen purity but can decrease hydrogen yield. Results indicate that the presence of potassium aids in gasification of the reactant and help prevent carbon formation on the catalyst. The soaps and unreacted triglycerides found in crude glycerol increase coke and tar formation in the reactor and will eventually cause plugging. Future work needs to be performed to fully determine the role of these impurities in crude glycerol reforming.

Overall, the viability of acid-washed glycerol reforming was demonstrated. Future work in optimizing the process and determining proper catalysts should be studied.

Table of Contents

Chapter 1

Introduction

1.1 Overview

Rising petroleum prices and increased concerns with global warming have forced the search for alternative, renewable (non-petroleum based) fuels to increase dramatically throughout the past decade. One of the major sources for alternative fuels can be produced from biomass derived biodiesel. This bio-based diesel can replace non-renewable petroleum-based diesel. Unfortunately, there are several shortcomings that need to be overcome before biodiesel production can be both economically and physically viable. For example, one of the major by-products of biodiesel production is crude glycerol. Crude glycerol is expensive to refine. Initially, this was not a problem because unrefined glycerol could be distilled and purified into pure glycerol. Then as the production of biodiesel increased, the market for pure glycerol became oversaturated and the price of crude glycerol plummeted [5]. Instead of purifying and selling crude glycerol, biodiesel plants were forced to pay to dispose of it. As a result, biodiesel production costs rose. To make biodiesel production more cost-effective, it is vital that a use for this crude glycerol is found. There are several different opinions about how this issue should be addressed. Some argue that crude glycerol should be converted into highly valued commodity chemicals, such as succinic acid [6] or 1,3 propanediol [7, 8]. In the short term or on a small scale, converting crude glycerol to a commodity chemical could offset biodiesel production costs. Still, as biodiesel production increases, these markets will become oversaturated and alternative uses for crude glycerol will need to be found. It is important that alternative methods are developed.

Another method that could be used to prevent this future problem is using steam reforming techniques to reform the crude glycerol into synthesis gas. This gas can then be converted to make additional jet or diesel fuel by using Fischer-Tropsch principles. Also, it is possible to produce a hydrogen rich gas that could be used as a hydrogen source for different industries (hydrogen fuel cells, hydrocracking, etc.). This is the focus of the present study: to address and check the viability of the steam reforming method.

In this study, the effects of the impurities in crude glycerol on catalytic life and activity were compared to pure glycerol reforming over Ni/MgO and Ni/γ-Al_2O_3. Although initially showing similar results, the impurities typically found in crude glycerol (specifically KOH and FFA) will limit the effectiveness of glycerol steam reforming over time. The impurities tend to increase coke and tar formation which impeded flow through the packed bed and reactor. A simple pre-wash of crude glycerol using acetic acid removed many of the impurities in the glycerol. This slowed down the formation of coke and tar in the reactor and dramatically increased the productivity of the reaction.

1.2 Scope

The objectives of this work included:

1) Demonstrate the need and importance for creating techniques that utilize the reforming of crude glycerol into hydrogen or synthesis gas.

2) Develop simple pre-treatment methods for crude glycerol that increase hydrogen or synthesis gas formation and limit coking in glycerol steam reforming that mirrors or surpasses pure glycerol reforming.

3) Use steam reforming techniques to produce hydrogen or synthesis gas using pure, crude, and acid-washed glycerol over a commercial Ni/Al_2O_3 and a self-made Ni/MgO catalyst.

4) Demonstrate the viability of further research of this technology.

1.3 Thesis Structure

Chapter 1 has provided a quick overview and motivation for this project. Chapter 2 will provide a background of the current status of glycerol steam reforming in literature. It will go into detail about the promise and current shortcomings of this technology. A description of the equipment, along with the experimental procedures, used in this project is provided in Chapter 3. Then, Chapter 4 provides a description and discussion of the experimental results and established procedures. Finally, Chapter 5 summarizes the findings of this project and presents recommendations for future work.

Chapter 2

Background and Literature Review

2.1 Biodiesel Production and Industry

The idea to use a renewable resource as a fuel in a diesel engine has been around for over a century. The first recorded use of biodiesel was on August 10th, 1893 by Rudolf Diesel, the inventor of the diesel engine. He was able to use peanut oil to successfully run and provide power from a diesel engine. During his lifetime, he predicted that bio-based fuels would someday become as important as petroleum and coal products [9].

After Diesel, the low cost and high efficiency of petroleum-based products prevented the advancement of alternative fuels for many years. It was not until the gas scare of the 1970s, that supply and security concerns again prompted interest in developing alternative forms of energy. Solar, wind, geothermal, biomass, and other renewable energies were becoming more and more desirable. Still, even now, many countries are heavily dependent on fossil fuels to meet their energy needs. The technologies to successfully use many forms of renewable energy sources are not developed enough to use cheaply and efficiently on a widespread scale. Until technology and research progresses far enough, it is important that any new technology has the ability to be implemented into the current infrastructure with little or no difficulties.

In terms of the energy required in the transportation sector, biofuel is able to meet many of these requirements. It is a renewable resource that can be produced in many different countries, which helps limit political and security concerns. Also, biofuels can be implemented directly into the current infrastructure and used in modern engines with little or no modifications [10]. In fact, bio-derived ethanol and biodiesel are already being used in several countries

(typically as blends), including the United States, Brazil, Germany, Australia and several others [10].

Biodiesel, in particular, is a promising alternative fuel for diesel engines. It is a renewable resource that can be derived from a variety of naturally produced feedstocks. One reason that biodiesel is promising is that it is the only available commercial fuel that meets the renewable fuel standards (RFS) laid out by the Environmental Protection Agency (EPA) for a biomass based diesel [11]. This means that biodiesel reduces greenhouse gas emissions by at least 50 percent compared to petroleum diesel. Also, biodiesel is classified as an advanced biofuel by the EPA under the latest renewable fuel standards (RFS2) [11].

These standards are having a significant impact on the biodiesel industry in the United States. Part of the mandate laid out in the RFS2 is the dramatic increase in the mandated use of renewable fuels. According to the EPA, the annual usage of renewable fuels in the United States needs to be at least 36 billion gallons by 2022 [11]. A significant portion of this increase is estimated to be from the increased production of biodiesel. Federal and state tax breaks and subsidies are provided to encourage biodiesel producers to increase production and help offset the costs of a developing industry [11]. Without government support, the development of the biodiesel industry would be hampered.

Currently, the majority of the biodiesel is produced from vegetable oil. Both edible and non-edible oils are used. In the USA, most biodiesel uses canola or soybean oil as feedstocks. Other commonly used vegetable oils are jatropha, rapeseed, palm, and castor oils [10]. Every oil source is different compositionally and has different fatty acid profiles. The composition of the oil affects the potential yield and the qualities found in the biodiesel. Table 2.1a [12] provides the fatty acid profiles of several vegetable oils commonly used to make biodiesel.

Table 2.1a - Fatty acid profiles of vegetable oils commonly used for biodiesel production. Adapted from Thompson et al. [11]

	Composition (%wt)						
Fatty Acids	**IdaGold Mustard**	**PacGold Mustard**	**Rapeseed**	**Canola**	**Soybean**	**Crambe**	**Waste Vegetable Oils**
Palmitic (16:0)	2.8	3.1	2.8	4.4	10.7	2	18.6
Stearic (18:0)	1	1.6	1	1.8	4.3	0.9	6.3
Oleic (18:1)	24.9	23.9	13.6	60.9	24.9	17.8	40.4
Linoleic (18:2)	10.4	21.6	11.8	19.1	51.6	8.1	28
Linolenic (18:3)	9.4	9.9	7.5	9.5	7.3	4.5	1.5
Eicosic (20:1)	10.7	12.1	8.6	1.8	0.2	3.7	-
Erucic (22:1)	34.3	22.1	47.9	0.8	-	54.2	-
Avg. MW (kg/kmol)	946.3	924.6	968.5	882.1	872.8	978.5	867.2

Even though vegetable oils are renewable resources, there are downsides to using them to produce biodiesel. The growth of vegetable oils creates competition for land traditionally used for food production and it also increases the destruction of natural habitats in locations where new land is required to grow energy crops [13]. Because of this, studies are looking into replacing vegetable oils, which have many other uses, with other feedstocks (e.g. waste vegetable oils and greases, animal fats, and algae). Many of these other methods are promising because they do not require additional arable land normally used for food crops. Algae, in particular, are promising because they have higher yields and productivities than land plants, they can accumulate large amounts of triglycerides, the main component for biodiesel production, and it does not require much agricultural land to grow [14]. Table 2.1b [15] compares the estimated land needed for different potential feedstocks for biofuels. If the values from Table 2.1b for algae yield can be approached or surpassed during large scale production, algal-based biodiesel may be the ultimate replacement for petroleum transport fuels.

Table 2.1b - Comparison of some sources of biodiesel. Adapted from Chisti et al. [14]

Crop	Oil yield (L/ha)	Land area needed to meet 50% of transport needs of US (M ha)	Percent of existing US cropping area
Corn	172	1540	846
Soybean	446	594	326
Canola	1190	223	122
Jatropha	1892	140	77
Coconut	2689	99	54
Oil palm	5950	45	24
Microalgae (70% oil)	136,900	2	1.1
Microalgae (30% oil)	58,700	4.5	2.5

Currently, studies are being performed to look into the effectiveness of growing algae in non-potable water: such as, saline, brackish, industrial or municipal wastewater [16-18]. These types of water do not compete with land or water that could be used for other products. Depending on the algal strain, the algae could also remove contaminants or impurities found in wastewater. For example, algae can use nitrogen or phosphorous as a growth nutrient [19] or it could help sequester CO_2 to generate carbon credits for power industries [20]. The idea is to have algae serve multiple purposes and not use water that has other purposes. Needless to say, algae are promising feedstocks for biodiesel production.

After a feedstock is chosen, it is necessary to convert it into a usable or efficient form. There are several ways to develop vegetable oil, or for algae the extracted fatty acid methyl esters, into a form that can be used in a diesel engine. The main methods are direct use and blending, microemulsion, thermal cracking, or transesterification [10]. The most commonly used method is transesterification. Biodiesel made through transesterfication produces a dynamic fuel that can best imitate petroleum diesel. During transesterification, the triglycerides in the oil are reacted with an alcohol and a catalyst to produce fatty acid methyl esters and

glycerol. Typically, biodiesel production facilities choose methanol or ethanol as the alcohol. The following equation shows the transesterification reaction:

$$\text{Triglyceride} + 3*CH_3OH + \text{Catalyst (e.g. KOH)} \leftrightarrow C_3H_5(OH)_3 + 3*R\text{-}C(OCH_3)O$$

$$\text{Triglyceride} + \text{Methanol} \leftrightarrow \text{Glycerol} + \text{Methyl Esters}$$

In terms of catalysts, there are three main types of solid heterogeneous catalysts used in making biodiesel: acid, base, and enzyme [13]. There are advantages and disadvantages to each type of catalyst. Solid based catalysts, such as KOH, $Ca(OH)_2$, and CaO, are effective for the transesterification of triglycerides. They tend to have a higher reactivity than solid acid catalysts, which means that base catalysts require lower operating conditions (lower temperatures) and have a quicker reaction time [13]. On the other hand, solid base catalysts can easily be poisoned by water and tend to dissolve in the solvent and become difficult to remove [21]. Solid acid catalysts, on the other hand, are more able to ignore the presence of water and free fatty acids [22]. Also, they can simultaneously perform the esterification of fatty acids in the feedstock with the transesterification of the triglycerides simultaneously. Therefore, a solid acid catalyst can use lower grade feedstock; thereby, lowering biodiesel production costs [13]. The final main area of heterogeneous catalysts typically looked into for triglyceride transesterification are enzyme catalysts. These catalysts tend to be renewable and can help promote the "greenness" of biodiesel production. One example of an enzyme catalyst is lipase [13]. Lipase has a high activity for this process and is a renewable commodity, which makes it promising. Unfortunately, lipase and other enzyme catalysts have issues, such as, higher production costs, enzyme leaching from solid supports, and deactivation due to glycerol production, that need to

be addressed by future research [13]. Currently, the KU Biodiesel Initiative uses a solid base catalyst (KOH) as its triglyceride catalyst.

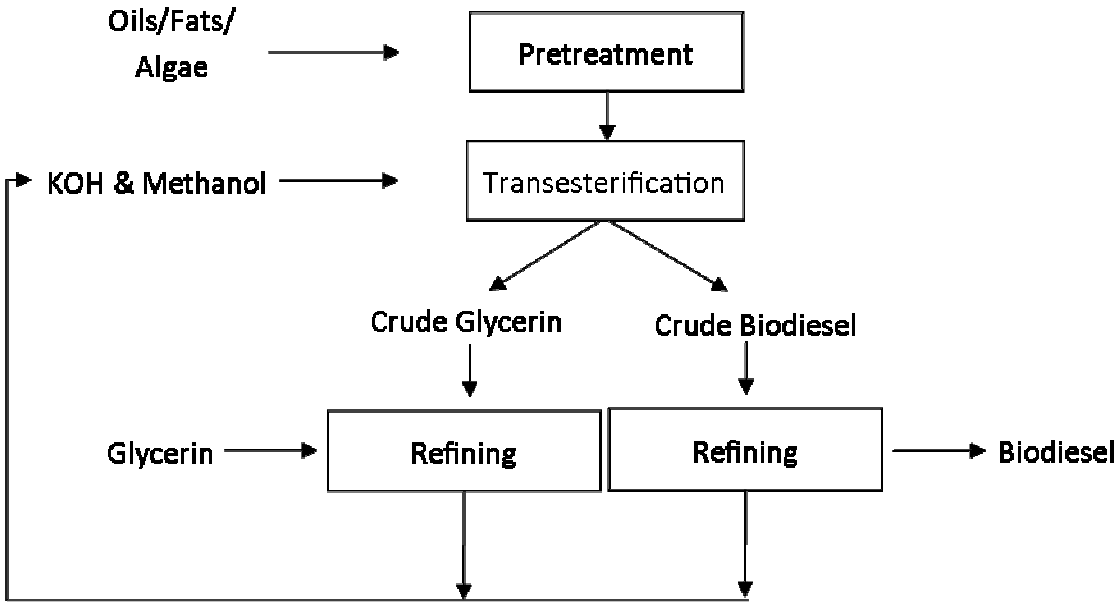

Figure 2.1a – Flow diagram for biodiesel

Figure 2.1a provides an example flow diagram for biodiesel production. In general, the fats/oils/algae require some form of pretreatment before they can be sent for transesterification. For example, the algal oils in algae need to be extracted from the algal biomass before they can be converted into biodiesel [23]. After the oils have been pretreated, the catalyst and alcohol are added and the oils are sent for transesterification. The transesterification reaction will produce two different phases. The top phase will contain crude biodiesel and the bottom crude glycerol. The crude biodiesel will be sent on to be refined and purified to the point where it is acceptable to be used as biodiesel. The crude glycerol phase contains unreacted methanol and free fatty acids, spent catalyst, and glycerol. Currently, larger scale biodiesel plants refine the crude

glycerol phase to produce non-fossil fuel based glycerol that can be used in traditional glycerol industries. For example, Cargill Inc. has a 14 million kg yr^{-1} glycerol refinery built next to their biodiesel plant [16]. In general, the remaining methanol and spent catalyst are recycled and reused.

2.2 Potential Uses for Crude Glycerol

The by-product glycerol is very important to the future growth of the biodiesel industry. Initially, biodiesel plants could refine and purify their crude glycerol. They could sell it on the open market because glycerol is traditionally used in many different industries, such as, pharmaceutical, cosmetic, food, paint, etc. Around two-thirds of pure glycerol is used in personal care products, food or beverages, oral care products, and tobacco (24%, 23%, 16%, and 12% respectively) [1]. Unfortunately, due to the glut of additional glycerol produced via biodiesel production, the market for glycerol has suffered. In 2005, the yearly worldwide demand for glycerol was about 2 billion pounds per year [5]. Even though the worldwide production of biodiesel is still in its early stages, the market price of glycerol has dropped significantly because of the glycerol added by biodiesel production [24]. If biodiesel production continues growing as expected, glycerol will lose even more value. Crude glycerol, the actual product of biodiesel production, is particularly worthless. Its value ranges from 3-10 cents per pound. Table 2.2a [5] provides details about the production of biodiesel and glycerol. Figure 2.2a shows the decrease in glycerol price versus time.

Table 2.2a - Biodiesel Production Information [4]

US Production Capacity (2008)	19	10^9 lb/year
US Production (2008)	5.2	10^9 lb/year
US Crude Glycerol from Biodiesel (2008)	0.52	10^9 lb/year
World Production of Glycerol (2008)	3.8	10^9 lb/year
World Demand for Glycerol (2005)	2	10^9 lb/year
Price of Crude Glycerol (2008)	3 –10	cents/lb
Price of Refined Glycerol (2008)	40 –50	cents/lb

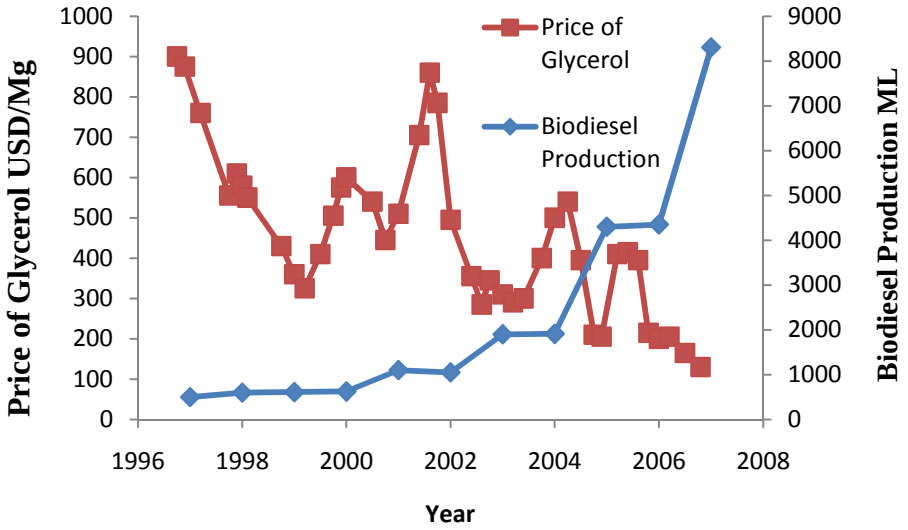

Figure 2.2a – Global biodiesel production and the cost of glycerol in Europe from 1997 to 2007. Adapted from Stelmachowski [2] and Gui [4].

When the growth of biodiesel production is considered, the low price of crude glycerol creates concern about the future viability of the industry. The Department of Energy (DoE) estimates that if the United States were to produce enough biodiesel to displace only 2% of the current petroleum diesel usage, an additional 800 million pounds of glycerol would be produced per year (They estimate the US glycerol market in 2004 at 600 million pounds/yr) [25]. Looking further ahead, at the rate of consumption in 2007, replacing all of the transport fuel consumed in the United States would require 0.53 billion m^3 annually (~1.40 x 10^{11} gallons) of biodiesel [15].

For every gallon of biodiesel produced during biodiesel production about 0.66 pounds of crude glycerol is made [12], that means approximately 9.2×10^{10} pounds of glycerol could be made a year in the USA alone. If biodiesel ends up replacing diesel completely, the picture does not change significantly. In 2010, the total estimated production of diesel worldwide was approximately 620 million metric tons (~1.37 trillion pounds) [26]. This means over 125 billion pounds of crude glycerol could be made a year in this scenario. It is true that these values cannot be reached anytime soon but it is clear that the status quo is not acceptable. Eventually, other uses for crude glycerol must be found.

Several large scale biodiesel plants continue to purify their crude glycerol but it is becoming less and less economically feasible as glycerol prices decrease [27]. Smaller facilities are forced to treat crude glycerol as a waste product and discard it [27]. These factors make biodiesel more expensive and less competitive with traditional fuels. Instead of being a valuable commodity that can be sold to offset biodiesel production costs, glycerol is quickly becoming a hindrance to making biodiesel production cost effective. It is important that alternative uses for crude glycerol are found so that pure and crude glycerol will maintain their value and ensure lower biodiesel costs.

2.2.1 Crude Glycerol Composition

The composition of crude glycerol varies significantly depending on which method is used to produce biodiesel (e.g. acid catalysts, base catalysts, etc.) and the feedstock the biodiesel is made from. In 2006, Thompson and He [12] performed a study to characterize crude glycerol composition from a variety of different feedstocks. Some of the results of their study are shown in Table 2.2.1a and Table 2.2.1b. Table 2.2.1a shows the amounts of salt impurities found in crude glycerol.

Table 2.2.1a - Analysis results of macro elements, carbon and nitrogen in crude glycerol. Adapted from Thompson et al. [12]

Feedstock	IdaGold Mustard	PacGold Mustard	Rapeseed	Canola	Soybean	Crambe	WVO
Calcium (ppm)	11.7 ± 2.9	23.0 ± 1.0	24.0 ± 1.7	19.7 ± 1.5	11.0 ± 0.0	163.3 ± 11.6	BDL[a]
Potassium (ppm)	BDL	BDL	BDL	BDL	BDL	216.7 ± 15.3	BDL
Magnesium (ppm)	3.9 ± 1.0	6.6 ± 0.4	4.0 ± 0.3	5.4 ± 0.4	6.8 ± 0.2	126.7 ± 5.8	0.4 ± 0.0
Phosphorus (ppm)	25.3 ± 1.2	48.0 ± 2.0	65.0 ± 2.0	58.7 ± 6.8	53.0 ± 4.6	136.7 ± 57.7	12.0 ± 1.5
Sulfur (ppm)	21.0 ± 2.9	16.0 ± 1.4	21.0 ± 1.0	14.0 ± 1.5	BDL	128.0 ± 7.6	19.0 ± 1.8
Sodium (%wt)	1.17 ± 0.15	1.23 ± 0.12	1.06 ± 0.07	1.07 ± 0.12	1.20 ± 0.10	1.10 ± 0.10	1.40 ± 0.16
Carbon (%wt)	24.0 ± 0.00	24.3 ± 0.58	25.3 ± 0.58	26.3 ± 0.58	26.0 ± 1.00	24.0 ± 0.00	37.7 ± 0.58
Nitrogen (%wt)	0.04 ± 0.02	0.04 ± 0.01	0.05 ± 0.01	0.05 ± 0.01	0.04 ± 0.03	0.06 ± 0.02	0.12 ± 0.01

[a] BDL indicates values that are below the detection limit for corresponding analytical method. The detection limits in ppm were as follows: calcium – 2, potassium – 40, Magnesium – 0.20, sodium – 80, phosphorus – 5, sulfur – 15, carbon – 200 and nitrogen – 100. Data shown are in the format of "average ± standard deviation."

The most significant impurity they found was sodium, which was due to the use of a NaOH catalyst during transesterification. If a KOH catalyst was used instead, the sodium and potassium values would essentially be switched.

Table 2.2.1b shows the liquid composition Thompson found in crude glycerol. From this data, it seems that crude glycerol is only around 60-80% glycerol. The rest of crude glycerol is methanol (23-38%), spent catalyst, soaps, glycerides, and esters [12].

Table 2.2.1b - Composition of glycerol layer after transesterfication. Adapted from Thompson et al. [12].

Feedstock	IdaGold Mustard	PacGold Mustard	Rapeseed	Canola	Soybean	Crambe	WVO
Glycerol+MeOH+Cat (g)	13.61 ± 0.19	13.27 ± 0.40	15.23 ± 0.20	15.94 ± 0.27	16.16 ± 0.47	17.58 ± 1.07	25.26 ± 0.62
Glycerol (g)	8.56 ± 0.35	8.35 ± 0.16	10.01 ± 0.06	10.80 ± 0.26	10.96 ± 0.48	10.98 ± 0.40	19.35 ± 0.82
Glycerol concen. (%wt)	62.9 ± 2.30	62.9 ± 0.65	65.7 ± 1.19	67.8 ± 1.02	67.8 ± 1.12	62.5 ± 2.16	76.6 ± 4.11

From this data, it is clear that many different components need to be considered, in addition to glycerol, before a potential pathway can be chosen for crude glycerol usage. It may be desirable to reclaim the methanol for recycling in biodiesel production, but distillations can be expensive. Also, the salts, soaps, and other residual compounds may cause harm to or prevent several different applications that could utilize crude glycerol.

One promising idea that has been suggested, that avoids expensive refining techniques, is to perform an acid wash on the crude glycerol to remove the extra salts and non-glycerol organics. Meyer et al. [28], in their study concerning the production of commodity chemicals

from crude glycerol, use hydrochloric acid to wash crude glycerol derived from palm oil. Table 2.2.1c shows their results.

Table 2.2.1c - Crude glycerol composition and pH values before and after acid wash. Adapted from Meyer et al. [28]

	Components (%w/w)				pH (20% in water)
	Glycerol	Water	Ash	Non-Glycerol Organics	
Crude Glycerol	60.04	11.77	4.7	23.49	10.2
Acid-Washed Glycerol	65.54	25.09	2.94	6.43	2.1

This data shows that acid-washing crude glycerol may be an option for improving potential reactions, if salt or non-glycerol organics prove problematic. The acid-washed glycerol provides a cleaner reactant.

Potential uses

Since the existing market cannot accommodate for the current levels of glycerol production other uses for this dynamic compound are being studied. Currently, glycerol can be utilized as boiler fuel or the supplement for animal feed [7] or disposed of as a waste. However, many experts feel that glycerol should be used to produce high-value commodity chemicals [29].

There are several different ways to convert crude glycerol into a commodity chemical. One of the main ways is through fermentation. Microbial fermentation can be used to convert crude glycerol into 1,3-propanediol [7, 8], propylene glycol [30] (1,2-propanediol), succinic acid [6], ethanol [31], and several other compounds. The advantage of crude glycerol fermentation is that it requires little pretreatment, can produce several different liquid products at once, and it is able to produce valuable biogases [28].

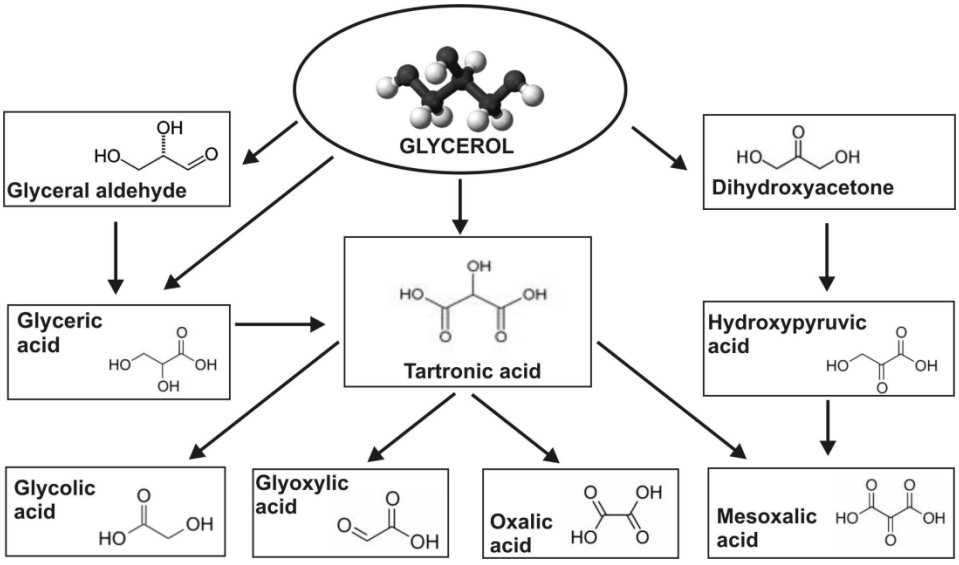

Figure 2.2.1a[2] – Possible reaction pathways and products obtained by selective catalytic oxidation of glycerol

Another way to convert crude glycerol into a valuable commodity chemical is through chemical conversion techniques. Catalytic oxidation of glycerol can be used to make several different acids and other valuable compounds (e.g. Figure 2.2.1a, tatronic acid, etc.) [2],[32]. Pyrolysis of glycerol can be used to make valuable chemicals; such as, acroelin, acetaldehyde, ethanol, methanol, etc. [33]. Additional techniques and products are shown in Figure 2.2.1b [2].

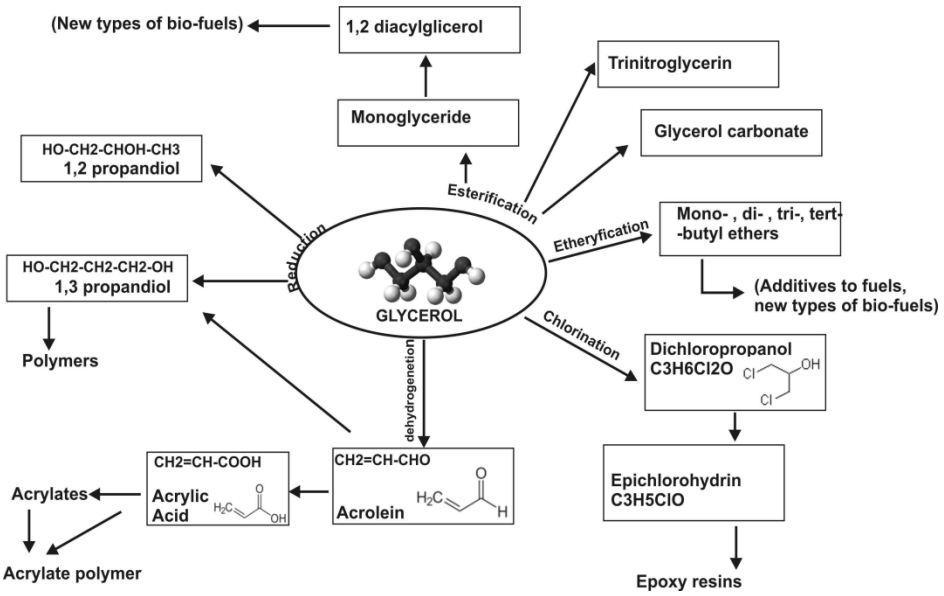

Figure 2.2.1b[2] – Methods of conversion of glycerol into useful products (excluding selective oxidation)

It is clear that there are many different pathways for producing valuable chemicals from crude glycerol. Unfortunately, many of these pathways will turn out to be unrealistic. One reason these pathways are not viable is because the current methods of production are too cheap and effective. One example of this is acrylic acid. The estimated cost to produce acrylic acid from glycerol is more than twice as expensive as the current commercial methods [25]. Similar problems occur with polyester fibers and polyurethane foams [25]. Other potential products are not feasible because the commercial selling price is similar to the estimated raw material cost of crude glycerol [25]. This is true for pathways that convert crude glycerol into aromatic polyester polyol foam [25] and acetone [29]. Other pathways, such as converting glycerol into lactic acid or malonic acid, are not viable because they lack large market capacities [29]. Still, all things considered, there are some promising candidates. A few of the most promising are succinic acid, 1,3-propanediol, 1,2-propanediol, polyglycerols, and dihydroxyacetone [34].

Unfortunately, these promising chemicals are only able to meet a part of the need for the biodiesel market. By comparing the annual yearly production and demand for these potential compounds with the potential amount of crude glycerol that may hit the market, it is clear that alternative methods for crude glycerol must be considered.

For example, by looking at one of the most promising commodity chemicals, 1,3-propanediol, this becomes clear. 1,3-propanediol has a current yearly market demand of 100 million pounds per year and growing.[35] It is very possible that this number may go up to 500 million pounds a year.[29] Several studies have attempted to produce 1,3-propanediol; hence, it is possible to determine the amount of glycerol needed to reach these values. Current studies have been able to get yields of up to 0.85 mol 1,3-propanediol/mol of glycerol (~0.70 g of 1,3-propanediol produced per gram of glycerol) for 1,3-propanediol production from crude glycerol via fermentation.[8] Therefore, to produce the 1,3-propanediol in the world from crude glycerol it would take approximately 1 billion pounds of crude glycerol per year (assuming 70% purity of crude glycerol). This value is billions of pounds less than the amount of crude glycerol currently produced by biodiesel production. As early as 2008, there was already an excess of ~2 billion lbs of crude glycerol produced per year.[5] Even in this extreme scenario, there are potentially billions and billions of pounds of crude glycerol that cannot possibly be used to produce 1,3-propanediol. Plus, it is likely that 1,3-propanediol yields from crude glycerol will continue to improve, which means that even less crude glycerol would be required in the future.

The situation is similar for the other promising options. The total market size (2000) for commodity chemicals, rated as promising derivatives of crude glycerol by the US Department of Energy, was approximately 7.4 billion pounds per year [25]. If it was assumed that the product yield of around 0.2 grams per gram of crude glycerol and that glycerol became the only

feedstock, this would require 37 billion pounds of crude glycerol a year. Even though this situation is idealistic and it is unlikely that crude glycerol could be converted into every promising product, 37 billion lbs/yr is lower than the potential 125 billion lbs/yr of crude glycerol that could be produced by making diesel fuel completely renewable.

Crude glycerol should be converted into 1,3-propanediol, succinic acid, and other commodity chemicals. Research should still continue in those areas but the amount of crude glycerol that could hit the market far exceeds the demand for these chemicals. It is necessary to find additional uses for crude glycerol.

2.3 Reforming

One very promising method that can address the glycerol glut is to use reforming techniques to make a hydrogen rich gas or synthesis gas (CO-H_2 rich gas) [36]. There are several advantages for using crude glycerol to produce hydrogen. First, the reforming of hydrocarbons is a well-known, mature and efficient technology [37]. Second, the need for hydrogen is growing drastically (for fuel cells, renewable hydrogenation reactions, etc.) [1]. Reforming techniques can be successful to produce synthesis gas as well. Reforming can produce a product gas that is mostly syngas at a H_2/CO ratio of about two [38]. Syngas ratios in this range are suitable for use in Fischer-Tropsch reactions to produce products like green diesel [39], methanol [40], and many others [40]. Figure 2.3a[3] shows the wide range of products that can be produced from synthesis gas. Many of these different methods can be incorporated into a biodiesel production facility to lower operating costs and elimanate the glycerol glut.

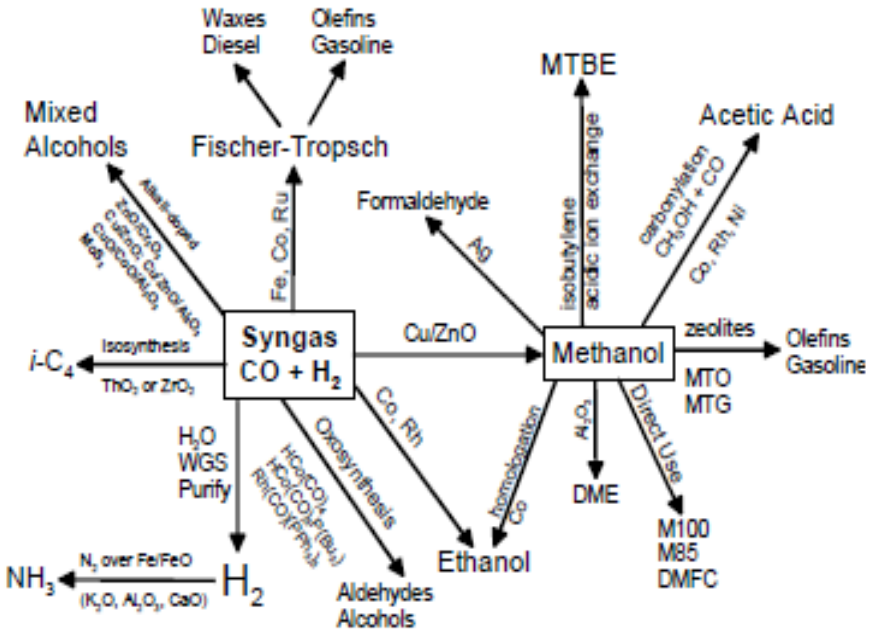

Figure 2.3a[3] – Different potential products of synthesis gas.

Reforming Methods

There are several different types of reforming that are being studied: steam reforming, aqueous-phase, autothermal, and supercritical reforming processes. Another process that produces similar results is partial oxidation. All of these reactions have their advantages and disadvantages. For example, supercritical water reforming of glycerol can produce a high yield of hydrogen [41]. Also, it shows the ability to limit tar and coke formation and the product gas comes available with high pressure [36]. Unfortunately, it requires high temperatures and pressures to operate (~900 °C and 240 atm [41]), which are expensive.

Steam reforming is the most common method to produce hydrogen in the chemical industry [1]. It is effective at providing complete conversion and high hydrogen yields [37, 42]. The main downside to this type of reforming is its highly endothermic nature which requires a large amount of added heat to overcome [43].

According to Luo [44], aqueous-phase reforming (APR) is a newer technique that operates at much lower temperatures than other methods, the reaction occurs in the liquid phase, and it is efficient at limiting CO production. The downside to APR is that current studies have not been able to produce high conversions and hydrogen yields compared to more traditional methods [1]. Also, if the production goal is synthesis gas and not highly purified hydrogen, limiting CO production is counter-productive.

Partial oxidation is when glycerol is converted in the presence of air [1]. This process has some significant advantages. First, the partial oxidation reaction is exothermic instead of endothermic. Therefore, the reaction does not require additional heat to be self-sustaining. This means that a partial oxidation reactor would be more compact and have a faster start-up time than other reforming reactors [45]. Also, due to the nature of the reaction, partial oxidation can be performed with or without a catalyst [39]. The downsides to partial oxidation can be just as significant, depending on the product goal. Partial oxidation reactions have lower hydrogen yields and a high rate of side-reactions [45]. If a high purity product is desired, partial oxidation is not the pathway of choice.

Autothermal reforming is a combination of partial oxidation reforming and steam reforming [1]. It does this by simultaneously feeding glycerol, air, and water into the reactor. This enables an autothermal reformer to react at the thermal neutral point (net reactor heat duty is zero or Q = 0) [43]. Autothermal reforming can have a relatively high hydrogen yield and selectivity, but still inhibit coke and char formation on the catalyst due to the presence of oxygen [46, 47]. Still, on a thermodynamic basis, the amount of hydrogen produced from autothermal reforming would be less than traditional steam reforming [1].

Table 2.3a - Common operating conditions and expected experimental results for different methods of hydrogen production from glycerol. Adapted from Adhikari et al. [1], Luo et al. [44], and Byrd et al. [48].

	Temp	Pressure	Q	Hydrogen Selectivity	Conversion
Steam Reforming	400 - 900 °C	1 bar	Endothermic	70-90%	~100%
Partial Oxidation	800 - 1055 °C	1 bar	Exothermic	50-60%	~100%
Autothermal Reforming	500 - 1055 °C	1 bar	0	~79%	~100%
Auqueous-phase Reforming	225 - 265 °C	29-56 bar	Endothermic	50-60%	~57%
Supercritical reforming	700 - 800 °C	241 bar	Endothermic	90-95%	~100%

Table 2.3a [1, 44, 48] compares the partial oxidation and the reforming methods. For this paper, the steam reforming method was chosen because it is simple and it has the ability to produce high levels of H_2 or syngas (depending on the operating conditions).

Kinetics of Glycerol Steam Reforming

There are several possible side reactions in glycerol steam reforming. Still, if the reaction occurs ideally, the overall reaction should be [37]:

$$C_3H_8O_3 + 3\ H_2O \rightarrow 3\ CO_2 + 7\ H_2 \qquad \text{(Eq. 1)}$$

Ideally, seven moles of H_2 are produced for every mole of glycerol fed to the reactor. This type of hydrogen production is hard to achieve due to the presence of side reactions. The main side reactions are listed below [49]:

$$C_3H_8O_3 \rightarrow 3\ CO + 4\ H_2 \qquad \text{(Eq. 2)}$$

$$CO + H_2O \leftrightarrow CO_2 + H_2 \qquad \text{(Eq. 3)}$$

$$CO + 3\ H_2 \leftrightarrow CH_4 + H_2O \qquad \text{(Eq. 4)}$$

$$CH_4 + H_2O \leftrightarrow CO + 3\ H_2 \qquad \text{(Eq. 5)}$$

$$CH_4 + CO_2 \leftrightarrow 2\ CO + 2\ H_2 \qquad \text{(Eq. 6)}$$

Equations 2 and 3 end up being the most important. Equation 2 is the direct decomposition of glycerol into gaseous products. This is often the first step of the overall ideal reaction (Eq. 1). Equation 3 is the water gas shift (WGS) reaction. The direct decomposition reaction and the WGS reaction combine to form the overall ideal reaction (Eq. 1). Whether the final product goal is hydrogen or synthesis gas, the water gas shift reaction is extremely important to understand. It determines whether the product gas is suitable as a hydrogen rich gas or a synthesis gas.

The other reactions are methanation (Eq. 4), methane steam reforming (Eq. 5), and a methane dry reforming reaction (Eq. 6). They play a large role in determining the amount of methane in the product gas. Table 2.3.1a[50] provides a list of reactions (along with their heat of reaction) that can occur during glycerol steam reforming.

Table 2.3.1a – List of Potential Reactions in Glycerin Steam Reforming. Adapted from Slinn et al. [50].

1	$C_3H_8O_3 + 3H_2O \leftrightarrow 7H_2 + 3CO_2$	+ 128 kJ/mol
2	$C_3H_8O_3 \leftrightarrow 4H_2 + 3CO$	+ 250 kJ/mol
3	$C + H_2O \leftrightarrow CO + H_2$	+ 131 kJ/mol
4	$CO + H_2O \leftrightarrow CO_2 + H_2$	- 41 kJ/mol
5	$C + 2H_2 \leftrightarrow CH_4$	- 75 kJ/mol
6	$CO + 3H_2 \leftrightarrow CH_4 + H_2O$	- 206 kJ/mol
7	$CO_2 + 4H_2 \leftrightarrow CH_4 + 2H_2O$	- 165 kJ/mol
8	$C + CO_2 \leftrightarrow 2CO$	+ 172 kJ/mol

As can be seen in Table 2.3a, glycerol steam reforming is highly endothermic and will require signigicant amounts of added energy to maintain the reaction. It is also important to have an excess of water to help prevent the formation of CH_4 gas and coke on the catalyst surface.

According to Czernik et al [51], the typical reaction mechanism in glycerol steam reforming is that the glycerol molecules are dissociatively adsorbed onto the metal crystallite sites. At the same time, water molecules adsorb onto the surface of the support. Hydrogen is produced by the dehydrogenation of the organic molecules and the reaction of the broken up organic fragments with nearby hydroxyl groups. These migrate to the support at the metal crystallites/support interfaces. This second reaction also results in the formation of carbon oxides (CO and CO_2). Some side-reactions can occur at the same time that lead to carbon deposits forming on the catalyst surface.

If the reactant does not contain enough water, or another oxidizing component, coking will start to form [50]. Coking will eventually cause the blockage of the catalyst pores and in extreme cases the complete failure of the reactor.

Crude glycerol adds additional complications to glycerol reforming. For example, reactor plugging is a problem that could possibly occur during crude glycerol steam reforming [36]. Char formation or polymerization of reforming products can cause this reactor plugging to occur. Also, precipitation of inorganic salts in the heating zone could cause plugging [36]. To prevent tar and coke formation, and thereby reactor plugging, it is very important to understand the pyrolysis of crude glycerol [52].

If these complications can be prevented, it is possible that crude glycerol reforming can compare favorably to pure glycerol reforming. For example, crude glycerol has shown the ability to improve H_2 and total gas production. Valliyappan et al. [39] contribute this to the

presence of potassium in the crude glycerol. Potassium has the tendency to favor the gasification process. This helps to prevent deactivation of the catalyst by limiting reactions that cause coking.

Thermodynamic Analysis

Several different thermodynamic studies have been performed for glycerol steam reforming [49, 53-56]. They provide estimates for product gas compositions over a range of steam reforming operating conditions. It is very important to understand the thermodynamics behind glycerol steam reforming. For example, if the operating conditions are not correct, the catalyst will not be effective and a large range of products could be formed. Figure 2.3b [1] shows the potential reaction pathways in the glycerol reforming process. A wide range of products can be formed from glycerol.

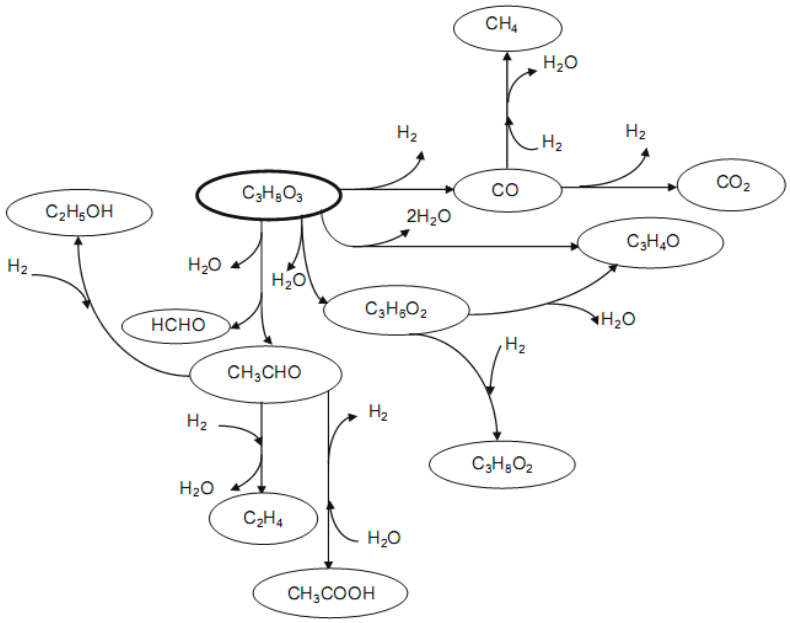

Figure 2.3b [1] - Potential reaction pathways in the glycerol reforming process.

According to Dou et al.[52] in their study about the thermogravimetrics of crude glycerol, the initial products of pyrolysis of glycerol are CO, acetaldehyde, and acrolein. When acetaldehyde and acrolein decompose further, they mostly produce CO, CH_4, and H_2. Still, if the operating temperature drops, due to the endothermic nature of glycerol steam reforming, the decomposition of acetaldehyde and acrolein into gas can be slowed. Therefore, it is important to maintain high temperatures in the reactor.

According to Chen et al. [54], in their thermodynamic study for glycerol steam reforming, there are five main parameters to consider during glycerol steam reforming. They are reaction temperature, reaction pressure, water to glycerol feed ratio, ratio of reactants to inert gas, and the feeding gas flow rate (residence time). For these five parameters, they found that the optimum reaction conditions for hydrogen production are at high temperatures, low pressures, low reactant to carrier gas fed rates, and a low gas flow rate (or a higher residence time). Also, they found that the optimum water to glycerol ratio is about 9.0. Of these parameters, they found that the water to glycerol ratio is the most important for determining glycerol conversion in the reactor.

Adhikari et al. [53] gave similar values for the optimum operating conditions for hydrogen production. They said that the optimum temperature was approximately 960 K (687 °C). Below this temperature, hydrogen production dropped significantly; whereas, above 960 K, hydrogen production drop was slow but minimal. (e.g. Moles of hydrogen at 800K = 4.7, 960 K = 6, 1000 K = 5.8). The optimum pressure was atmospheric (1 atm) and the best water to glycerol ratio was 9:1.

2.3.1 Catalyst Choice

The steam reforming of pure glycerol has been studied extensively the last several years. According to Pairojpiriyakul [43], Ni/γ-Al_2O_3, Ni/α-Al_2O_3, Ni/MgO, Ni/CeO_2, Ni/TiO_2, Ni/CeO_2/Al_2O_3, $La_{1-x}Ce_xNiO_3$, Ru/Y_2O_3, Ir, Co/CeO_2, Rh/Al_2O_3, Pt/Al_2O_3, Pd/Al_2O_3, Ir/Al_2O_3, Ru/Al_2O_3, and Ce/Al_2O_3 catalysts have been developed and tested for hydrogen production from steam reforming of pure glycerol. Iriondo et al. [37] compared Ni/La_2O_3/γ-Al_2O_3, Pt/La_2O_3/γ-Al_2O_3, and Pt/Ni/La_2O_3/γ-Al_2O_3. They found that a Ni/γ-Al_2O_3 catalyst modified with 6% La_2O_3 outperformed a regular Ni/γ-Al_2O_3 at producing hydrogen and limiting coking.

Adhikari et al. have performed several studies with a wide variety of catalysts (Ni/MgO, Ni/γ-Al_2O_3, Rh/γ-Al_2O_3, Pt/γ-Al_2O_3, Pd/γ-Al_2O_3, Ir/γ-Al_2O_3, Ru/γ-Al_2O_3, and Ce/γ-Al_2O_3) [42, 53]. They found the most effective catalysts to be Ni/MgO and Ni/γ-Al_2O_3. Chiodo et al. [57] looked at Rh/Al_2O_3, Ni/Al_2O_3, Ni/MgO, and Ni/CeO_2 and found that Rh/Al_2O_3 to be the most effective at limiting coke formation and producing hydrogen. Chirag et al. [24] used nickel catalysts (Ni/CeO_2 and Ni/ZrO_2/CeO_2) to reform pure glycerol. They found that at 700 C a Ni/ZrO_2/CeO_2 catalyst can maintain its activity and a H_2 yield of four for 14 hours. There are many other useful studies that, for the sake of brevity, are not listed here. The best places to start looking for more information are the review articles by Adhikari et al. and Vaidya et al. [1, 58].

There are several factors that need to be focused on when picking a catalyst for this process. First, just like any catalyst, it is important that the metal has a high order of reactivity. For glycerol steam reforming, the order of activity for a variety of metals is Ru≈Rh > Ni > Ir > Co > Pt > Pd > Fe [59]. Also, it is important that a glycerol steam reforming catalyst has the ability to successfully reform glycerol and methane simultaneously otherwise a significant amount of methane can be produced [54]. If the goal is to produce the most synthesis or

hydrogen gas possible, this is very important because for every mole of methane that is produced, two potential moles of hydrogen are lost.

One metal that has shown promise is nickel. Nickel has been shown to be an active catalyst for hydrogen production during the steam reforming of ethanol [60]. It should follow that it would be effective at glycerol reforming as well. Nickel has a high activity for C-C and O-H bond cleavage. Also, Ni is successful at making H atoms bond to form molecular H_2, because it has a high activity for hydrogenation [60]. Using a nickel catalyst does have its downsides. According to Ni et al. [60], nickel is less active for water-gas shift reactions. Also Ni et al. state that Ni-based catalysts suffer from coke formation caused by dehydration and that the nickel metals tend to sinter during reaction, which can lead to significant drops in production for long-term operations. The support of the catalyst can help address these issues. MgO, ZnO, and CeO_2 have tendencies to inhibit coke formation due to their basic nature. La_2O_3 promotes dehydrogenation and does not induce coke formation [60]. On the other hand, a support like γ-Al_2O_3 causes the coke formation to be more prevalent because it promotes dehydration due to its acidic nature [60].

Alumina is considered a good support because it has a high surface area that helps provide a higher metal dispersion. In addition, it shows good chemical and mechanical resistance [61]. The downside to alumina is that it has a tendency to promote catalyst coking [61] because it has a slightly acidic nature that attacks the carbon-carbon bond in organic molecules. Also, alumina can promote sintering at higher temperatures [37]. There are two main types of alumina supports: γ-Al_2O_3 and α-Al_2O_3. γ-Al_2O_3 provides higher metal dispersion and surface area but α-Al_2O_3 provides a better mechanical resistance [61].

In terms of crude glycerol reforming, research into appropriate catalysts is still in its infancy. Dou et al. [62] reformed crude glycerol with and without in-situ CO_2 removal over a Ni based commercial steam reforming catalyst (mostly MgO and CaO). They found that hydrogen selectivity was slightly higher for crude glycerol reforming than for pure glycerol reforming. Valliyappan et al. [39] reformed pure and crude glycerol over a Ni/γ-Al_2O_3 catalyst at 800 °C and atmospheric pressure. They further found that crude glycerol reforming initially provides a higher hydrogen yield than pure glycerol reforming. Additionally, they were able to produce a higher purity synthesis gas with crude glycerol (93 mol%, H_2/CO ratio of 1.94). Unfortunately, they do not provide information about the long-term effects of the crude glycerol on the catalyst besides providing the percentage of the reaction mixture that became char.

To fully understand the feasibility of using crude glycerol to produce hydrogen or synthesis gas, it is important to know more about the long-term effects of the impurities found in crude glycerol on steam reforming. This study attempts to look at this by using two low-cost, commonly used steam reforming catalysts: a commercial Ni/γ-Al_2O_3 catalyst and a homemade Ni/MgO catalyst. These two catalysts were chosen because they have been shown to be successful at providing some of the best hydrogen selectivity and catalytic activity for pure glycerol steam reforming in literature [37, 42, 53]. Furthermore, Ni/γ-Al_2O_3 was chosen because it was donated by the Evonik Degussa Corporation. Ni/MgO was chosen because it was believed Ni/γ-Al_2O_3 may cause coking and catalyst deactivation. MgO supports have been shown to inhibit coke and tar formation during steam reforming reactions [60]. Furthermore, this study looks into the pretreatment of crude glycerol, in an attempt to find cheap, easy methods to improve catalyst life and product purity.

Chapter 3

Experimental

3.1 Catalyst Production

Two different catalysts were used during this study. One was a commercial Ni/γ-Al_2O_3 catalyst. The other was a 5% Ni/MgO catalyst prepared by the incipient wetness impregnation technique.

3.1.1 Commercial Catalyst

Octolyst 1001, a commercial Ni/γ-Al_2O_3 catalyst, was donated by Evonik Degussa Corporation. According to the catalyst specifications sheet provided by Evonik, Octolyst 1001 is composed of 80-85% aluminum oxide (γ-Al_2O_3, 3-7% nickel (Ni), and 8-15% nickel monoxide (NiO). Overall, the nickel content is around 14-17 weight %. The initial catalyst diameter was 1.5-1.7 mm but it was ground down to 60 mesh before use.

Table 3.1.1a - Octolyst 1001

Physico-chemical data provided by Evonik		
Nickel	14 - 17	%
Diameter	1.5-1.7	mm
Bulk density	700-900	kg/m^3
BET surface area	>150	m^2/g

3.1.2 Incipient Wetness Technique

A 5% Ni/MgO catalyst was prepared via the incipient wetness technique. NanoActive MgO Plus support was obtained from NanoScale Corporation based in Manhattan, KS. Nickel was bought from Alpha Aesar in the form of Nickel(II) nitrate hexahydrate. After impregnation, the catalyst was dried for 12 hours at 110 °C. Then, it was calcined under an air environment for

seven hours at 500 °C with a ramp rate of 10 °C/min. After calcination, the catalyst was sieved to 60-80 mesh particle size.

3.2 Thermodynamic Analysis

A thermodynamic analysis was performed to determine the effect of methanol and to estimate the thermodynamic equilibrium of crude and acid-washed glycerol reforming. Several thermodynamic studies have been performed to determine the optimum operating conditions for pure glycerol reforming [53-57]. These studies, which have been previously discussed, go into significant detail about the effect WRR has on glycerol steam reforming. They show that the WRR has a direct relationship with hydrogen selectivity and yield. As the WRR increases, hydrogen yield and selectivity increase but at higher WRR the effect is slowed [53, 54]. The optimum WRR for hydrogen production from pure glycerol steam reforming is 9:1or a steam to carbon atom ratio (S/C) of 3:1 [53, 54].

For this study, the thermodynamic equilibrium versus temperature was based off of the minimization of Gibbs free energy. The calculations were performed in ChemCad for a variety of different reactant feed conditions using a Gibbs free energy reactor. Equilibrium values were calculated every 25 °C from 450 °C to 1100 °C for reactant feeds of 9:1 WRRs with different amounts of methanol: 0.0 mol %, 1.0 mol %, 2.5 mol %, 3.5 mol %, and 5 mol %. The compositions listed are based off the methanol content of the entire reactant (e.g. 1.0 mol % methanol is 90 mol % water, 9 mol % glycerol, and 1 mol % methanol). The remaining operating conditions were based off those used in the experimental procedure (P = 1 atm, carrier gas flow rate = 50 mL/min, reactant (liquid) flow rate = 0.15 mL/min). In addition, equilibrium values were calculated from 450 °C to 1100 °C for reactant feeds based off of the feed compositions used for the crude and acid-washed runs in this project. Table 3.2a provides the

molar compositions of the feeds used in the thermodynamic equilibrium analysis. The steam to carbon atom ratio is provided as well because it has a greater effect on equilibrium than the WRR.

Table 3.2a - Molar composition of feeds used in thermodynamic equilibrium analysis

Run	% Glycerol	% Methanol	% Water	WRR	S/C
Pure Glycerin (0 mol % methanol)	10.0	0.0	90.0	9.0	3.0
1.0 mol % methanol	9.0	1.0	90.0	9.0	3.2
2.5 mol % methanol	7.5	2.5	90.0	9.0	3.6
3.5 mol % methanol	6.5	3.5	90.0	9.0	3.9
5.0 mol % methanol	5.0	5.0	90.0	9.0	4.5
Crude Glycerol	8.8	3.3	87.9	7.3	3.0
Ni/MgO acid-washed run	5.0	4.0	91.0	10.1	4.8
Ni/γ-Al_2O_3 acid-washed run	6.1	4.4	89.4	8.5	3.9

3.3 Reactor Set-up

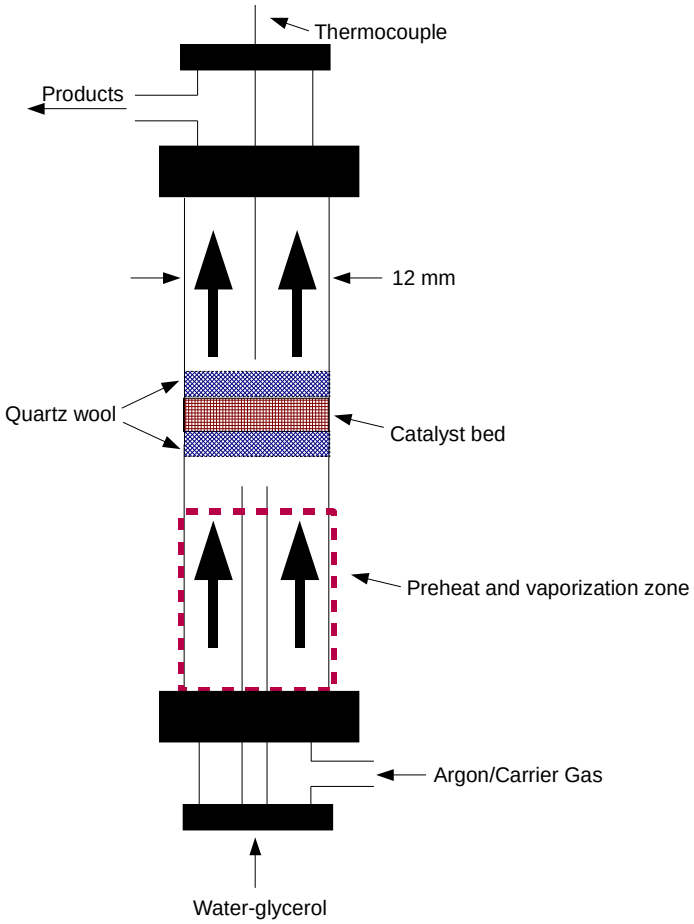

Figure 3.3a – Schematic of Reactor Tube

Catalytic tests were performed in a 12 mm O.D. quartz tube packed-bed reactor. Figure 3.3a shows the set-up of the reactor. The reactor was composed of two different zones: a preheating and vaporization zone and a reaction zone. The heating zone was necessary to gasify the liquid reactant. Inside this heating zone, a small inner tube (O.D. 6 mm) was placed inside the reactor. The liquid reactant (water/glycerol) was passed through this inner tube and would gasify before reaching the outlet. The rest of the heating zone was filled with a 5% N_2 in argon carrier gas (50 ml/min). The inner-tube ended at least 2 cm below the reaction zone to allow radial dispersion of the gasified reactant throughout the reactor.

The reaction zone's catalyst bed was filled with approximately 0.2 g of 60 mesh catalyst and 0.2 g of inert SiO_2 (Sigma Aldrich Part # 342831-100G), for heat control. These were mixed thoroughly and packed between two layers of quartz wool (Grace Davison Discovery Science Cat # 4033) for support. Directly above the catalyst bed, a K-type thermocouple, from Omega, was placed to monitor reactor bed temperature.

The thermocouple sent a signal to a computer equipped with National Labatories Labview version 8.6 software. This software was used was to control the oven and monitor reactor bed temperature. For these tasks, Labview used a National Instruments (NI) NCI PCI-6221 37-pin board (part # 779418-01), a SH37F-37M connector cable (NI part # 778621-02), and a CB-37FH-unshielded, horizontal DIN railmount (NI part # 778673-01) to control the reactor oven through a solid state relay. The thermocouple signal was hooked up to the 37-pin board.

The 50 amp solid state relay (Omega part # SSR330DC50) was enclosed within a polycarbonate enclosure (McMaster-Carr part # 7360K63). The oven was comprised of two semi-cylindrical ceramic fiber heaters (Watlow part # VS402A06S-000AR). These were bought through the Richard Greene Company and assembled to make an open-holed cylindrical heater that had a 2" ID and was 6" long. The power output for each semi-cylindrical heater was 60 vac and 275 Watt.

Depending on the run, either pure glycerol (ultrapure, HPLC Grade CAS # 56-81-5) from Alpha Aesar or crude glycerol, obtained from the KU Biodiesel initiative was mixed with distilled water (approximately 70 volume % H_2O/ 30% pure/crude/acid-washed glycerol). This mixture was pumped into the heating zone of the reactor by a Gilson 305 Pump with a 10 SC pumphead at 0.15 ml/min.

A Porter CM 4 mass flow controller was used to control two Porter mass flow meters to regulate carrier and reduction gas flows through the reactor. The carrier gas was a 5% N_2 in Ar. The reduction gas was a 5% H_2 in Ar. Both tanks were bought from Matheson Gas, the parent company of Linweld Inc.

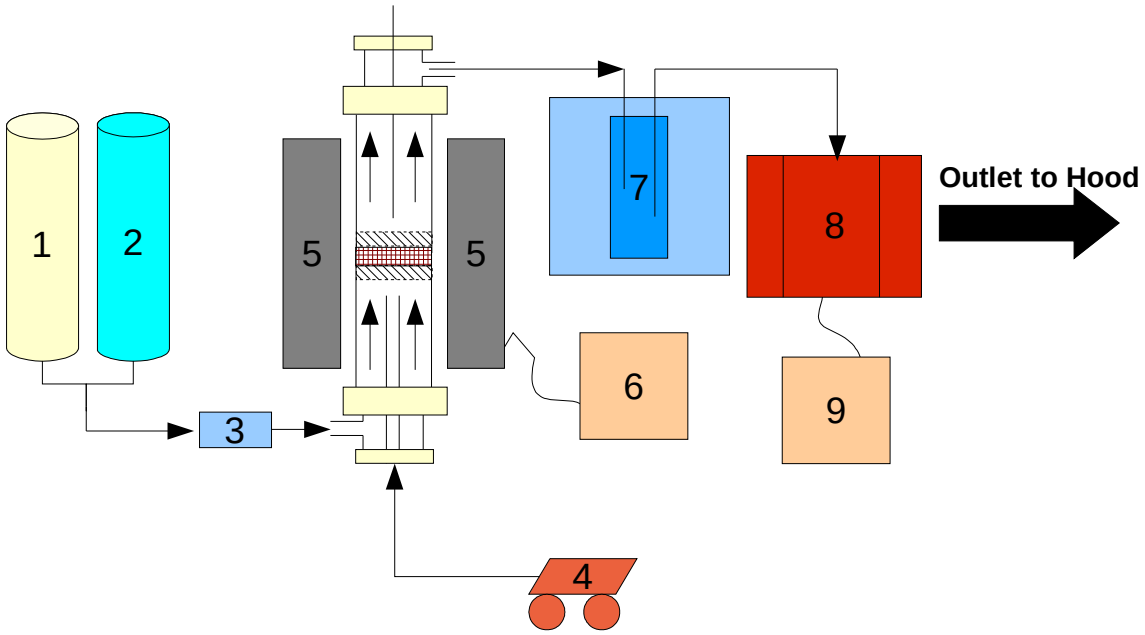

Figure 3.3b - Overall schematic diagram of the small scale reformer. (1) 5% nitrogen/argon cylinder; (2) 5% hydrogen/argon cylinder; (3) mass flow controller for inlet gases; (4) Inlet pump for liquid water-glycerol mix; (5) Reactor Oven; (6) Computer (temperature control); (7) Ice Bath and Liquid Product Collection; (8) SRI 8610 Gas Chromatograph;(9) Computer (GC control);

After leaving the reactor, the reaction mixture was directed to a Pyrex condenser through Swagelok stainless steel ¾" tubing. This condenser was placed directly above a three-mouthed 1000 ml glass collection vessel, which was placed in an ice bath to ensure complete condensation of H_2O. One mouth was blocked off with a rubber cork, the middle mouth led to a gas chromatograph for analysis, and the last mouth was attached to a Pyrex condenser. The reaction mixture would flow into the condenser where the water would condense. The water would flow into the 1000 ml glass vessel for collection. The gases would flow through the condenser and the collection vessel to the GC for analysis.

All tubing and fittings were bought from Swagelok. Quartz tubing was purchased from GM Associates. The overall reactor set-up is shown in Figure 3.3b.

3.4 Operating Conditions

Before the reaction, it was necessary to reduce each catalyst with 50 ml/min of 5% H_2 in Argon. Ni/γ-Al_2O_3 was reduced at 600 °C for an hour and a half. Ni/MgO was reduced at 825 °C for an hour and a half. These reducing conditions were based off conditions used in literature [57, 63]. The reduction temperatures will not be the same because Ni interacts differently with MgO and γ-Al_2O_3.

There were three different runs for each catalyst. For each catalyst, pure, crude, and acid-washed glycerol runs were performed. The conditions for producing acid-washed glycerol and its components are discussed later. The reaction conditions were kept constant for every run. The operating temperature was at 725 °C, with a liquid flow rate of reactant at 0.15 ml/min. This reaction temperature was based on the results of thermodynamic studies found in literature [53, 56]. These studies show that the optimum operating temperature for hydrogen production during pure glycerol steam reforming is above 900 K or (627 °C). Past this point the hydrogen yield will hold steady around 6 but if the temperature drops below this temperature the hydrogen yield drops quickly (e.g. at 550 °C the hydrogen yield drops to 5). Due to the endothermic nature of the reaction and the response time lag of the heating program, the operating temperature was set to 725 °C to ensure the temperature would remain above 627 °C. The carrier gas flow rate was set at 50 ml/min. The gas hourly space velocity (GHSV) for Ni/γ-Al_2O_3 was 44000 hr^{-1} and for Ni/MgO it was 29000 hr^{-1}. The main reason for the large difference in GHSV is due to the density differences between the two catalysts.

3.5 Reaction Analysis

A SRI GC 8610C was used with Peaksimple 3.85 32 bit software (SRI) to collect chromatographs. The SRI GC 8610C was equipped with a TCD (Thermal Conductivity Detector) and a FID (Flame Ionization Detector). The TCD was used to detect and analyze N_2 and H_2, concentrations but could also detect CO, CH_4, CO_2, and higher level hydrocarbons. The FID was not able to detect N_2 and H_2 but could more precisely detect CO, CH_4, CO_2, and higher level hydrocarbons (like ethane and ethylene) than the TCD. The operating conditions of the GC are shown in Table 3.5a.

Table 3.5a - GC operating conditions

Hold at 50 C for 1 min
T_{start} = 50 C Hold for 1 min
T_{ramp} = 15 C/min
T_{final} = 170 C Hold for 2 min

Before each run, the GC was calibrated with a calibration gas. This gas contained equal parts H_2, CO, CO_2, CH_4, C_2H_6, and C_2H_4. Overall, the concentration for each of these gases was 16.89%, 16.64%, 16.61%, 16.59%, 16.65%, and 16.62% for H_2, CO, CO_2, CH_4, C_2H_6, and C_2H_4, respectively. The calibration gas tank was obtained through Matheson Gas, the parent company of Linweld Inc.

After the reaction was finished, the performance of the reactions was determined by the following equations:

$$\%\text{Glycerol conversion to gas} = \frac{\text{C atoms in gas products}}{\text{total C atoms in the feedstock}} * 100 \qquad \text{(Eq. 7)}$$

$$\text{Carbon selectivity} = \frac{\text{C atom in species "i"}}{\text{C atoms produced in gas phase}} * 100 \qquad \text{(Eq. 8)}$$

Where species "i" is CO, CO_2, CH_4, C_2H_4, and C_2H_6.

$$\text{Hydrogen Yield} = \frac{\text{moles of hydrogen produced}}{\text{moles of glycerol and methanol fed}} * 100 \qquad \text{(Eq. 9)}$$

$$\text{Hydrogen selectivity} = \frac{\text{moles of hydrogen produced}}{\text{C atoms produced in gas phase}} * \frac{1}{\text{RR}} * 100 \qquad \text{(Eq. 10)}$$

Where, for pure glycerol:

$$RR = \frac{7}{3}$$

And for crude glycerol:

$$RR = \frac{7}{3} * \%\, Glycerin + \frac{3}{1} * \%\, Methanol$$

3.6 Liquid Product Analysis

To ensure conversion was 100%, the final liquid product was analyzed with an index refractometer and distilled to remove all of the water. A Reichert Digital/Briz/RI-Chek refractometer from Reichert compared the liquid product with distilled water. If conversion was 100%, the liquid product and distilled water provided the same signal. Also, if conversion is complete, there no liquid will be left in the boiling flask after a distillation. For the distillation, 15 ml of product was placed in a glass vessel with boiling stones. The glass flask was placed

into a heating bath set for 110 C and the liquid was boiled off until completion. The steam was sent through a condenser where it was collected and measured.

3.7 Crude Glycerol Refining

It was determined early on that the impurities found in crude glycerol may necessitate some reactant pretreatment. The soap and salt impurities would greatly inhibit catalyst and reactor performance and prevent crude glycerol steam reforming from being feasible. It was deemed necessary to find a way to prevent these impurities from negatively affecting the reaction.

3.7.1 Acid-Wash Experiment

If the impurities found in crude glycerol prevented crude glycerol reforming from being viable, it was decided to attempt a simple cleaning of the reactant to improve the performance of the reaction. Literature has shown that a simple acid wash can remove many of the salts and free-fatty acids present in the crude glycerol [28]. The first step was to determine the proper amount of acetic acid needed to get phase separation between the glycerol and soap/fatty acid layers. A simple acid wash experiment was prepared; the procedure is shown in Appendix A. After the results of this experiment, it was determined that the best ratio for the crude glycerol acid wash was ~3.25 ml of 5 M acetic acid for every 20 ml of crude glycerol for crude glycerol containing around 20000 mg/L of catalyst. This ratio provided two distinct phases. The top phase contained the free fatty acids, unreacted triglycerides, and some of the salts. The bottom phase contained crude glycerol, methanol and the rest of the remaining salts.

3.8 Catalyst Characterization

3.8.1 Bruanauer-Emmett-Teller (BET)

BET analysis was performed on both catalysts to determine surface area and pore volume of the catalysts. This information was collected to gain a better understanding of any potential mass transfer limitations. Low surface areas and small pore diameters can indicate the catalyst is not performing at a kinetically optimum rate. Analysis was performed by a Micrometrics-Gemini 2360 at the Center for Environmentally Beneficial Catalysis (CEBC). Before analysis, samples were dried for 2 hours at 90 C with a Micrometrics Flowprep 060 under a slow N_2 flow. During the run, the catalyst was placed in a test tube that was placed in a liquid nitrogen bath. The pressure was slowly evacuated from the tube to determine the number of absorbed gas particles attached to the catalysts. Gemini 2360 v.5.01 software was used to control and analyze the run.

3.8.2 Electron Microscopy (TEM/STEM)

Transmission electron microscopy (TEM) and scanning transmission electron microscopy (STEM) analysis was performed at the Microscopy and Analytical Imaging Laboratory at KU. A FEI Tecnai F20 XT Field Emission Transmission Electron Microscope was used for TEM and STEM. The samples were placed on Lacey Carbon Film on 200 mesh copper grids from Electron Microscopy Sciences. The images were taken at a variety of resolutions with assistance from the Microscopy and Analytical Laboratory staff. From these images, an estimate for average nickel particle size can be determined. Also, these images provide a visible representation of the dispersion of the nickel on the catalyst surface.

3.8.3 X-Ray Diffraction (XRD)

XRD was performed at the Structural Biology Center at the University of Kansas to determine the identity of nickel bonds on the catalyst surface. From this data, it could be determined how the nickel was bonding to the catalyst support. Room temperature x-ray powder

patterns were obtained using monochromated CuKα radiation (λ= 1.54178 Å) on a Bruker Proteum Diffraction System equipped with Helios high-brilliance multilayer optics, a Platinum 135 CCD detector and a Bruker MicroStar microfocus rotating anode x-ray source operating at 45kV and 60mA. The powders were mixed with a small amount of Paratone N oil to form a paste that was then placed in a small (< 0.5 mm.) nylon kryoloop and mounted on a goniometer head. The specimen was then positioned at the goniometer center-of-motion by translating it on the goniometer head. Two overlapping 1 minute 180º φ-scans were collected using the Bruker Apex2 V2010.3-0 software package with the detector at 2θ = 35º and 90º using a sample-to-detector distance of 50.0 mm. These overlapping scans were merged and converted to a .RAW file using the Pilot/XRD2 evaluation option that is part of the APEX2 software package. This .RAW file was then processed using the Bruker EVA powder diffraction software package.

3.8.4 Chemisorption

Chemisorption was performed to determine nickel dispersion on both catalysts. Approximately, 0.2 grams of fresh unreduced catalyst was loaded into a Micrometrics AutoChem 2910 at the Center for Environmentally Beneficial Catalysis. The catalyst was prepped by flowing argon over the catalyst and ramping the temperature to 850 °C at a ramp rate of 10 °C/min. After the temperature cooled, the catalyst was reduced by flowing 10.3% H_2 in argon and ramping the temperature at 10 C/min to 850 °C. The temperature was ramped down to 50 °C, where chemisorption was performed by pulsing 10% CO in helium until the peaks caused by the pulses were equal. Win 2920 v 4.02 software was used to control and analyze the experiment.

3.8.5 Temperature Programmed Reduction (TPR)

TPR analysis was performed at the Center for Environmentally Beneficial Catalysis to determine the temperature at which the nickel oxides would reduce. A Micrometrics AutoChem 2910, with Win 2920 v. 4.02 software, was used to perform TPR. Approximately, 0.2 grams of fresh unreduced catalyst was loaded into the Micrometrics AutoChem. The sample was prepared by flowing argon over the catalyst and ramping the temperature to 850 °C at a ramp rate of 10 °C/min. The temperature was allowed to cool and the gas flow was changed to 10.3% H_2 in argon. The temperature was ramped to 925 °C at 15 °C/min. A thermal conductivity detector (TCD) signal was plotted versus time to find the reduction peaks.

3.8.6 Fourier Transform Infrared Spectroscopy (FTIR)

FTIR analysis was performed on both catalysts to identify the species that absorbed to the surface of the fresh and spent catalysts. FTIR was performed at the KU Bioengineering Research Center on a Perkin Elmer Spectrum 400 FT-IR/FT-NIR Spectrometer. A Pike Technologies GladiATR was attached to the FTIR. The spectra were collected from wavelengths of 4000 to 650 cm^{-1} with a 4.0 cm^{-1} resolution.

3.9 Crude Glycerol Analysis

ICP analysis was performed on crude glycerol to determine salt and metal content. Samples were sent to Trinity Analytical Laboratories, Inc. in Mound Valley, KS. Samples were tested for Ca, Mg, K, Na (EPA 6010 B) and P (SM 4500-P B, 5).

In addition to ICP, crude and acid-washed glycerol was distilled to determine methanol and water content. Distillations were two-stage processes. First, methanol was boiled off, collected, and measured. After measuring the remaining liquid (water, glycerol, etc.), the water was boiled off, collected, and measured.

Chapter 4

Results and Discussion

4.1 Catalyst Characterization

4.1.1 BET

BET analysis was performed on both catalysts. Figure 4.1.1a shows the results of the findings. 15% Ni/γ-Al_2O_3 was found to have a surface area of 224 m^2/g and a pore volume of 0.48 cm^3/g. The average pore diameter was 8.48 nm. 5% Ni/MgO was shown to have a surface area of 62.2 m^2/g and a pore volume of 0.28 cm^3/g. Its average pore diameter was 17.8 nm.

Table 4.1.1a - BET Analysis Results

Catalyst	BET Surface Area	Pore Volume	Avg. Pore Diameter
15% Ni/Al_2O_3	224 m^2/g	0.48 cm^3/g	8.48 nm
5% Ni/MgO	62.2 m^2/g	0.28 cm^3/g	17.8 nm

4.1.2 TEM/SEM

Metal sintering and the average metal particle size were evaluated by TEM and SEM analysis. Figure 4.1.2a shows a TEM of fresh, reduced Octolyst 1001. From this image and others, an average metal particle size between 5-7 nm was found. Figure 4.1.2b shows a SEM image of fresh, reduced Octolyst 1001. The average metal particle size found in this image corresponded with the TEM images. Figures 4.1.2e and 4.1.2f are images of fresh, reduced Ni/MgO. From these images and others, an average nickel particle size for Ni/MgO of approximately 20 nm was determined. Figure 4.1.2c shows a TEM image of spent Octolyst 1001 from a pure glycerol reforming reaction. In this image and others, it is clear that the average nickel particle size has increased dramatically due to sintering during the reaction. The average nickel particle size increased from approximately 6 nm to approximately 17 nm.

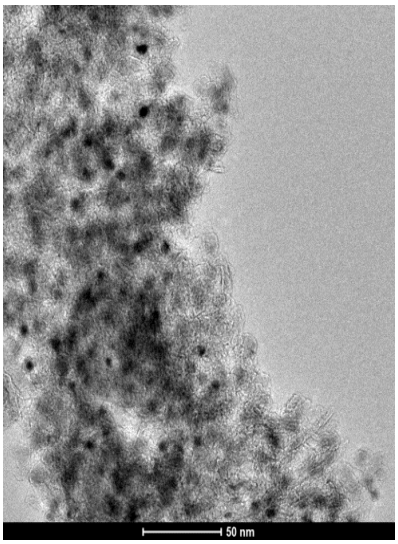

Figure 4.1.2a – TEM image of reduced Octolyst 1001. The dark spots are nickel deposits on the

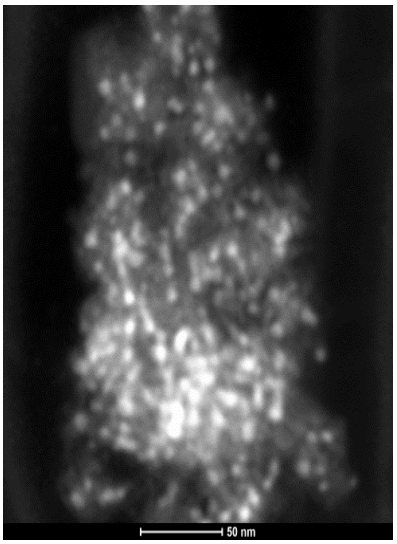

Figure 4.1.2b – SEM image of reduced Octolyst 1001. The nickel deposits can be seen on the catalyst support.

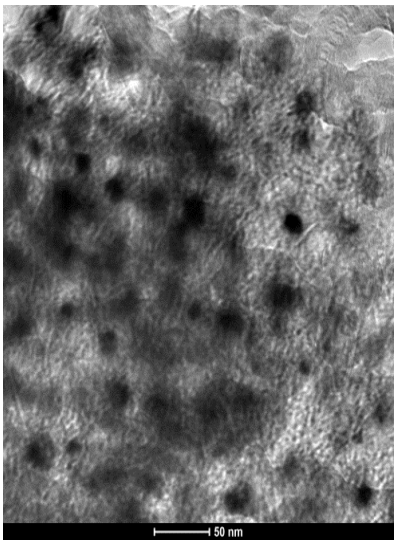

Figure 4.1.2c – TEM image of spent Octolyst 1001 from pure glycerol reforming. The average metal particle size has increased during reaction.

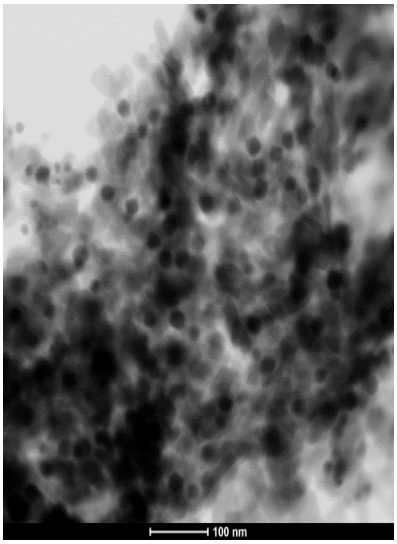

Figure 4.1.2d – TEM image of reduced Ni/MgO.

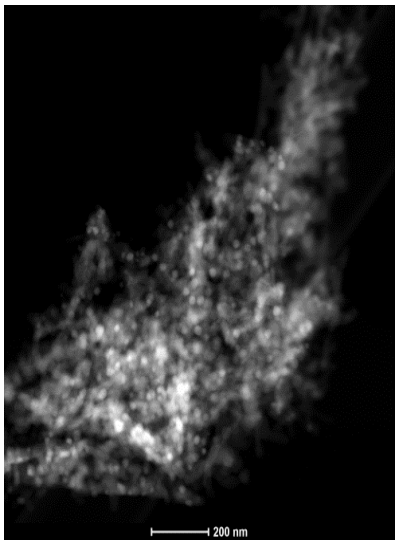

Figure 4.1.2e – SEM image of reduced Ni/MgO.

4.1.3 XRD

Identity of different metal species was determined on both catalysts by XRD. Figures 4.1.3a and 4.1.3b show the XRD spectra for Ni/γ-Al_2O_3 and Ni/MgO respectively. Gamma-Al_2O_3 and $NiAl_2O_4$ peaks were found at 2-Theta values of 17.7, 37.4, 45.6, 60.6, 66.9, 76.4, and 85.2. Ni and Ni O peaks were found at 39.8, 52.0, 63.1, and 93.3. Two NiO peaks should have appeared but were absorbed in the 45.6 and 76.4 peaks because of the magnitude of those peaks. The identities of these peaks were found in literature.[64-66]

For Ni/MgO, XRD showed the presence of several metal species. It is difficult to determine which peaks belong to NiO and MgO because they have similar disfraction patterns. The peaks found at 2-Theta values of 37.1, 43.1, 62.5, 74.9, and 78.8 belong to NiO or $MgNiO_2$. Peaks at 47.2 and 58.7 signify the presence of Ni. The identity of these peaks was based off previous studies found in literature.[67-69].

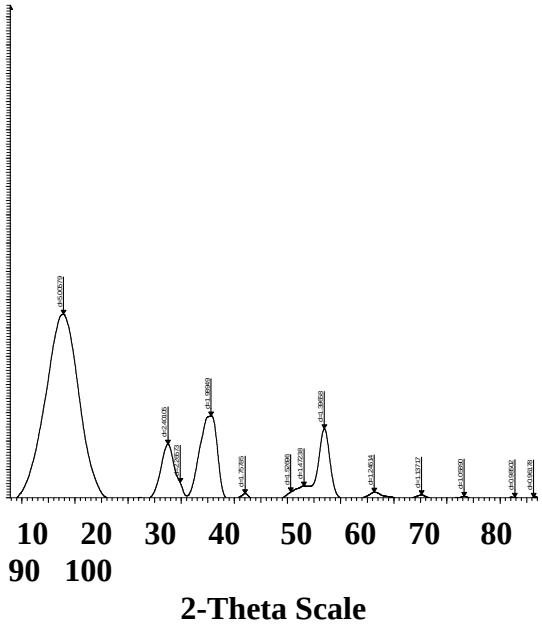

Figure 4.1.3a – XRD spectra for fresh, reduced Ni/γ-Al_2O_3.

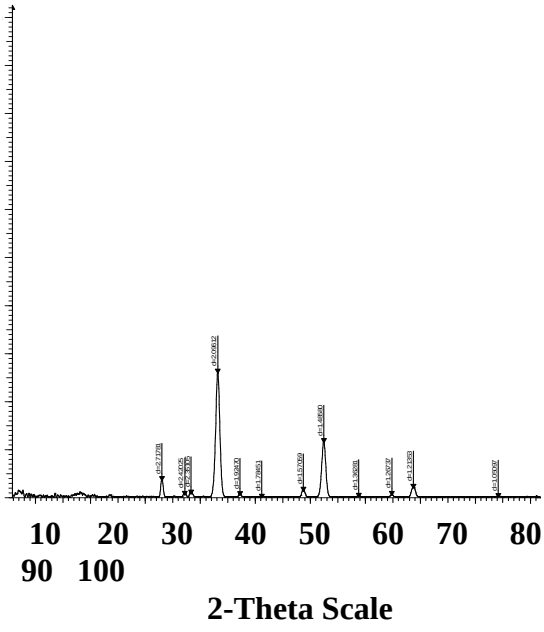

Figure 4.1.3b – XRD spectra for fresh, reduced Ni/MgO.

4.1.4 Chemisorption

Determination of metal dispersion and active particle size was performed by chemisorption analysis on fresh, reduced catalysts. From these values, an estimate for active metal sites per gram of catalyst was calculated. Table 4.1.4a shows the results of the chemisorption analysis. It was found that Ni/γ-Al_2O_3 had a metal dispersion of about 5.4% and an average particle diameter of 18.8 nm. The average particle diameter found here is higher than the value calculated by TEM/SEM analysis for fresh, reduced Ni/γ-Al_2O_3. This is due to the fact that prior to chemisorption analysis, TPR analysis was performed. The TPR analysis was performed up to 850 °C. For TEM/SEM analysis, the catalyst was reduced at 600 °C. This was the temperature used to reduce the catalyst prior to reaction. The TPR analysis maximum temperature was required to be higher than the normal reduction temperature to ensure that reduction peaks were not missed. The higher reduction temperature used during TPR analysis caused nickel sintering to occur and increased the average nickel particle size. In the future, TPR analysis and Chemisorption analysis should be performed separately.

The results for Ni/MgO corresponded closely to the results found by TEM/SEM analysis. This is due to the fact that Ni/MgO was reduced at a high temperature for both studies (825 and 850 °C). The reduction temperature for Ni/MgO was different because nickel and MgO interact differently than nickel and γ-Al_2O_3. This causes the two catalysts to require different reduction temperatures. Chemisorption analysis found that metal dispersion was approximately 4.8% and the active particle diameter was 21.2 nm.

Table 4.1.4a - Chemisorption Results

Catalyst	Metal Dispersion	Active Particle Diameter	Active sites per gram of catalyst
Ni/γ-Al_2O_3	5.39%	18.7947 nm	8.30E+19
Ni/MgO	4.77%	21.2174 nm	2.45E+19

From this data and the metal loading information, the active sites per gram of catalyst were calculated. This was done so that the two catalysts performances could be more accurately analyzed. For Ni/γ-Al_2O_3, this value was found to be 8.30 x 10^{19} sites per gram catalyst. For Ni/MgO, this value was found to be 2.45 x 10^{19}. This means that the Ni/γ-Al_2O_3 catalyst had about 3.4 times as many active sites as Ni/MgO. The difference between the two catalysts can be tied to the increased metal loading and surface area of Ni/γ-Al_2O_3 compared to Ni/MgO.

4.1.5 TPR

The reduction properties of the catalysts and support were analyzed by TPR. Figure 4.1.5a shows the resulting TPR graph for Ni/γ-Al_2O_3. There were four peaks found in this graph. A main peak is located at 820 °C. Smaller peaks were located at 165, 255, and 338 °C. Figure 4.1.5b provides a closer view of the smaller peaks found by TPR analysis. The lowest peaks are associated with the reduction of large particles of NiO that do not form significant bonds with the alumina support.[70] The largest peak (~820 °C) is a combination of several peaks. It indicates the reduction of $NiAl_2O_4$ and $NiAl_xO_y$.[71]

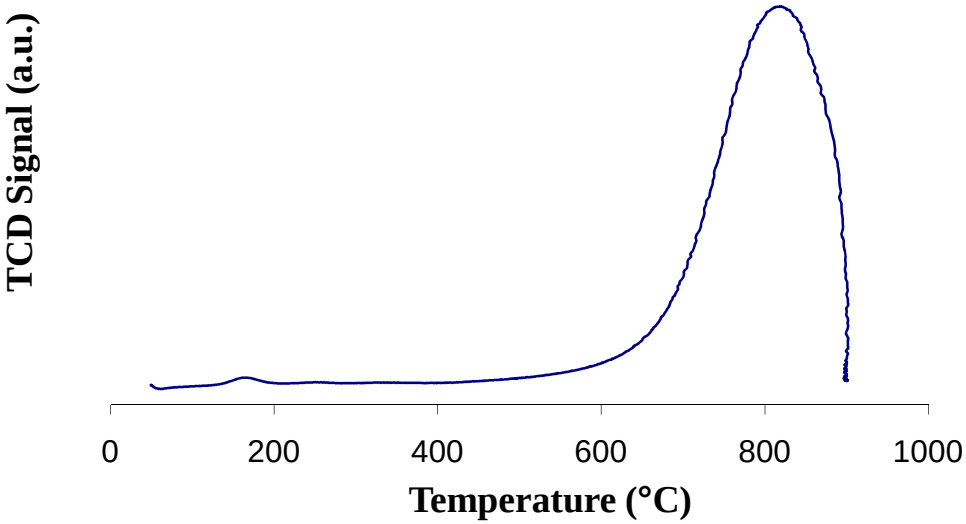

Figure 4.1.5a – TPR graph of Ni/γ-Al_2O_3

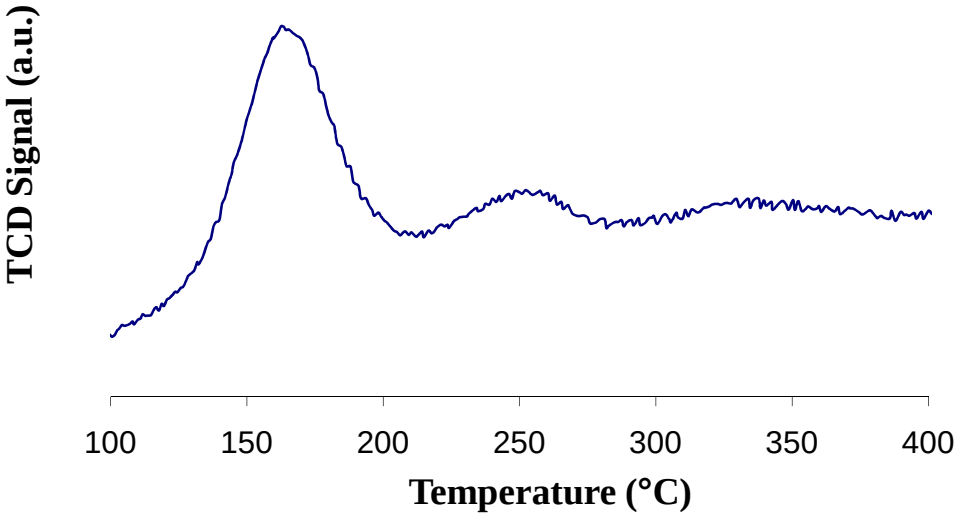

Figure 4.1.5b – Smaller TPR peaks found for Ni/γ-Al_2O_3

Figure 4.1.5c shows the TPR graph for Ni/MgO. A main peak was found at 910 °C. Four smaller peaks were found at 117, 276, 383, and 830 °C. It can be difficult to find TPR

peaks for Ni/MgO catalysts because of the similarity in behavior of NiO and MgO. Metallic nickel has been shown to be supported on MgO in an amorphous or a highly dispersed state.[72] The large peak, containing the peaks at 830 and 910 °C, shows the presence of nickel bonded into the MgO matrix and are a clear indication of a NiO-MgO solid solution.[73]

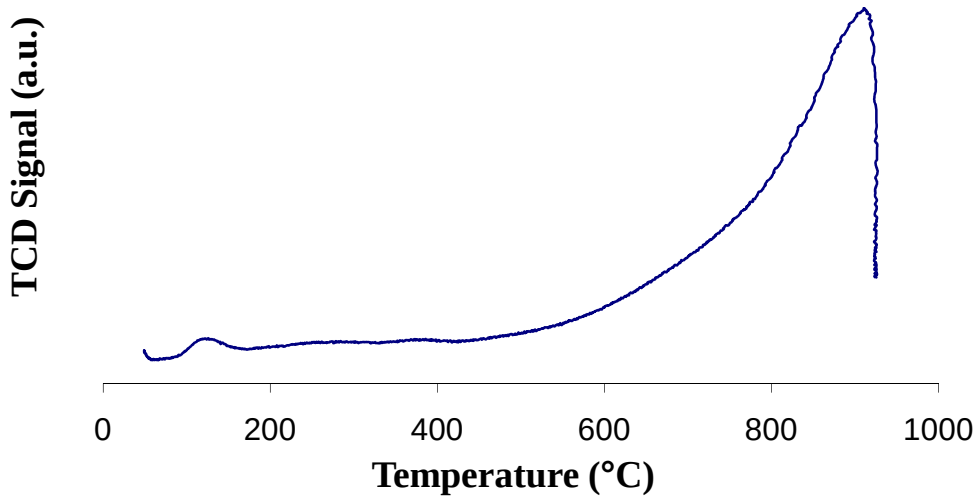

Figure 4.1.5c – TPR graph of Ni/MgO

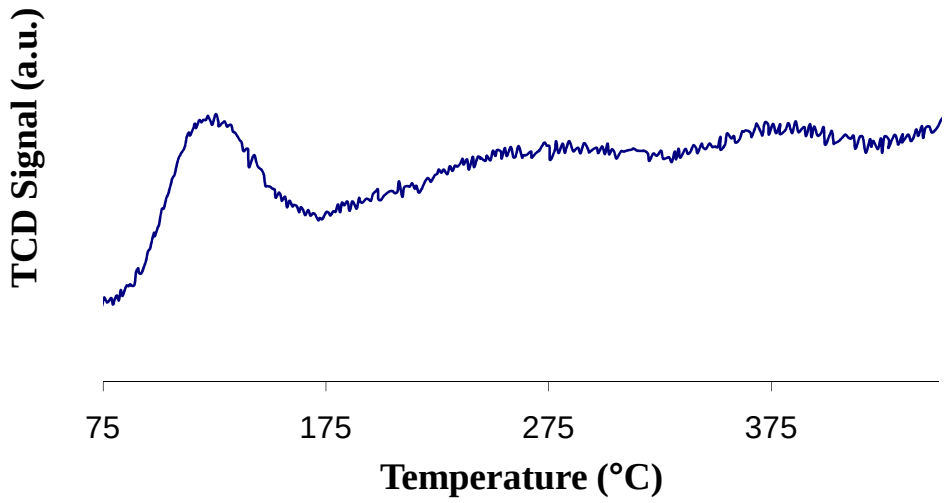

Figure 4.1.5d – Smaller TPR peaks found for Ni/MgO

4.1.6 FTIR

Figure 4.1.6a shows the FTIR spectra for Ni/γ-Al_2O_3. The goal was to identify the organic compounds that adhere to catalyst surface during reaction. Several peaks were identified but only one peak was clearly unique for the spent catalysts. Most peaks were found on both the fresh and spent catalysts. A unique peak was found at approximately 2975 cm^{-1}. Figures 4.1.6b, c compare reduced Ni/γ-Al2O3 and the Ni/γ-Al_2O_3 used in acid-washed glycerol reforming from a wavelength of 2700 to 3200 cm^{-1}. These graphs show that there is a peak on the used acid-washed glycerol catalyst but not on the reduced catalyst. This peak fits in ranges that indicate the formation of –OH bonds on the catalyst.

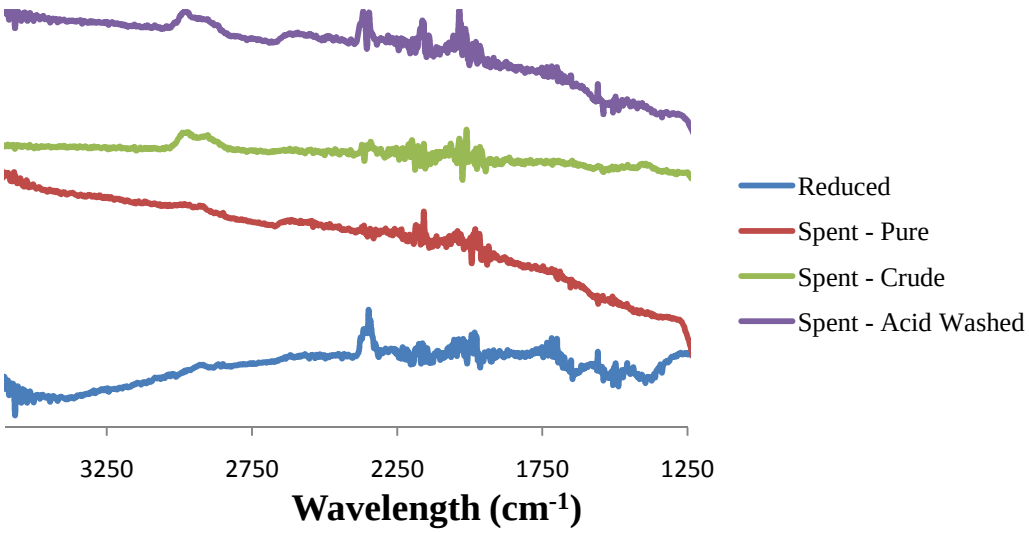

Figure 4.1.6a – FTIR graph of Ni/γ-Al_2O_3

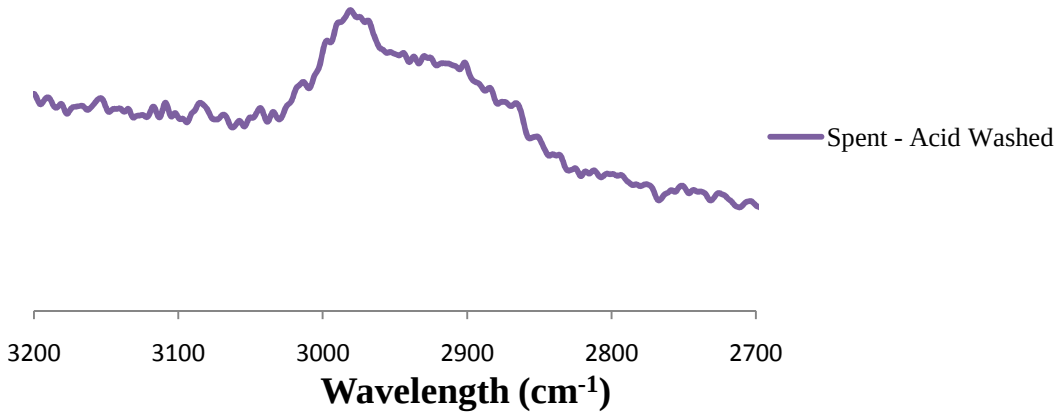

Figure 4.1.6b – FTIR graph of Ni/γ-Al_2O_3 used in acid-washed glycerol reforming

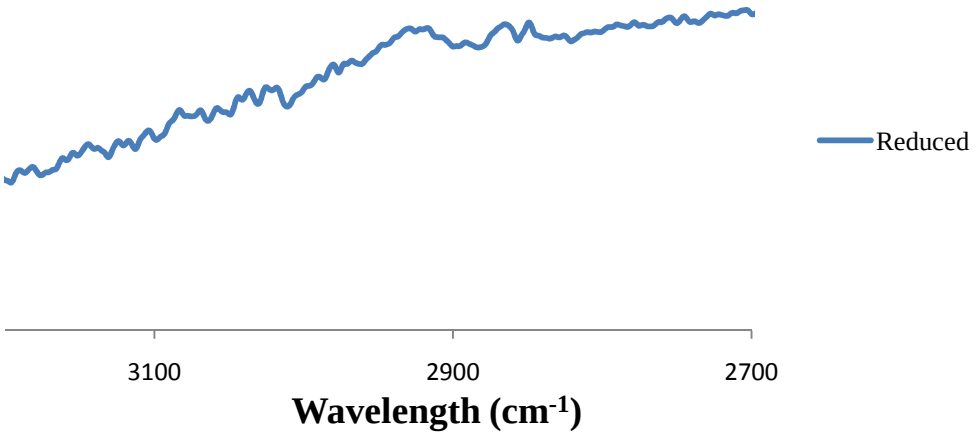

Figure 4.1.6c – FTIR graph of fresh, reduced Ni/γ-Al_2O_3

Figure 4.1.6d shows the FTIR spectra for the various runs that used Ni/MgO as a catalyst. Several more unique peaks were identified in the spent catalyst. Unique peaks were located at wavelengths of 2970, 2940, 2875, 1730, 1380, 1235, and 1220 cm^{-1}. The 2970, 1235, and 1220 cm^{-1} peaks fit in ranges that indicate –OH bonds. The 2940 cm^{-1} peak may indicate the presence of a -CHO bond. The peak at 2875 cm^{-1} is in the range where a –CH bond peaks appear. 1730 cm^{-1} may indicate the presence of a $–C=CH_x$ bonds. Finally, 1380 cm^{-1} may indicate the presence of a $–COCH_3$ bond on the catalyst. Figures 4.1.6e, f, and g give closer looks at the areas where peaks are located. The FTIR spectra for Ni/MgO were successful at showing that organic compounds are attaching to the catalyst during reaction. To gain a more precise understanding of what species are bonding to the catalyst, more detailed FTIR analyses need to be performed. The method used in this analysis was not quantitative and did not provide the detail necessary to conclusively identify every unique peak.

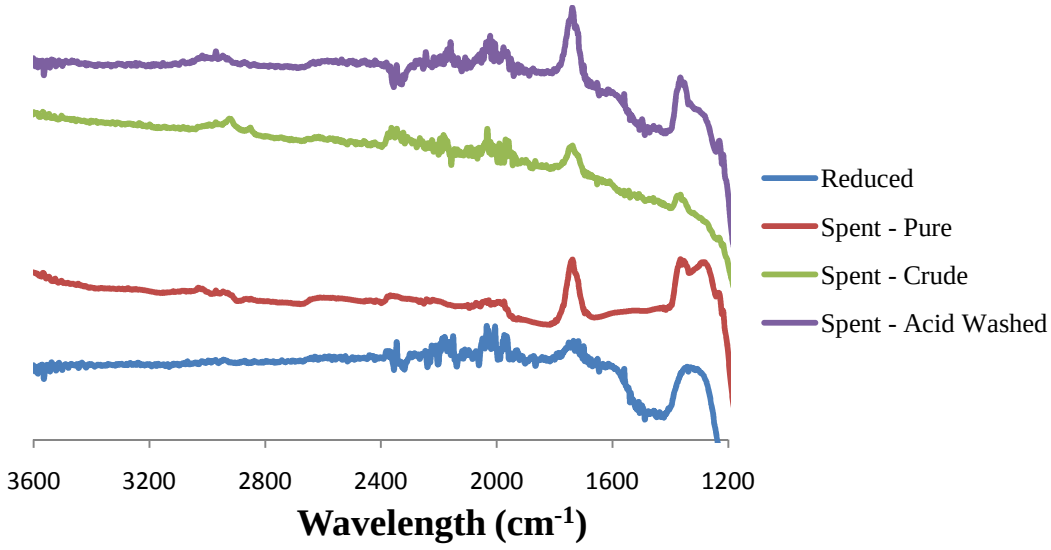

Figure 4.1.6d – FTIR for Ni/MgO

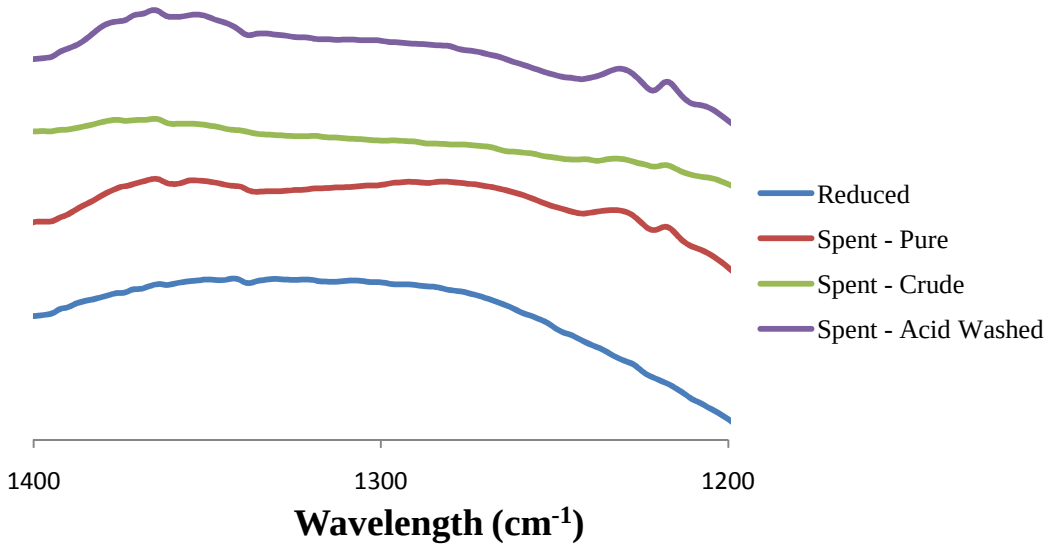

Figure 4.1.6e – FTIR for Ni/MgO from 1200 to 1400 cm^{-1}

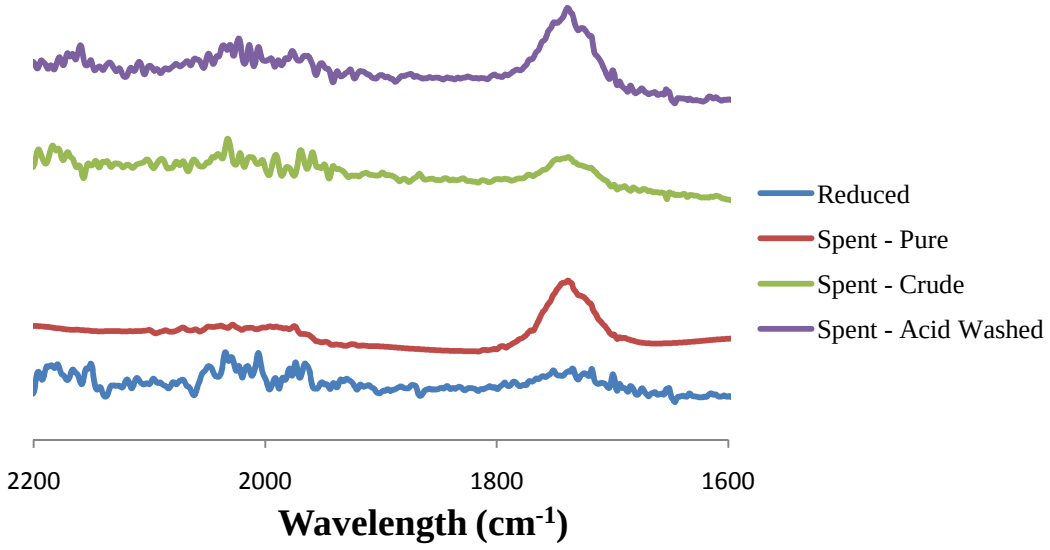

Figure 4.1.6f – FTIR for Ni/MgO from 1600 to 2200 cm^{-1}

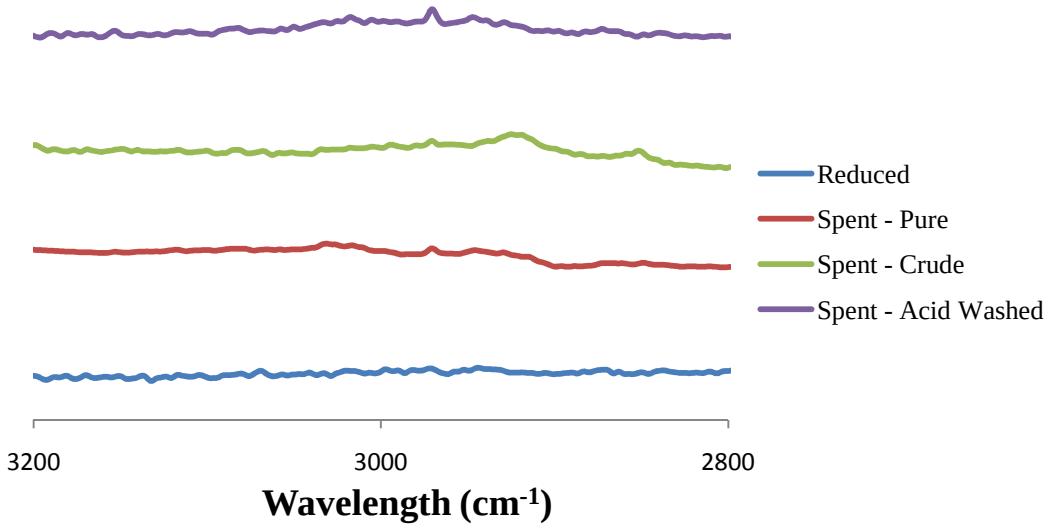

Figure 4.1.6g – FTIR for Ni/MgO from 2800 to 3200 cm^{-1}

4.2 Crude Glycerol

4.2.1 Composition Pre-Acid Wash

ICP analysis and a distillation were performed on the crude glycerol that was used in the reaction. The ICP analysis was performed on the glycerol before it was mixed with H_2O. The distillation was performed on a 9:1 molar mixture of water and glycerol.

Table 4.2.1a shows the results of the ICP analysis on crude glycerol. ICP analysis found that crude glycerol has a very large amount of potassium present, with lower amounts of sodium and phosphorus. The large amount of potassium present in the crude glycerol was due to the use of KOH as the catalyst for biodiesel transesterification.

Table 4.2.1a - ICP analysis of crude glycerol

Analyte	Result	Quantitation Limit	Units
Calcium	ND	20	mg/L
Magnesium	ND	20	mg/L
Potassium	20700	200	mg/L
Sodium	373	20	mg/L
Phosphorus	44.5	4	mg/L

Table 4.2.1b provides the results of the crude glycerol distillation. It was found that the crude glycerol was approximately 67% water, 5.6% methanol, and 27.4% glycerol. The glycerol contained many of the impurities left over from biodiesel transesterification (salts, unreacted triglycerides, etc.). This means that the actual glycerol content was probably a little lower.

Table 4.2.1b - Crude glycerol distillation

Total (mL)	% Glycerin	% Methanol	% Water
50.4	27.4	5.6	67.1

4.2.2 Composition Post-Acid Wash

Two different distillations were performed because different batches of acid-washed glycerol were used for Ni/MgO and Ni/γ-Al_2O_3. Table 4.2.2b provides the results of both acid-wash glycerol distillations. These solutions were used directly in the reaction without removing

any water or methanol. The acid washed glycerol used by the Ni/MgO catalyst was approximately 16.9% glycerol, 7.4% methanol, and 75.6% water. For Ni/Al_2O_3 was approximately 20.0% glycerol, 8.0% methanol, and 72.0% water. The glycerol/methanol ratio for both mixtures is close to the same. The main difference is the amount of water that is present. The glycerol used in the reaction over Ni/MgO was more diluted with water.

Table 4.2.2b - Acid-washed glycerol distillations

Catalyst	Total (mL)	% Glycerin	% Methanol	% Water
Ni/MgO	50.5	16.9	7.4	75.6
Ni/γ-Al_2O_3	25.0	20.0	8.0	72.0

4.3 Glycerol Steam Reforming

4.3.1 Pure Glycerol Reforming

4.3.1.1 Octolyst 1001

Pure (99.8%) glycerol steam reforming was performed over a 15% Ni/γ-Al_2O_3 catalyst (Octolyst 1001) in a packed bed reactor. 0.4876 g of catalyst and SiO_2 (55% catalyst/45% SiO_2) were placed into a quartz tube reactor between two pieces of quartz wool. The catalyst was reduced for an hour and a half with 5% H_2 in argon (50 ml/min) at approximately 600 °C. The reactor temperature was allowed to ramp up to 725 °C and allowed to stabilize before starting the reaction. Also, the GC was calibrated before the reaction was started. To start the reaction, a distilled water-pure glycerol mixture was fed to the reactor at a molar ratio of 9:1 (water:glycerol) at a liquid flow rate of 0.15 ml/min (GHSV = 44000 hr^{-1}). GC testing started within 15 minutes of starting the reactant flow to the reactor.

Reactant was sent to the reactor for 1166 minutes. During this time 166.5 ml of reactant was fed to the reactor (approximately 0.14 ml/min) and 138 ml of liquid product was collected.

The liquid product was clear for the first six hours of reaction but the final product had an oil layer on top of the water.

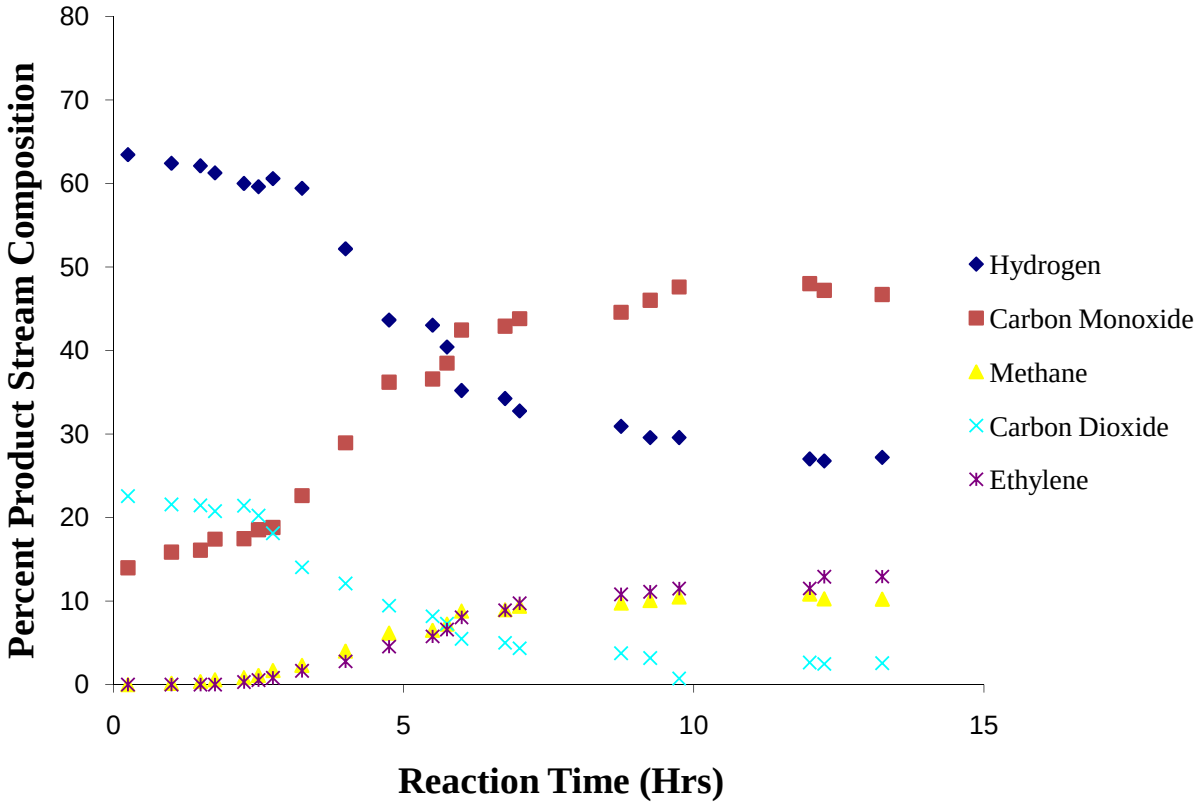

Figure 4.3.1.1a – Product gas composition for pure glycerol reforming over Ni/γ-Al_2O_3

Figures 4.3.1.1a shows the product gas composition for the life of the reaction.

As can be seen in the figure above, the catalyst loses its activity after three hours. This pattern of losing activity after the 3 hour mark is found in several other articles for Ni/γ-Al_2O_3 [63, 74]. Over the first three to four hours, the product gas composition was approximately 60-63% H_2, 15-18% CO, 18-22 % CO_2, and 0-2 % CH_4. Little to no higher level hydrocarbons (0.0-0.8 %) were present in the gas.

After the eight hour mark, the catalytic activity of the catalyst stabilized. The percent H_2, CO, CO_2, CH_4, C_2H_6, and C_2H_4 in the product gas was approximately 29%, 47%, 3%, 10%,

0.5%, and 11% respectively. These values are similar to the composition found when no catalyst is used [57, 75].

Figure 4.3.1.1b shows the selectivity of H_2, CO, CO_2, CH_4, C_2H_6, and C_2H_4 versus time. During the reaction, there is a drastic drop off in hydrogen selectivity. H_2 selectivity drops from 71% to 15%. The increase of ethylene and methane selectivity to ~15% is an obvious sign of catalyst deactivation.

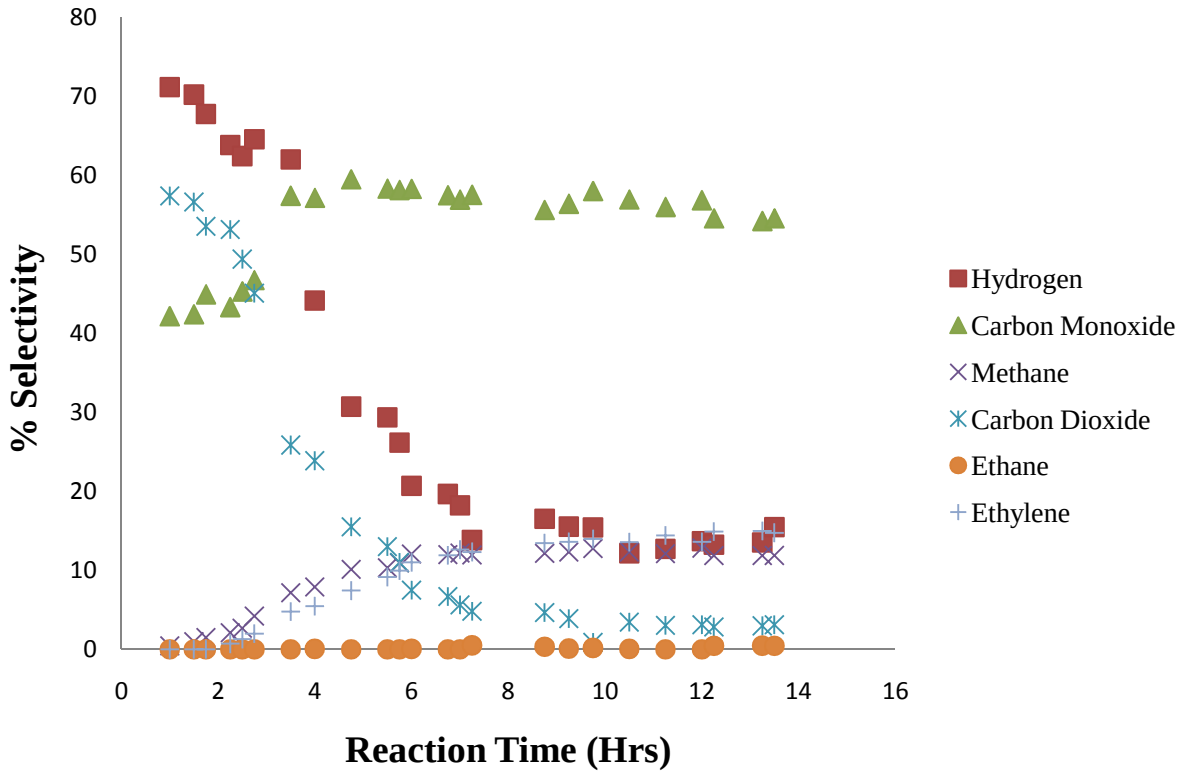

Figure 4.3.1.1b – Product gas selectivity for pure glycerol reforming over Ni/γ-Al_2O_3

Figure 4.3.1.1c shows the estimated conversion of glycerol into gaseous products versus time. Conversion levels are initially fairly close to 100%. Deactivation starts to occur after the two hour mark and after six hours conversion levels stay between 40-50%. During the reaction, the reactor tube gained 0.5102 g of weight due to coke and char formation.

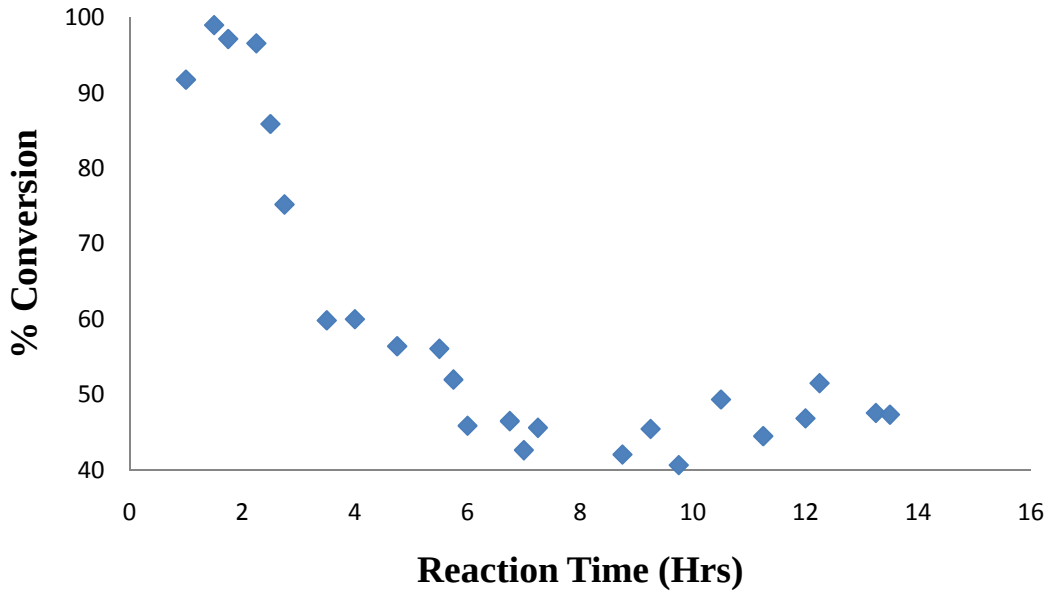

Figure 4.3.1.1c – Product gas Glycerol conversion over Ni/γ-Al_2O_3

Figure 4.3.1.1d shows the hydrogen yield versus time for this reaction. Initially, hydrogen yield is high. For every mole of glycerol fed, about 4.3 to 4.8 moles of hydrogen was produced. This value drops very quickly with the drop of activity. After the seven hour mark, the hydrogen yield drops to 0.4-0.5 moles.

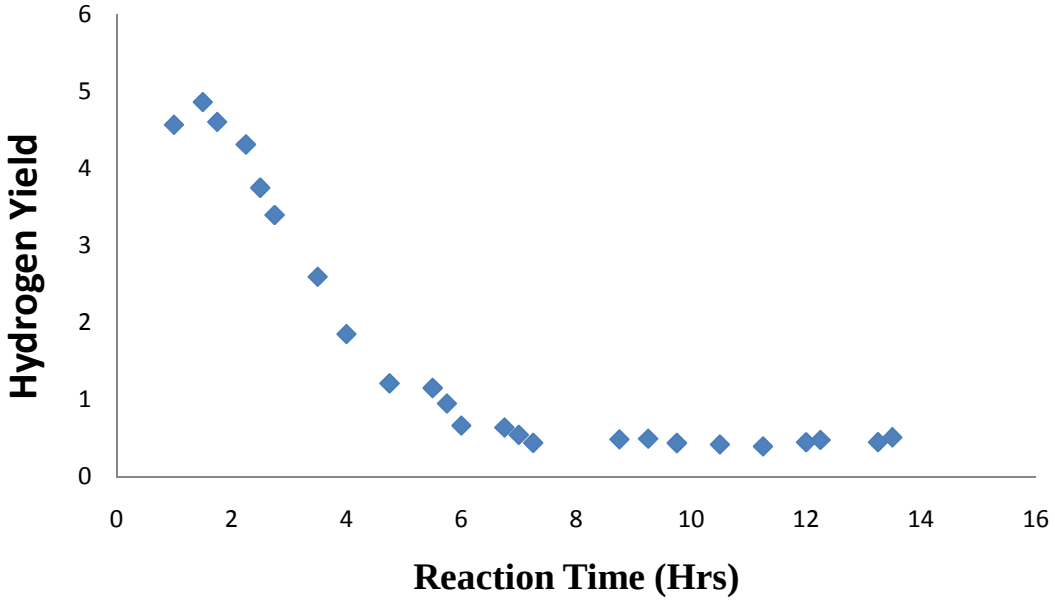

Figure 4.3.1.1d – Hydrogen yield for pure glycerol reforming over Ni/γ-Al_2O_3

The syngas ratio of the product gas versus reaction time is presented in Figure 4.3.1.1e. The syngas ratio starts at a little below four for the first several hours of reaction. After seven hours of reaction time, the syngas ratio stays between 0.5 to 0.6.

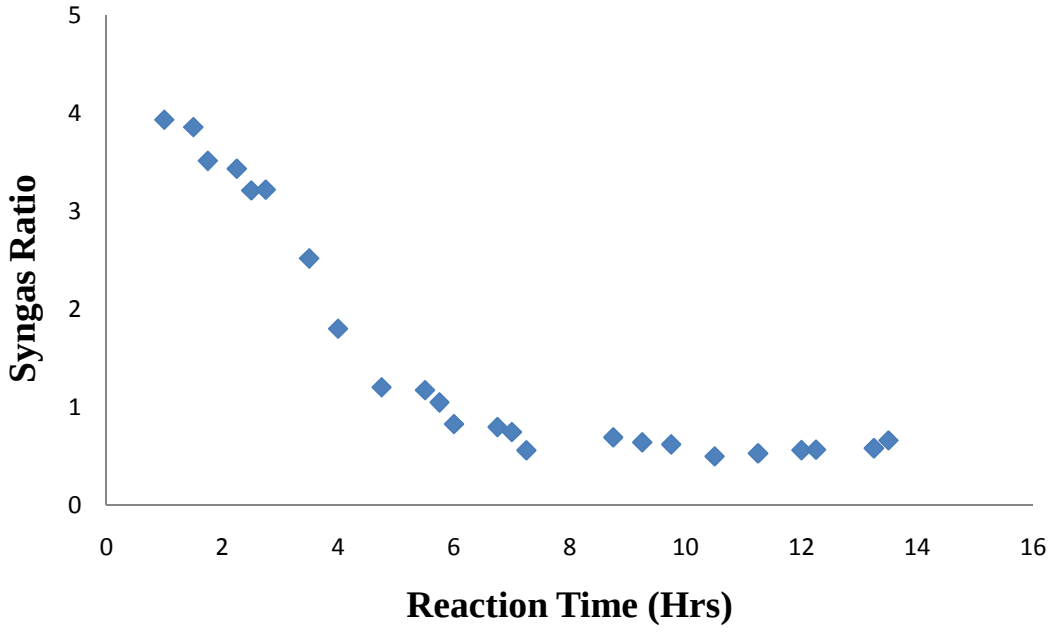

Figure 4.3.1.1e – Product gas syngas ratio for pure glycerol reforming over Ni/γ-Al_2O_3

Figure 4.3.1.1f shows the lower heating value (LHV) of the product gas versus reaction time. These values ignore the presence of the carrier.

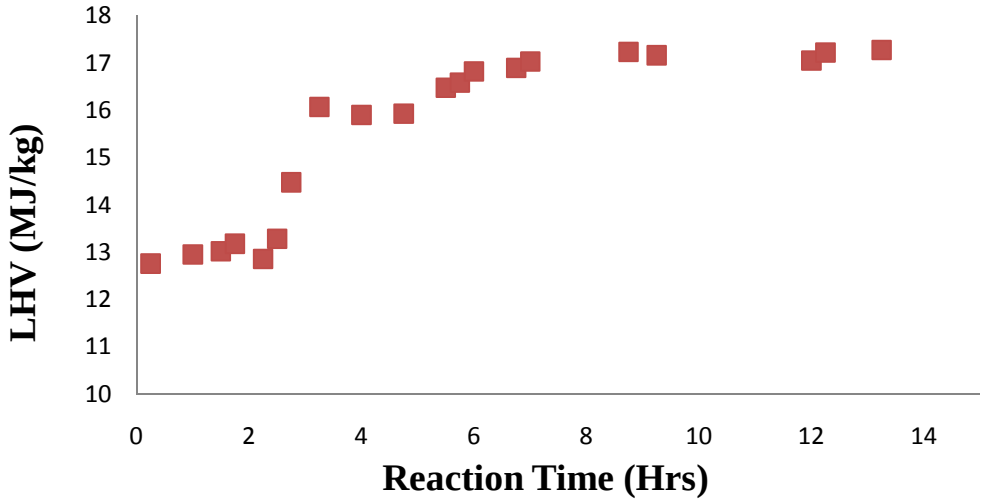

Figure 4.3.1.1f – Product gas LHV for pure glycerol reforming over Ni/γ-Al_2O_3

4.3.1.2 Ni/MgO

Pure (99.8%) glycerol steam reforming was performed over a 5% Ni/MgO catalyst in a packed bed reactor. 0.1954 g of catalyst and 0.2790 g of SiO_2 were placed into a quartz tube reactor between two pieces of quartz wool. The catalyst was reduced for an hour and a half with 5% H_2 in argon (50 ml/min) at approximately 825 °C. The reactor temperature was allowed to ramp up to 725 °C and allowed to stabilize before starting the reaction. Also, the GC was calibrated before the reaction was started. To start the reaction, a distilled water-pure glycerol mixture was fed to the reactor at a molar ratio of 9:1 (water:glycerol) at a liquid flow rate of 0.15 ml/min (GHSV = 28000 hr^{-1}). GC testing started within 15 minutes of starting the reactant flow to the reactor.

Reactant was sent to the reactor for 903 minutes. During this time 122.8 ml of reactant was fed to the reactor (approximately 0.14 ml/min) and 66.9 ml of liquid product was collected. The liquid product was clear throughout the length of the run.

The Ni/MgO catalyst activity drops steadily throughout the reaction. Figures 4.3.1.2a, b show the product gas composition and product gas selectivity for the life of the run. The initial composition of the product gas was approximately 66% H_2, 10% CO, and 24% CO_2. CH_4, C_2H_6, and C_2H_4 were not detected. After 14 hours, the product gas composition was about 60% H_2, 19% CO, 18% CO_2, 2% CH_4, 0.5% C_2H_6, and 0.2% C_2H_4. The gas selectivity behaves similarly. Hydrogen selectivity drops from over 80% to 57% during the reaction. CO_2 selectivity drops as well but CO selectivity increases. The overall drop in activity was around ~10%.

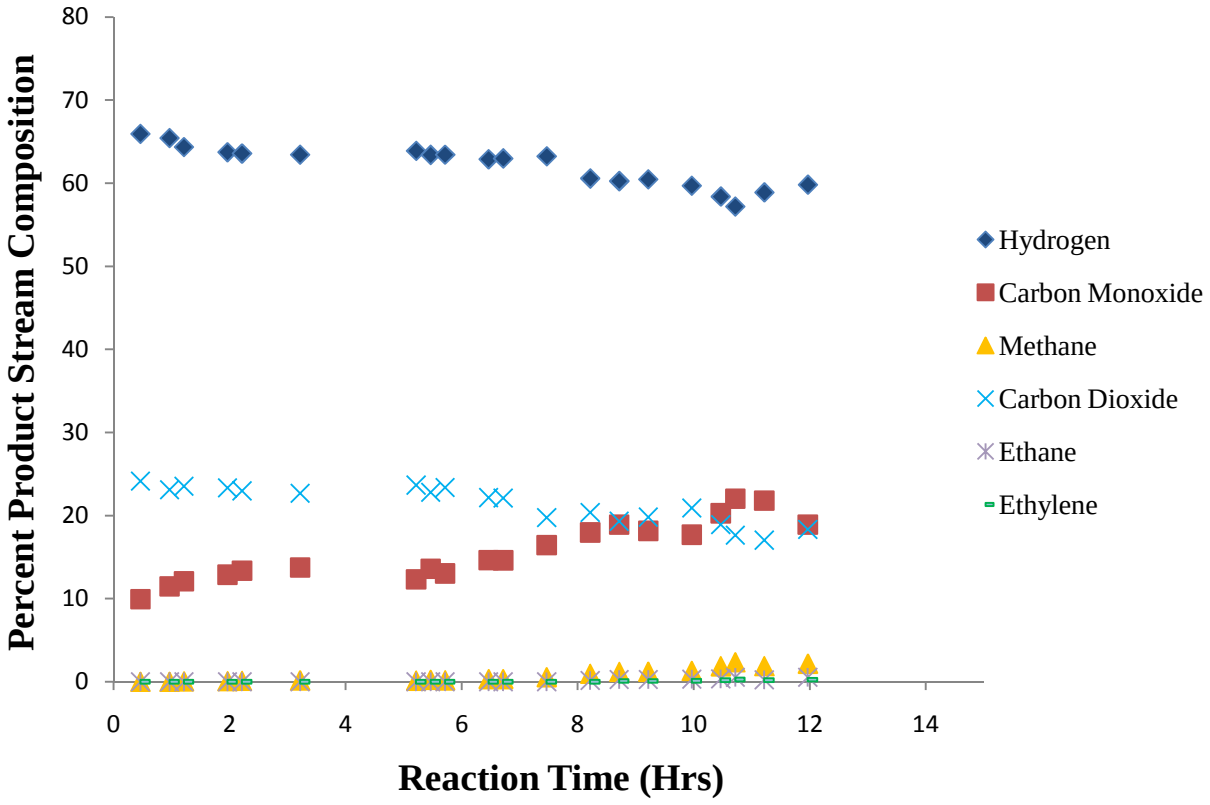

Figure 4.3.1.2a – Product gas composition for pure glycerol reforming over Ni/MgO

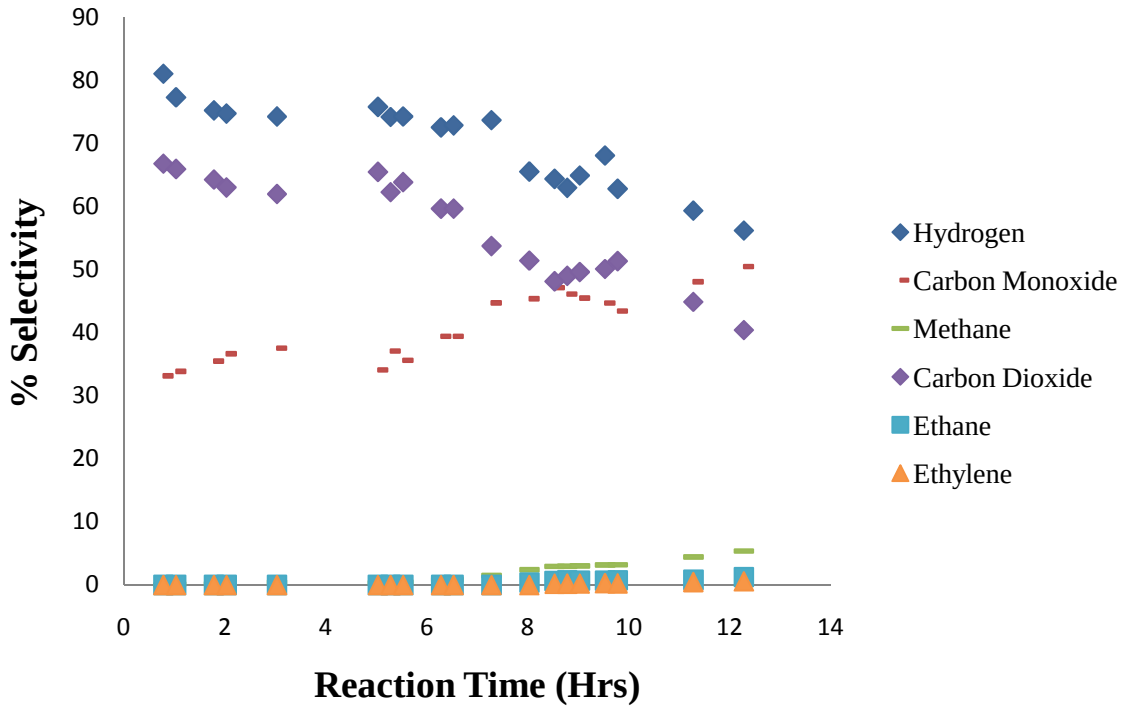

Figure 4.3.1.2b – Product gas selectivity for pure glycerol reforming over Ni/MgO

To determine whether or not the liquid product had any components besides water, index refractometry and a distillation were performed on the liquid product. This liquid product gave the same values as distilled water on an index refractometer. Also, 15 mL of the product were distilled at 105 °C to see if other products were present. Table 4.3.1.2a shows the results of these tests. Also, the reactor tube weighed an additional 0.9289 g after the reaction due to tar and coke formation. This comes out to be less than 2% of the total glycerol fed. These tests confirm that conversion of glycerol was close to 100%.

Table 4.3.1.2a - Conversion Estimates

Index Refractometer		Distillation	
Distilled H_2O	1.3326	Initial Volume	15.0 mL
Ni/MgO - Pure	1.3326	Volume after 105 °C Distillation	0.0 mL

Figure 4.3.1.2c shows the hydrogen yield versus time for this reaction. The hydrogen yield remains steady throughout the reaction. After two hours of reaction time, the hydrogen yield stabilizes and holds steady around 4.5 to 5.75 until after 12 hours of reaction time.

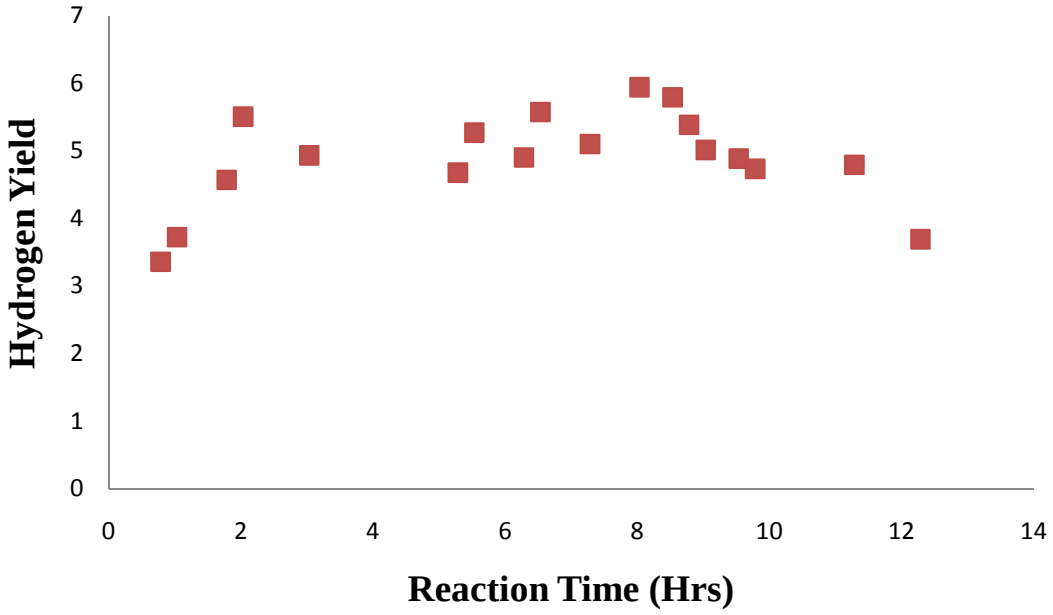

Figure 4.3.1.2c – Hydrogen yield for pure glycerol reforming over Ni/MgO

The syngas ratio of the product gas versus reaction time is presented in Figure 4.3.1.2d. The syngas ratio gradually decreases with the rise of CO production in the product gas. After 45 minutes of reaction time, the syngas ratio is 5.7. By the four and a half hour mark, the syngas ratio has dropped to about 4.5. It holds steady for the next several hours. Then there is another

drop in syngas ratio for the next two hours. For the rest of the reaction, the syngas ratio stayed around three.

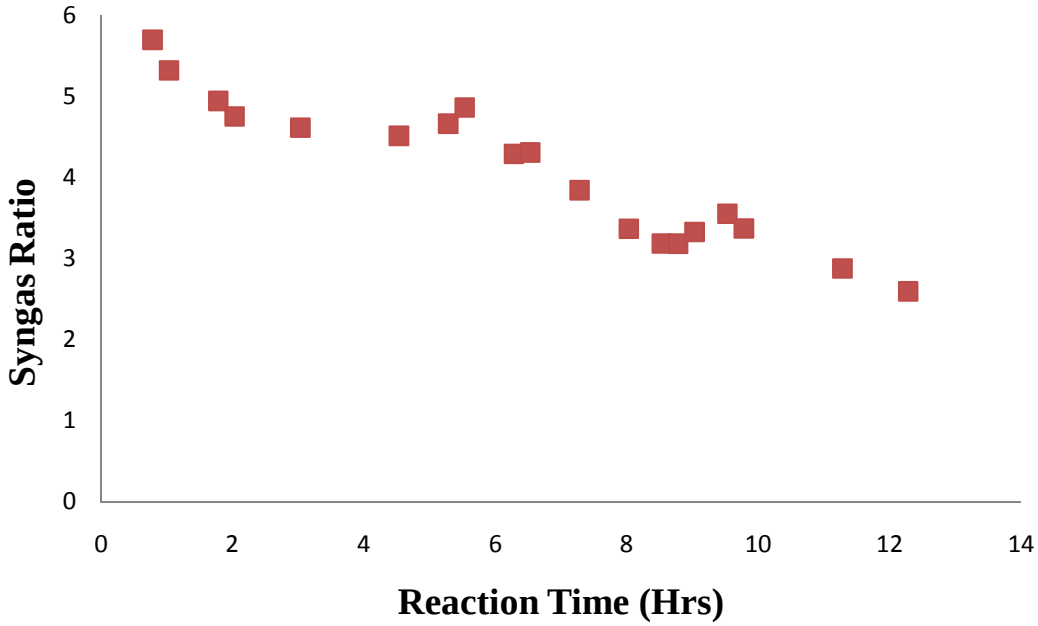

Figure 4.3.1.2d – Syngas ratio for pure glycerol reforming over Ni/MgO

Figure 4.3.1.2e shows the LHV of the product gas versus reaction time. These values ignore the presence of the carrier. The LHV of the product gas increases slightly as the reaction progresses. This is due to the increase in CO and CH_4 production.

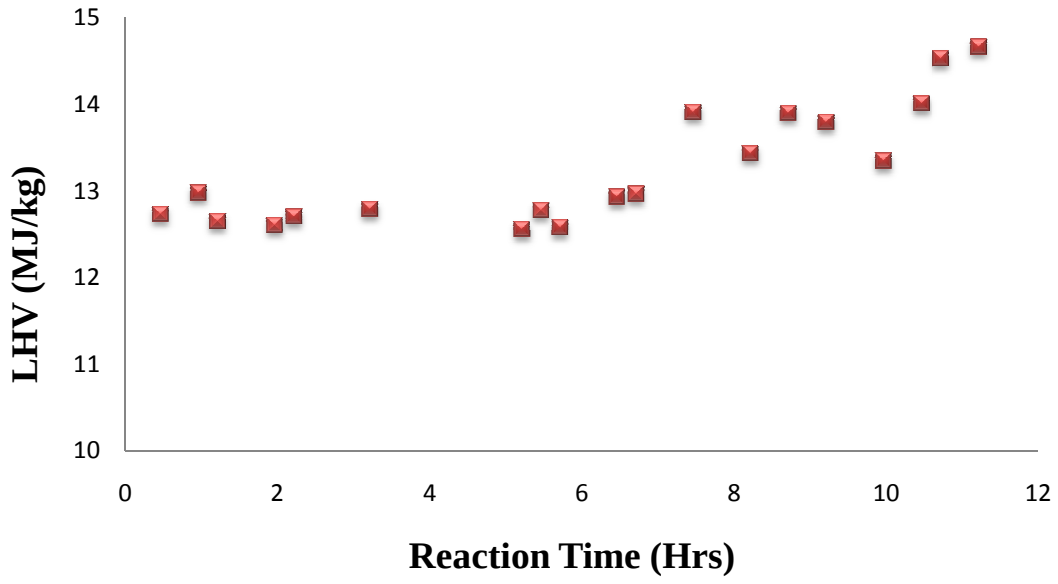

ng over

4.3.2 Crude Glycerol Reforming

4.3.2.1 Octolyst 1001

Crude glycerol steam reforming was performed over a 15% Ni/γ-Al_2O_3 catalyst (Octolyst 1001) in a packed bed reactor. 0.4981 g of catalyst and SiO_2 (55% catalyst/45% SiO_2) were placed into a quartz tube reactor between two pieces of quartz wool. The catalyst was reduced for an hour and a half with 5% H_2 in argon (50 ml/min) at approximately 600 °C. The reactor temperature was allowed to ramp up to 725 °C and allowed to stabilize before starting the reaction. Also, the GC was calibrated before the reaction was started. To start the reaction, a distilled water-crude glycerol mixture was fed to the reactor at a volume ratio of about 70:30 (water:crude glycerol) at a liquid flow rate of 0.15 ml/min (GHSV = 44000 hr^{-1}). This volume ratio was based off a 9:1 molar ratio for pure glycerol. The soap content in the crude glycerol could not be accurately tested with the present methods. Therefore to maintain consistency between the runs the volume ratio was kept constant. GC testing started within 15 minutes of starting the reactant flow to the reactor.

Reactant was sent to the reactor for 1140 minutes. During this time 122.8 ml of reactant was fed to the reactor (approximately 0.11 ml/min) and 31.2 ml of liquid product was collected. Despite the length of time glycerol was sent to the reactor, reactant did not reach the catalyst bed for the entirety of the run. After six hours of operation, the reactor started to show signs of blockage (e.g. outlet gas flow rate dropped significantly, liquid reactant leaked out of the stainless steel tubing). It is probable that the feeding rate was the same as the pure glycerol runs until reactor blockage started to occur (e.g. 0.14 mL/min).

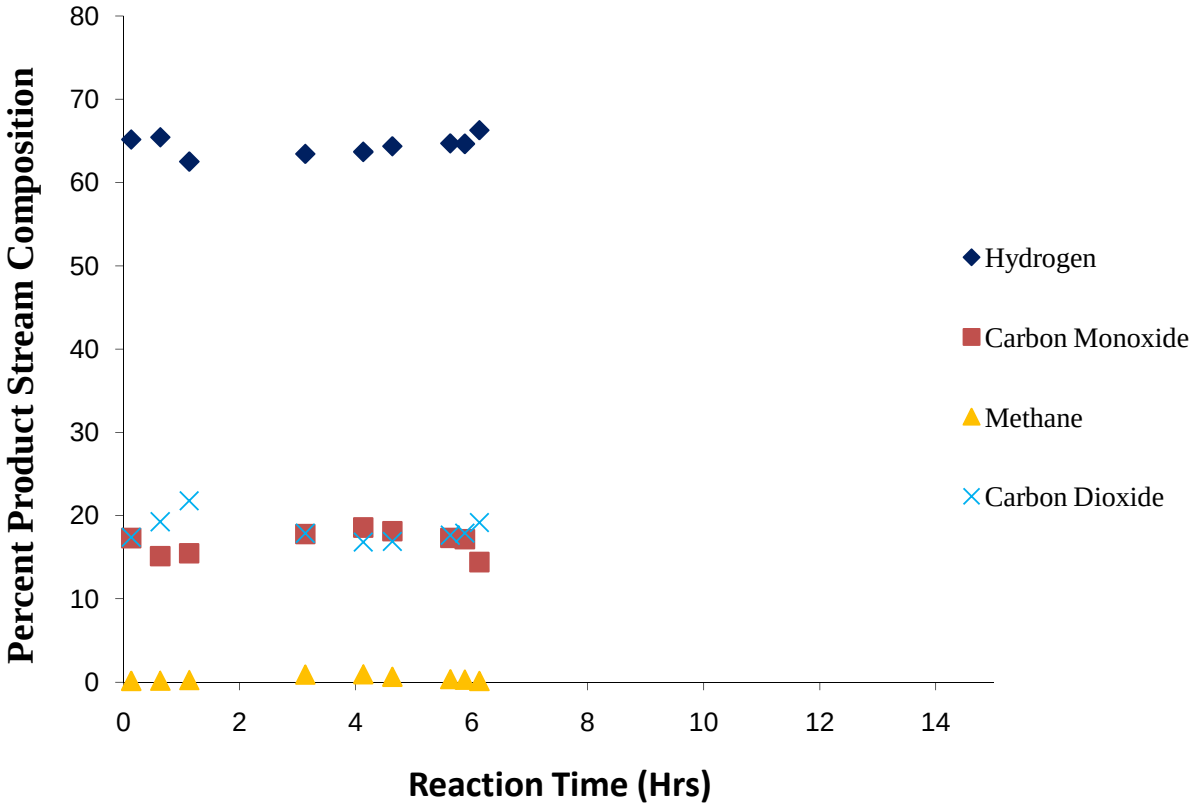

Figure 4.3.2.1a – Product gas composition for crude glycerol reforming over Ni/γ-Al_2O_3

Figure 4.3.2.1a shows the product gas composition for the life of the run. It is difficult to tell how the catalyst handles crude glycerol compared to the pure glycerol because of the blockage of the reactor after six hours. Still through the first six hours of reaction, crude glycerol

reforming outperforms pure glycerol reforming when using Octolyst 1001 because no signs of deactivation occur. Throughout the six hours before blockage, the activity holds very steady. The composition of the product gas was approximately 64-66% H_2, 16-19% CO, 17-19% CO_2, and 0.2-1% CH_4 throughout the run. C_2H_6, and C_2H_4 were not detected.

Figure 4.3.2.1b shows the selectivity of H_2, CO, CO_2, CH_4, C_2H_6, and C_2H_4 versus time. Despite the appearance of variance, the selectivity values hold steady. Hydrogen selectivity is approximately 70% throughout the reaction. CO and CO_2 selectivity stay between 45-55%.

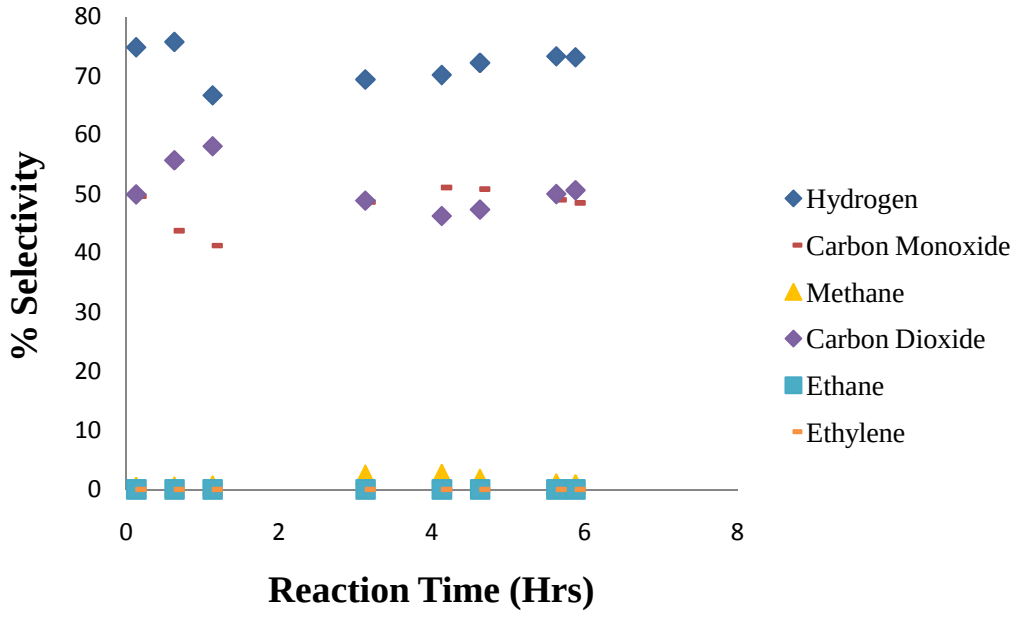

Figure 4.3.2.1b – Product gas selectivity for crude glycerol reforming over Ni/γ-Al_2O_3

To determine whether or not the liquid product had any components besides water, index refractometry and a distillation were performed on the liquid product. This liquid product gave the same values as distilled water on an index refractometer. Also, 15 mL of the product were distilled at 105 °C to see if other products were present. Table 4.3.2.1a shows the results of these tests. These tests indicate that the conversion of glycerol approached 100%.

Table 4.3.2.1a - Conversion Estimates

Index Refractometer		Distillation	
Distilled H_2O	1.3327	Initial Volume	15.0 mL
Ni/γ-Al_2O_3 - Crude	1.3328	Volume after 105 °C Distillation	0.0 mL

Due to the nature of the blockage in the reactor, it was difficult to weigh the reactor tube after the reaction. A significant amount of tar formation occurred in and around the inner reactor tube. This caused the inner tube to stick inside the outer reactor tube upon dismantling of the reactor. This prevented accurate measurement of the weight added to the reactor tube during reaction.

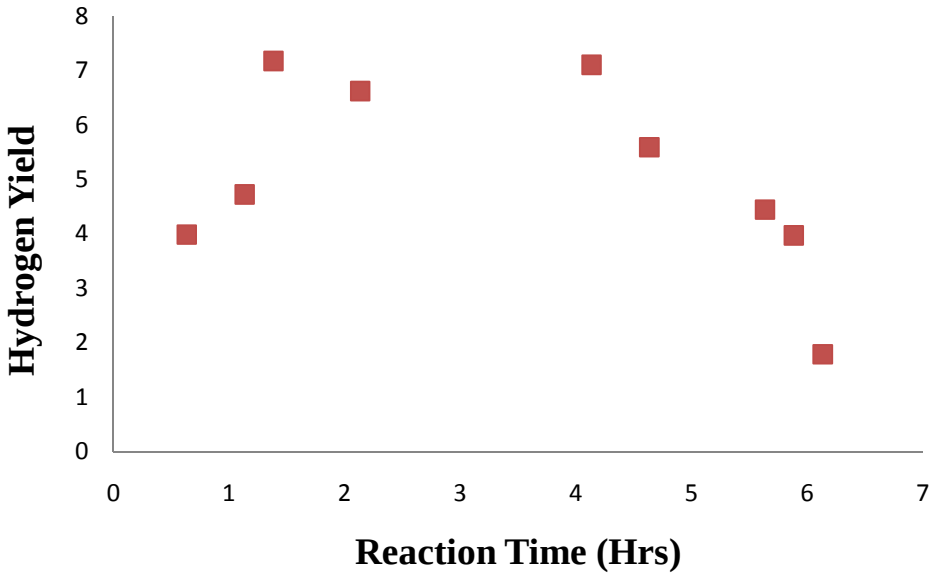

Figure 4.3.2.1c – Hydrogen yield for crude glycerol reforming over Ni/γ-Al_2O_3

Figure 4.3.2.1c shows the hydrogen yield versus time for this reaction. The data is scattered and does not provide the clearness that is desired. Still, it appears that the hydrogen yield holds steady until signs of blockage start to occur.

The syngas ratio of the product gas versus reaction time is presented in Figure 4.3.2.1d. The syngas ratio is constant throughout the reaction. For the six hour reaction period, the syngas ratio hovers between 3.5 and 4.25.

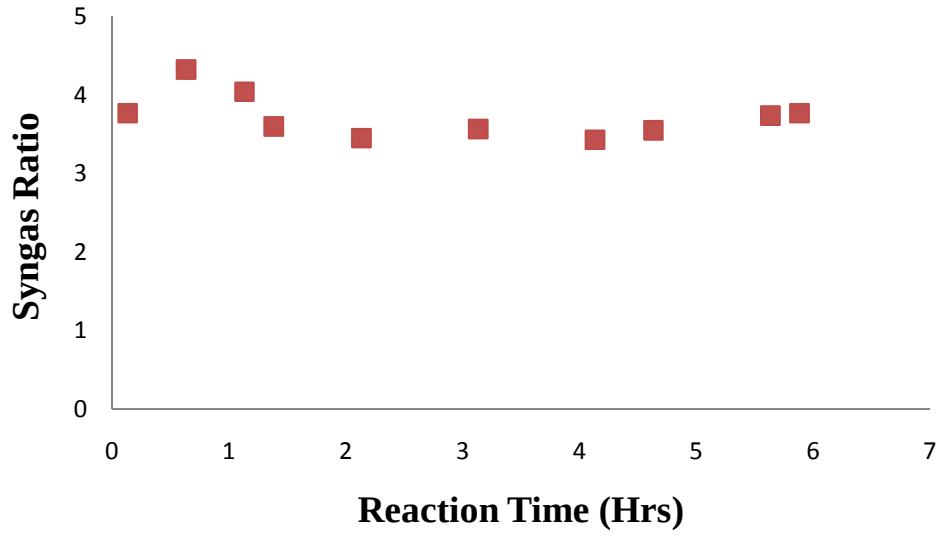

Figure 4.3.2.1d – Product gas syngas ratio for crude glycerol reforming over Ni/γ-Al_2O_3

Figure 4.3.2.1e shows the LHV of the product gas versus reaction time. These values ignore the presence of the carrier. The LHV of the product gas remains around 15 MJ/kg throughout the reaction.

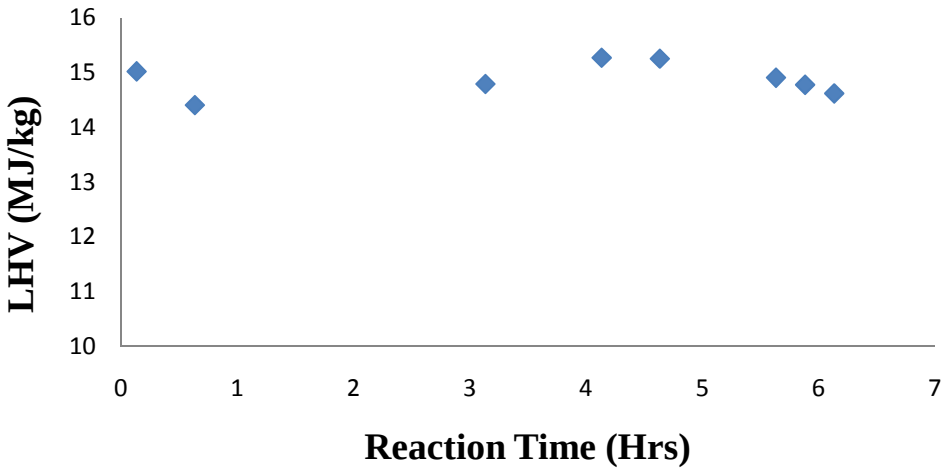

Figure 4.3.2.1e – Product gas LHV for crude glycerol reforming over Ni/γ-Al_2O_3

4.3.2.2 Ni/MgO

Crude glycerol steam reforming was performed over a 5% Ni/MgO catalyst in a packed bed reactor. This reaction was similar to its Ni/γ-Al_2O_3 counterpart. Both reactions lasted essentially six hours due to blockage of the heating zone of the reactor. Also, product gas composition did not change significantly over this period.

0.2053 g of catalyst and 0.3452 g of SiO_2 were placed into a quartz tube reactor between two pieces of quartz wool. The catalyst was reduced for over an hour and a half with 5% H_2 in argon (50 ml/min) at approximately 825 °C. The reactor temperature was allowed to ramp up to 725 °C and allowed to stabilize before starting the reaction. Also, the GC was calibrated before the reaction was started. To start the reaction, a distilled water-crude glycerol mixture was fed to the reactor at a volume ratio of 70:30 (water:crude glycerol) at a liquid flow rate of 0.15 ml/min (GHSV = 28000 hr^{-1}). GC testing started within 15 minutes of starting the reactant flow to the reactor.

Reactant was sent to the reactor for 702 minutes. During this time 106 ml of reactant was fed to the reactor (approximately 0.15 ml/min) and 64 ml of liquid product was collected. The reaction was started in the evening. By morning, the carrier gas flow was blocked, the temperature program failed, and reactor temperature had dropped significantly. The failure of the temperature program was, in all likelihood, due to the tar and coke formation in the heating zone.

From the data, the reaction behaved normally for the first five to six hours of the reaction. Signs of blockage started showing up soon after that. The temperature program failed around the nine hour mark. The final liquid product was clear but had a thin yellowish oil film on top. It

was completely clear for at least the first hour. It is likely that it remained clear until the drop in reactor temperature caused by the failure of the temperature control.

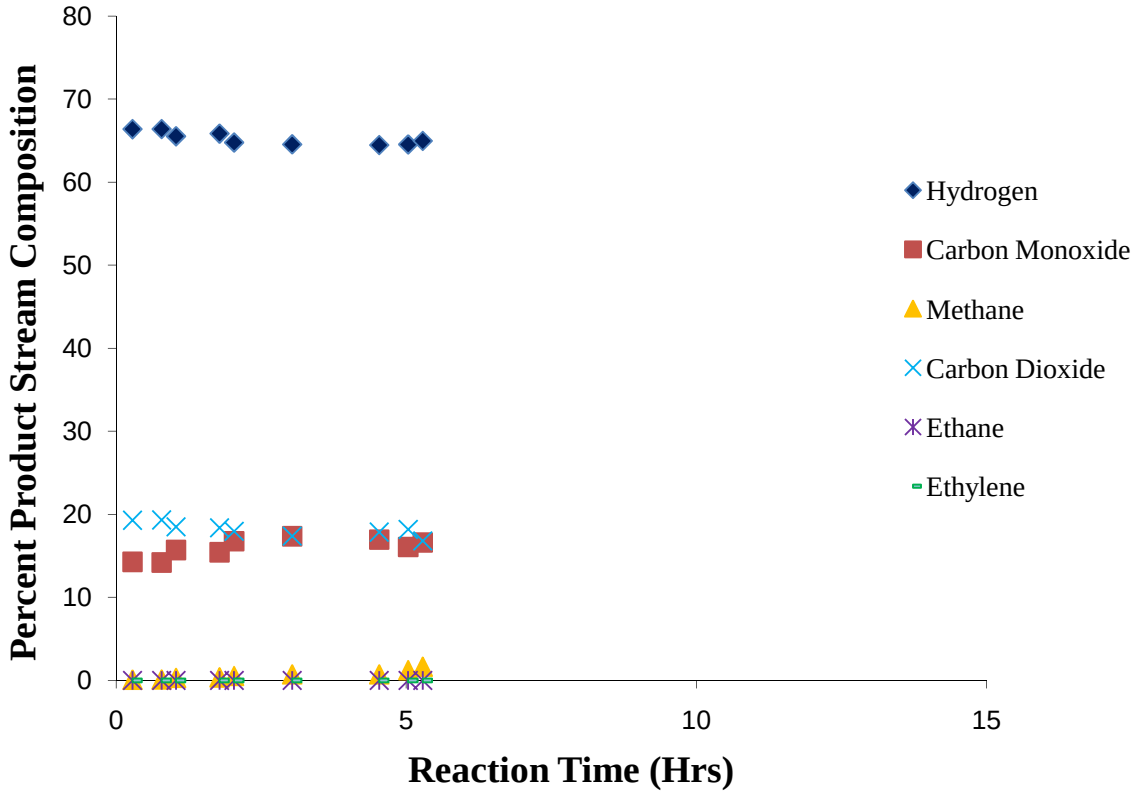

Figure 4.3.2.2a – Product gas composition for crude glycerol reforming over Ni/MgO

The Ni/MgO catalyst holds its activity for the first five hours of the run. Figure 4.3.2.2a shows the product gas composition for the first five hours of the run. The composition of the product gas was 64-66% H_2, 14-16% CO, 17-19% CO_2, and 0-1% CH_4 throughout this time period. C_2H_6, and C_2H_4 were not detected during the initial five hours.

Figure 4.3.2.2b shows the selectivity of H_2, CO, CO_2, CH_4, C_2H_6, and C_2H_4 versus time. These values change very little over time. Hydrogen and CO_2 selectivity decrease by 5-10%, whereas, CO production increases the same amount. Methane selectivity increases from 0-4%, indicating that the flow of glycerol to the catalyst was slowed over time.

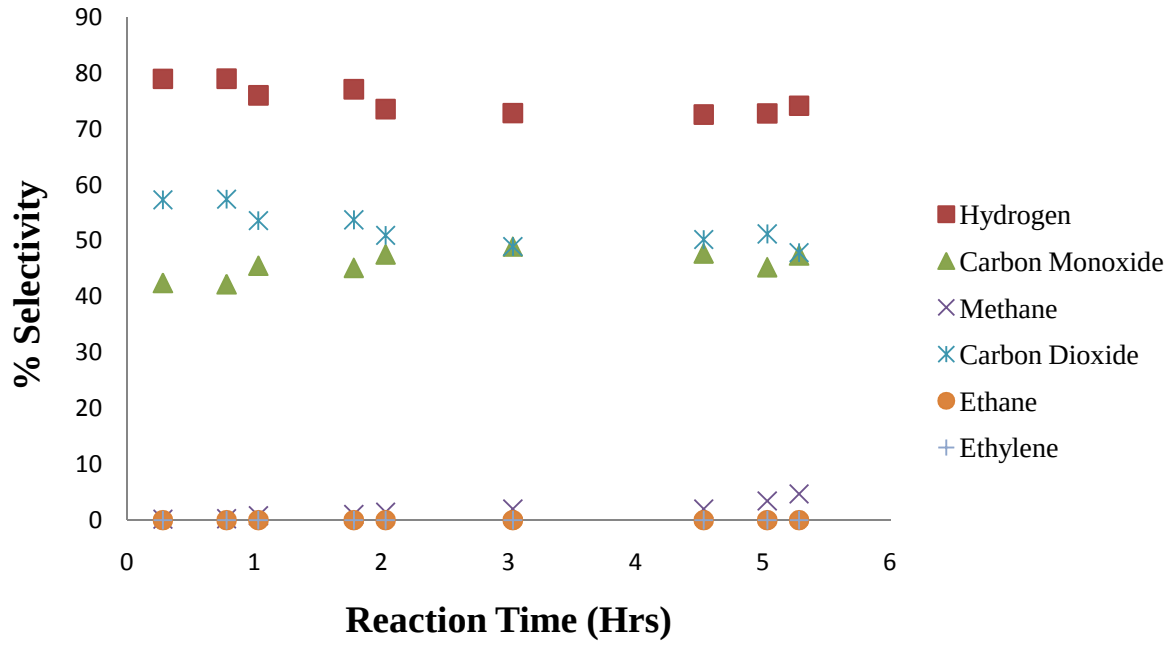

Figure 4.3.2.2b – Product gas selectivity for crude glycerol reforming over Ni/MgO

Conversion is difficult to quantitatively estimate for this reaction. The index refractometry and distillation methods used previously cannot be used because of the yellow oily film layer. The best method is to consider that the liquid product was initially clear (for at least one hour of operation). The product gas composition does not change significantly for the first five hours, which indicates that the reaction dynamics have not changed. Also, as will be shown later, acid-washed glycerol reforming using Ni/MgO gives water as its only liquid product. Based on these facts, it is very likely that crude glycerol reforming over Ni/MgO had water as its only liquid product for the first 5+ hours and that the conversion of glycerol to gaseous components was approximately complete (ignoring tar and coke formation).

Due to the nature of the blockage in the reactor, it was difficult to weigh the reactor tube after the reaction. A significant amount of tar formation occurred in and around the inner reactor tube (for the reactant feed).

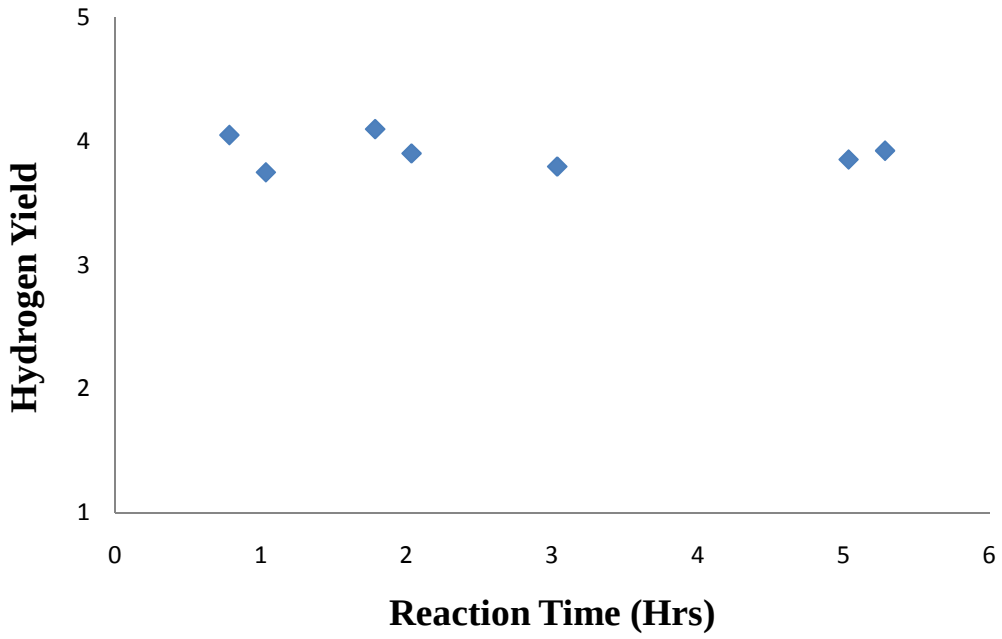

Figure 4.3.2.2c – Hydrogen yield for crude glycerol reforming over Ni/MgO

Figure 4.3.2.2c shows the hydrogen yield versus time for this reaction. The data is a fairly linear and the hydrogen yield holds around 4.0 until blockage of the reactor. The syngas ratio of the product gas versus reaction time is presented in Figure 4.3.2.2d. The syngas ratio holds drops slightly throughout the reaction. Initially the ratio is about 4.5. At the five hour mark, the syngas ratio is approximately 4.0.

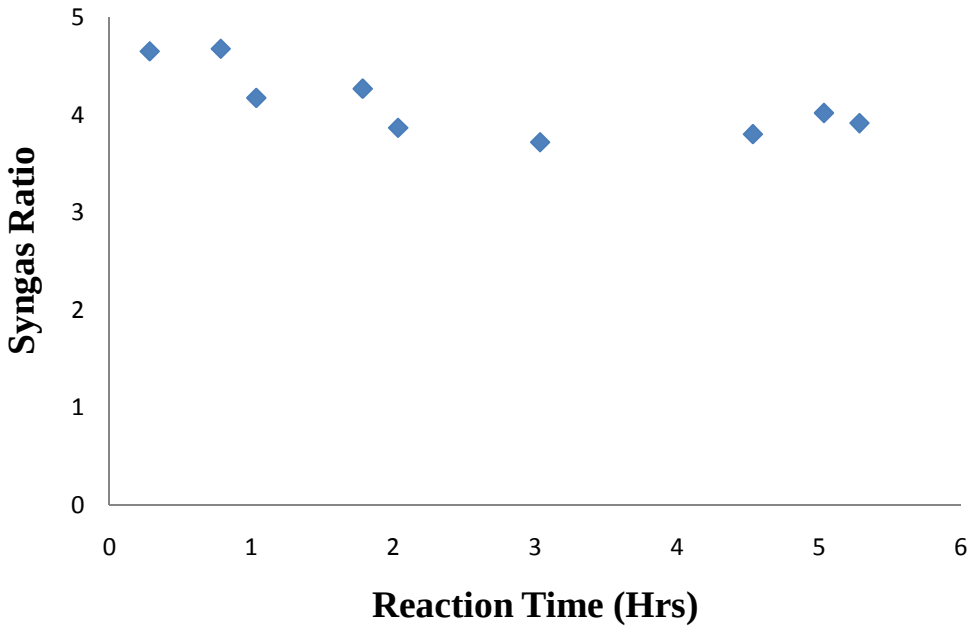

Figure 4.3.2.2d – Product gas syngas ratio for crude glycerol reforming over Ni/MgO

Figure 4.3.2.2e shows the LHV of the product gas versus reaction time. These values ignore the presence of the carrier. The LHV of the product gas increases slightly as the reaction progresses. This is due to the increase in CO and CH_4 production. Although CO has a low LHV, it still plays a role in increasing the overall LHV of the product gas because it replaces CO_2, which has no LHV.

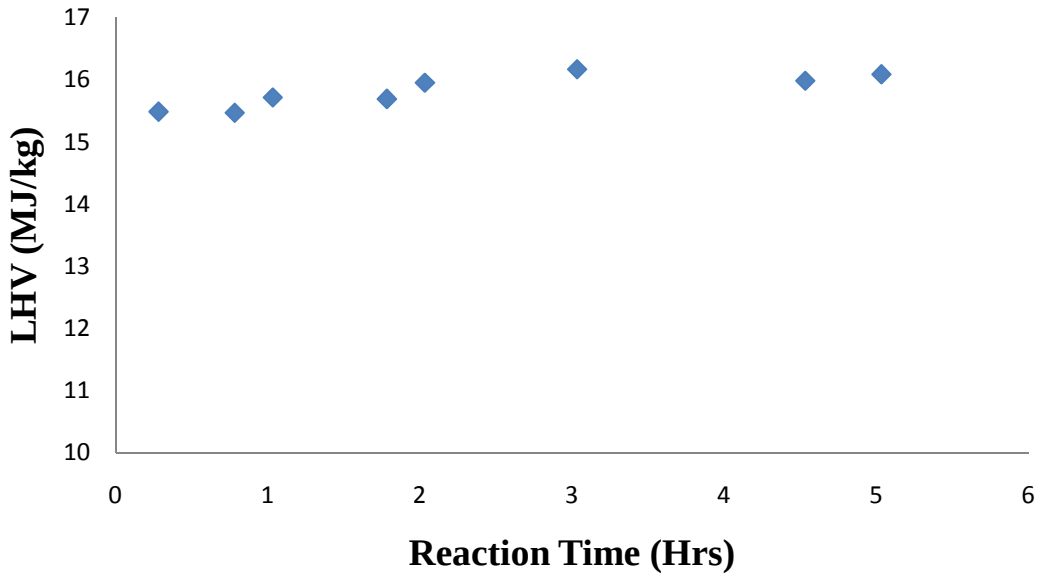

Figure 4.3.2.2e – Product gas LHV for crude glycerol reforming over Ni/MgO

4.3.3 Acid Washed Glycerol Reforming

4.3.3.1 Octolyst 1001

Acid-washed glycerol steam reforming was performed over a 15% Ni/γAl_2O_3 catalyst (Octolyst 1001) in a packed bed reactor. 0.4924 g of catalyst and SiO_2 (55% catalyst/45% SiO_2) were placed into a quartz tube reactor between two pieces of quartz wool. The catalyst was reduced for an hour and a half with 5% H_2 in argon (50 ml/min) at approximately 600 °C. The reactor temperature was allowed to ramp up to 725 °C and allowed to stabilize before starting the reaction. Also, the GC was calibrated before the reaction was started. To start the reaction, a distilled water-crude glycerol mixture was fed to the reactor at a volume ratio of about 70:30 (water:acid-washed glycerol) at a liquid flow rate of 0.15 ml/min (GHSV = 44000 hr^{-1}). The 70:30 volume ratio was not exact. It does not include any water present in the acid-washed glycerol. The actual composition of the reactant is provided later. GC testing started within 15 minutes of starting the reactant flow to the reactor.

Reactant was sent to the reactor for 975 minutes. During this time 143 ml of reactant was fed to the reactor (approximately 0.15 ml/min). During the reaction, a small leak formed in the reactant pump line and approximately 15 mL of reactant did not reach the reactor. Therefore, only about 130 mL of reactant made it to the reactor (flowrate = 0.13 mL/min). 74.3 ml of liquid product was collected.

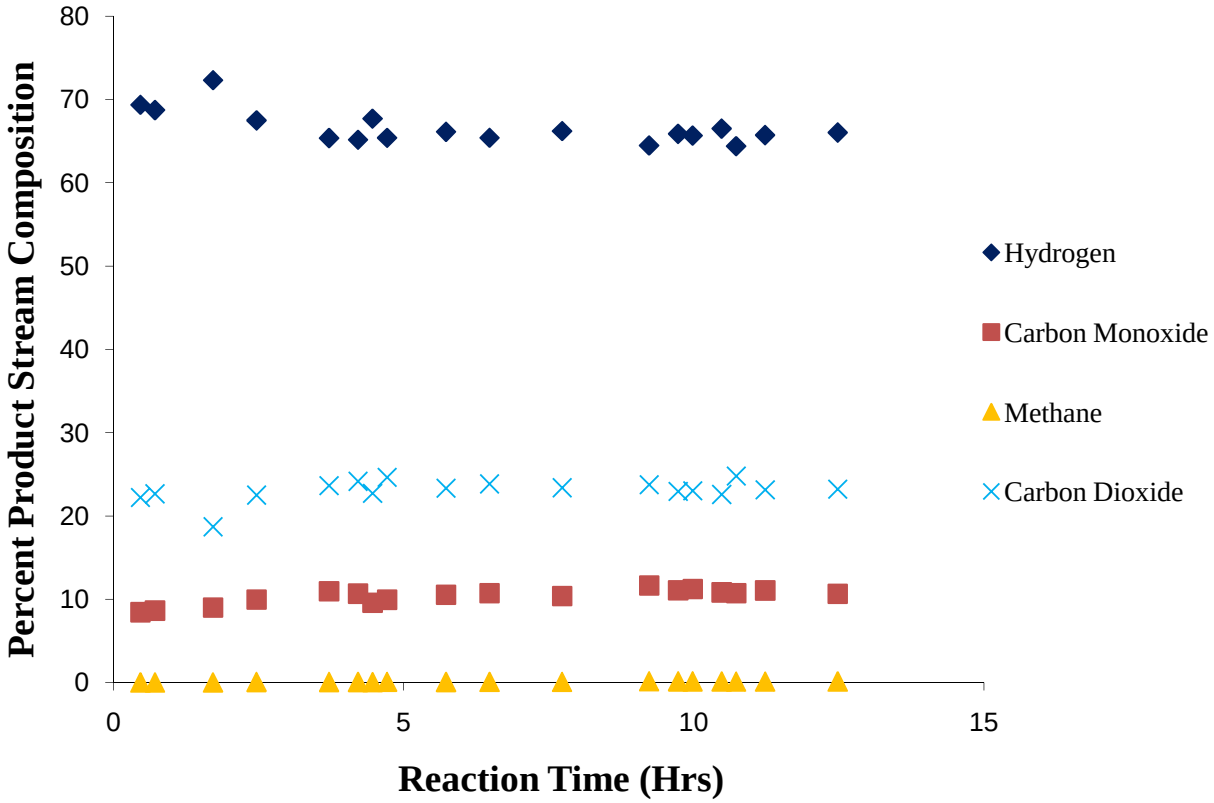

Figure 4.3.3.1a – Product gas composition for acid-washed glycerol reforming over Ni/γ-Al_2O_3

Figure 4.3.3.1a shows the product gas composition for the life of the run. The catalyst held its activity throughout the 12 hour run. Signs of blockage did not appear until after 13-14 hours. The acid-wash significantly improved the stability of the reaction. The composition of the product gas was between 65-69% H_2, 8-11% CO, 22-25% CO_2, and 0.0-0.2% CH_4 throughout the run. C_2H_6, and C_2H_4 were not detected.

Figure 4.3.3.1b shows the selectivity of H_2, CO, CO_2, CH_4, C_2H_6, and C_2H_4 versus time. After a slight initial drop, which may be due to start-up issues, the values stabilize and are steady throughout the run. After three hours, the H_2 selectivity remains approximately 77% for the rest of the reaction. CO and CO_2 selectivity stay around 31% and 69%, respectively.

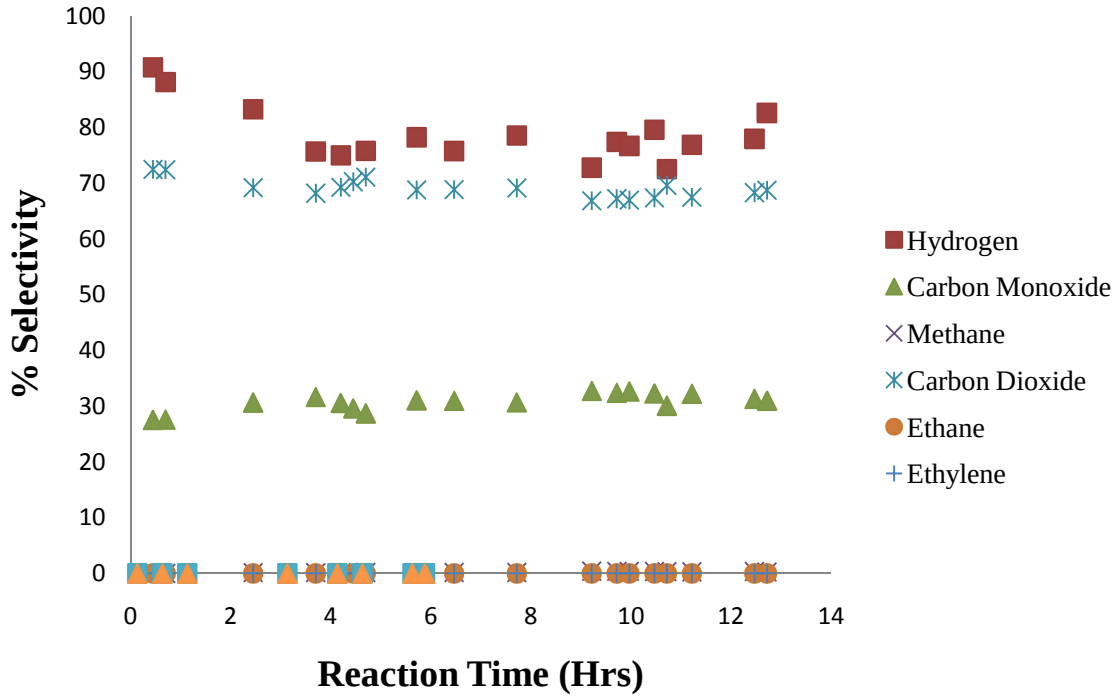

Figure 4.3.3.1b – Product gas selectivity for acid-washed glycerol reforming over Ni/γ-Al_2O_3

To determine whether or not the liquid product had any components besides water, index refractometry and a distillation were performed on the liquid product. This liquid product gave the same values as distilled water on an index refractometer. Also, 15 mL of the product were distilled at 105 °C to see if other products were present. Table 4.3.3.1a shows the results of these tests. During the reaction, the reactor tube gained 1.1196 g of weight due to coking and tar formation. This is about 2-3% of the total mass of reactant fed. These tests confirm that conversion of glycerol approached 100%.

Table 4.3.3.1a - Conversion Estimates

Index Refractometer		Distillation	
Distilled H_2O	1.3327	Initial Volume	15.0 mL
Ni/γ-Al_2O_3 - Acid-wash	1.3326	Volume after 105 °C Distillation	0.0 mL

Figure 4.3.3.1c shows the hydrogen yield versus time for this reaction. The data vary significantly initially but remain steady after four hours. Once the data stabilizes, the hydrogen yield stays between three and four.

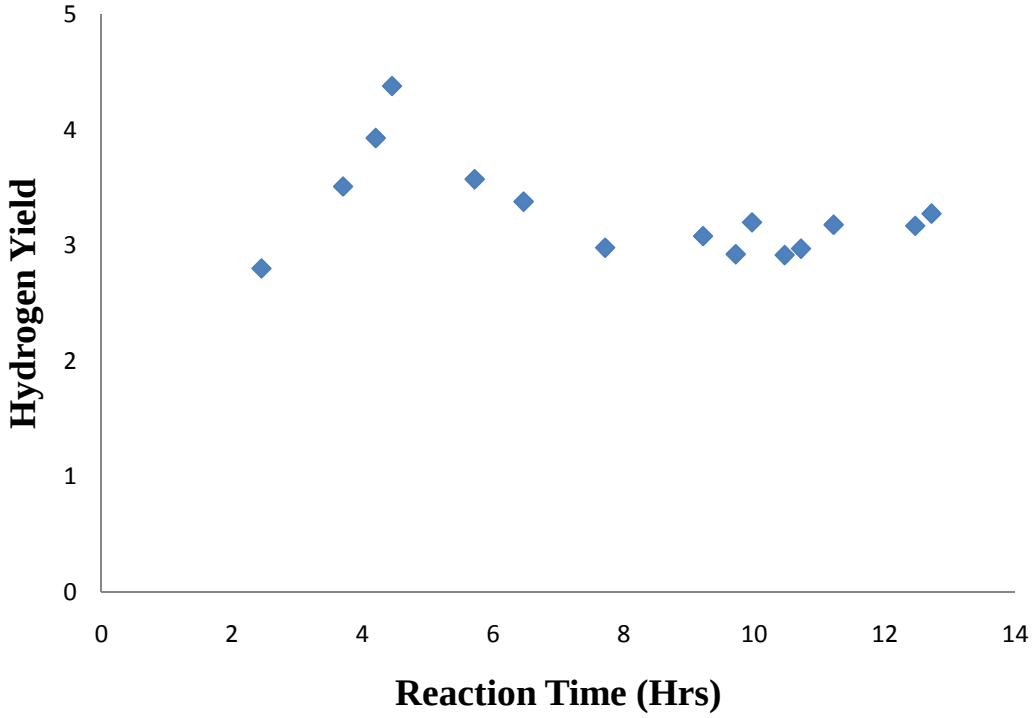

Figure 4.3.3.1b – Hydrogen yield for acid-washed glycerol reforming over Ni/γ-Al_2O_3

The syngas ratio of the product gas versus reaction time is presented in Figure 4.3.3.1d. The syngas ratio starts around eight but gradually drops for a few hours. Once the syngas ratio falls to six, around the four hour mark, it holds steady for the rest of the reaction.

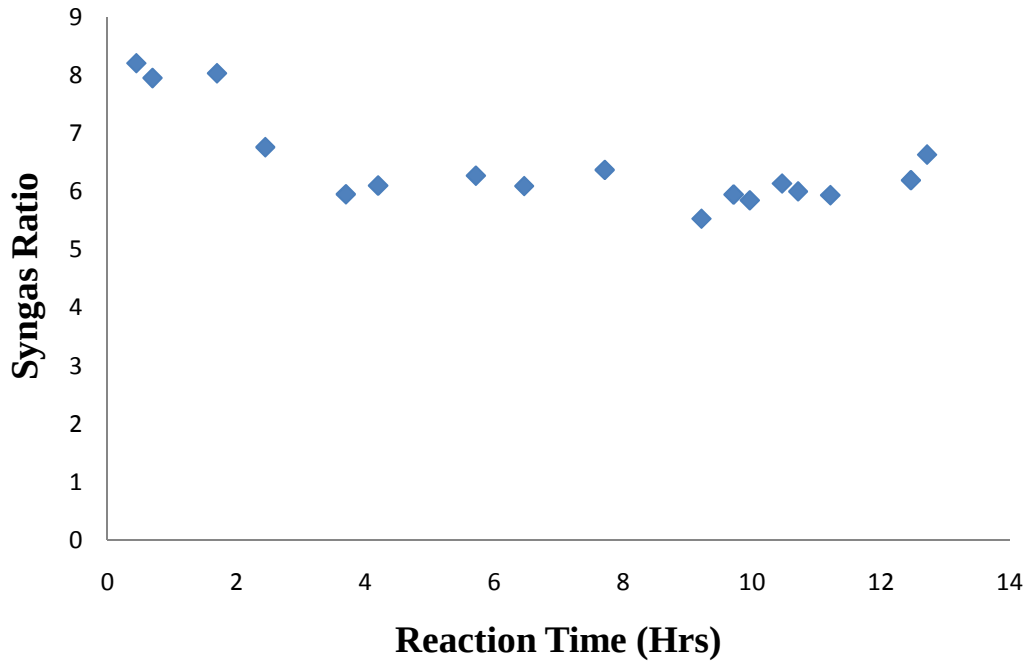

Figure 4.3.3.1d – Product gas syngas ratio for acid-washed glycerol reforming over Ni/γ-Al_2O_3

Figure 4.3.3.1e shows the LHV of the product gas versus reaction time. These values ignore the presence of the carrier gas. The LHV of the product gas has an initial slight decrease but quickly stabilizes and holds constant. This pattern is similar to the syngas ratio, gas selectivity graphs.

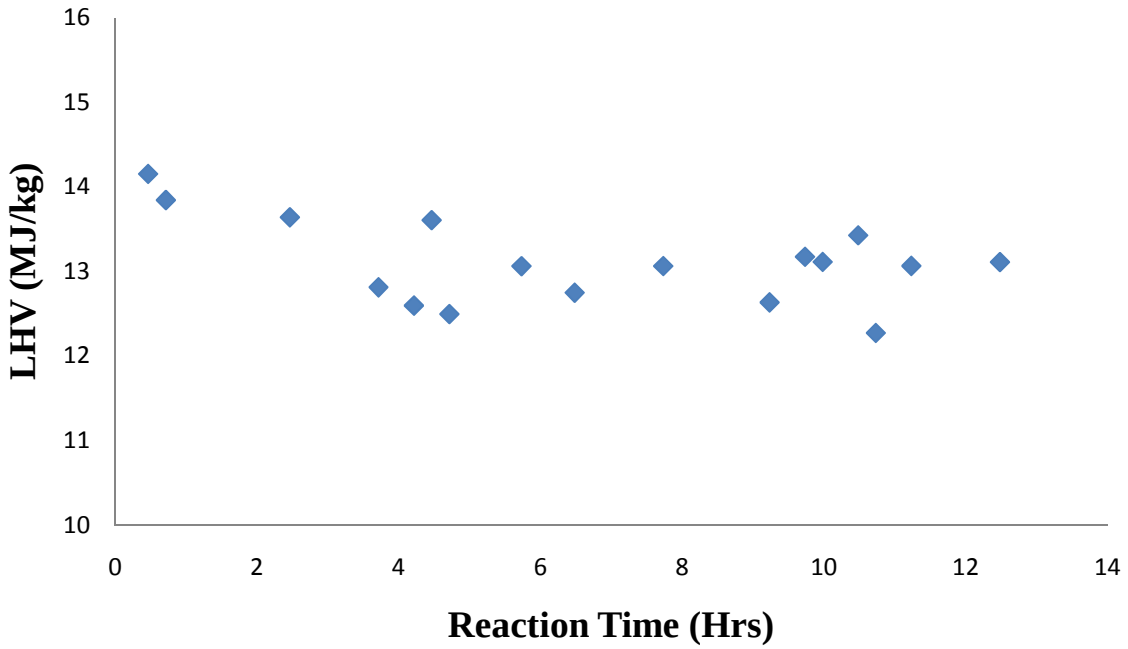

Figure 4.3.3.1e – Product gas LHV for acid-washed glycerol reforming over Ni/γ-Al_2O_3

4.3.3.2 Ni/MgO

Acid-washed glycerol steam reforming was performed over a 5% Ni/MgO catalyst in a packed bed reactor. 0.2029 g of catalyst and 0.3967 g of SiO_2 were placed into a quartz tube reactor between two pieces of quartz wool. The catalyst was reduced for over an hour and a half with 5% H_2 in argon (50 ml/min) at approximately 825 °C. The reactor temperature was allowed to ramp up to 725 °C and allowed to stabilize before starting the reaction. Also, the GC was calibrated before the reaction was started. To start the reaction, a distilled water-crude glycerol mixture was fed to the reactor at a volume ratio of about 70:30 (water:acid-washed glycerol) and at a liquid flow rate of 0.15 ml/min (GHSV = 28000 hr^{-1}). GC testing started within 15 minutes of starting the reactant flow to the reactor.

Reactant was sent to the reactor for 999 minutes. During this time 156 ml of reactant was fed to the reactor (approximately 0.15 ml/min) and 100.2 ml of liquid product was collected. The liquid product was completely clear.

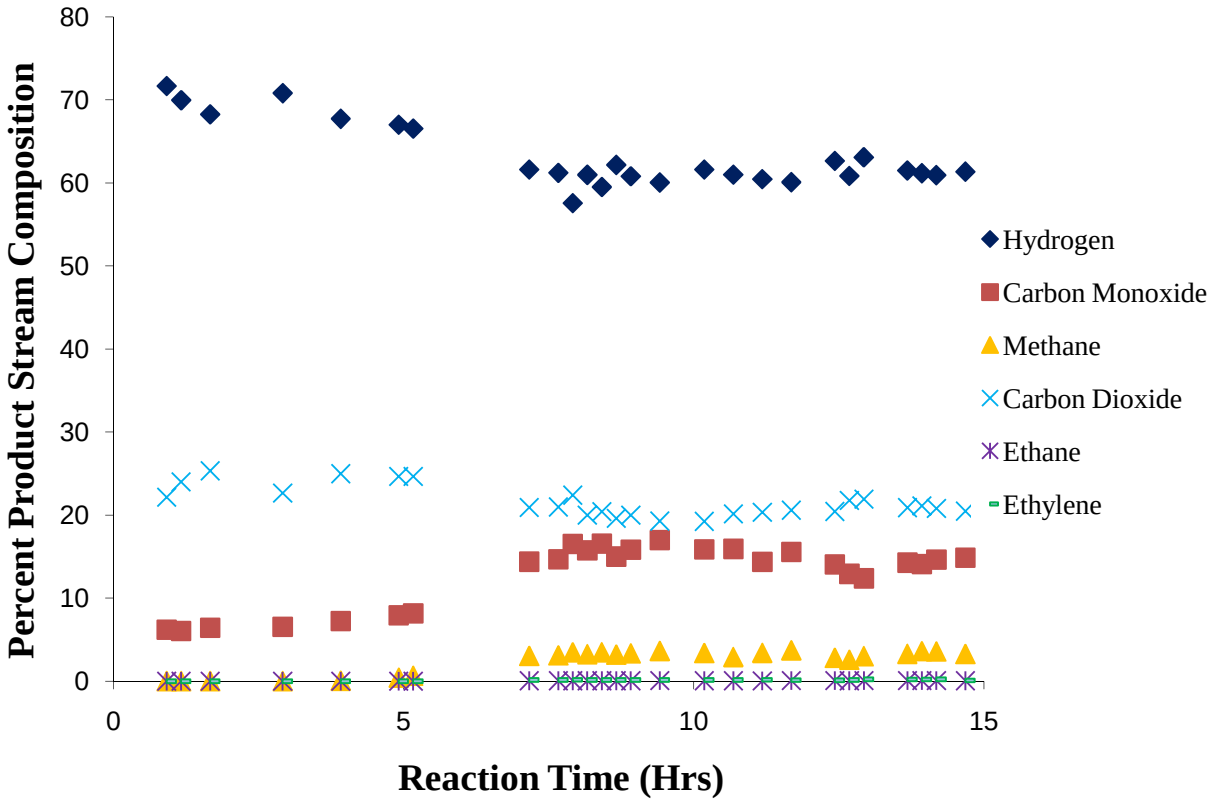

Figure 4.3.3.2a – Product gas composition for acid-washed glycerol reforming over Ni/MgO

Figure 4.3.3.2a shows the product gas composition for the life of the run. The catalyst decreases in activity throughout the 15 hour run. Signs of blockage did not appear until after 15 hours. The acid-wash improved the stability of the reaction. The initial composition of the product gas was between 67-70% H_2, 6-8% CO, 22-25% CO_2, and 0.0-0.1% CH_4. C_2H_6, and C_2H_4 were not detected. These values changed slowly until the eight hour mark where they stabilized . The stabilized composition of the product gas was between 60-62% H_2, 13-16% CO, 19-21% CO_2, and 3-4% CH_4. Very small amounts of C_2H_6 and C_2H_4 were detected (<0.1% and <0.2% respectively).

Figure 4.3.3.2b shows the selectivity of H_2, CO, CO_2, CH_4, C_2H_6, and C_2H_4 versus time. There is a significant change in gas selectivity from the start of the reaction to the six hour mark.

Hydrogen selectivity drops from 93% to 63% and CO_2 drops from 80% to 55%. CO selectivity increases from 20% to 37% and CH_4 selectivity increase from 0% to 7%. For last eight hours of the reaction, the gas selectivity remains the same.

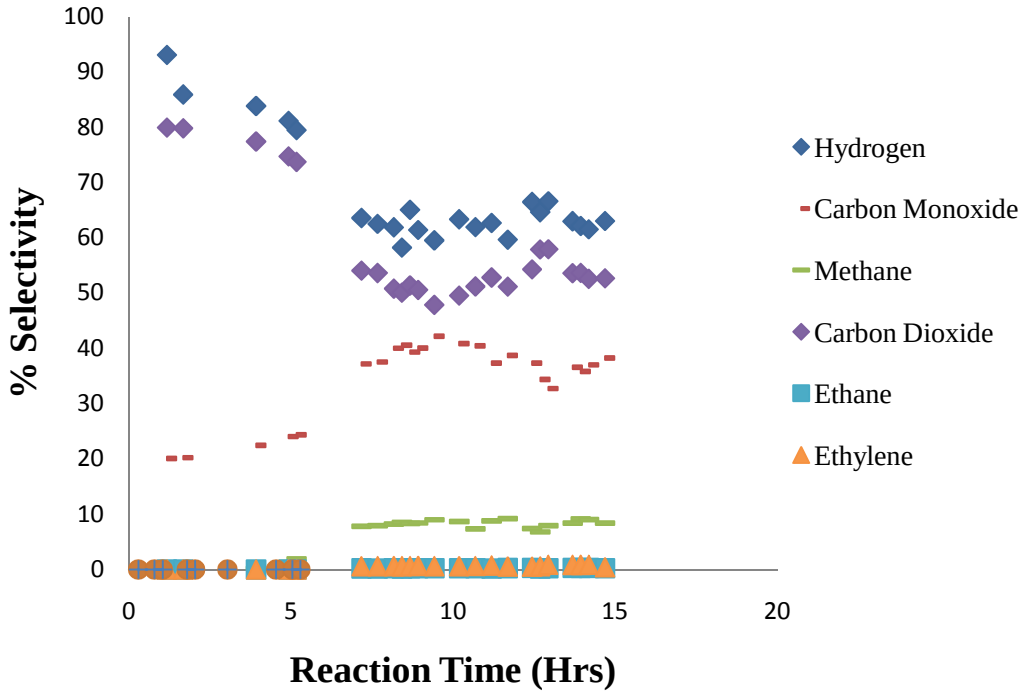

Figure 4.3.3.2b – Product gas selectivity for acid-washed glycerol reforming over Ni/MgO

To determine whether or not the liquid product had any components besides water, index refractometry and a distillation were performed on the liquid product. This liquid product gave the same values as distilled water on an index refractometer. Also, 15 mL of the product were distilled at 105 °C to see if other products were present. Table 4.3.3.2a shows the results of these tests. An accurate reactor tube measurement was not possible because the inner quartz tube broke and became lodged in the tar formation that had formed. Upon removal, significant amounts of deposits were lost. Still, the distillation and index refractometer results confirm that conversion of glycerol approached 100%.

Table 4.3.3.2a - Conversion Estimates

Index Refractometer		Distillation	
Distilled H_2O	1.3327	Initial Volume	15.0 mL
Ni/MgO - Acid-Wash	1.3327	Volume after 105 °C Distillation	0.0 mL

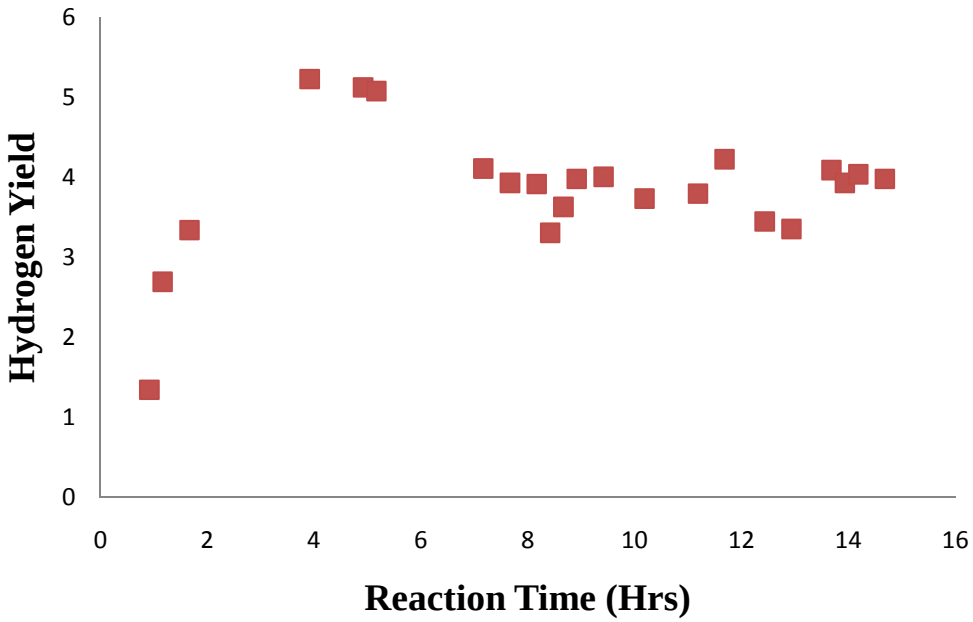

Figure 4.3.3.2c – Hydrogen yield for acid-washed glycerol reforming over Ni/MgO

Figure 4.3.3.2c shows the hydrogen yield versus time for this reaction. The data varies initially but is consistent after six hours. Once the data stabilizes, the hydrogen yield stays between 3-4.

The syngas ratio of the product gas versus reaction time is presented in Figure 4.3.3.2d. The syngas ratio starts at approximately 11 but gradually drops for a few hours. Once the syngas ratio falls to four, around the seven hour mark, it holds steady for the rest of the reaction.

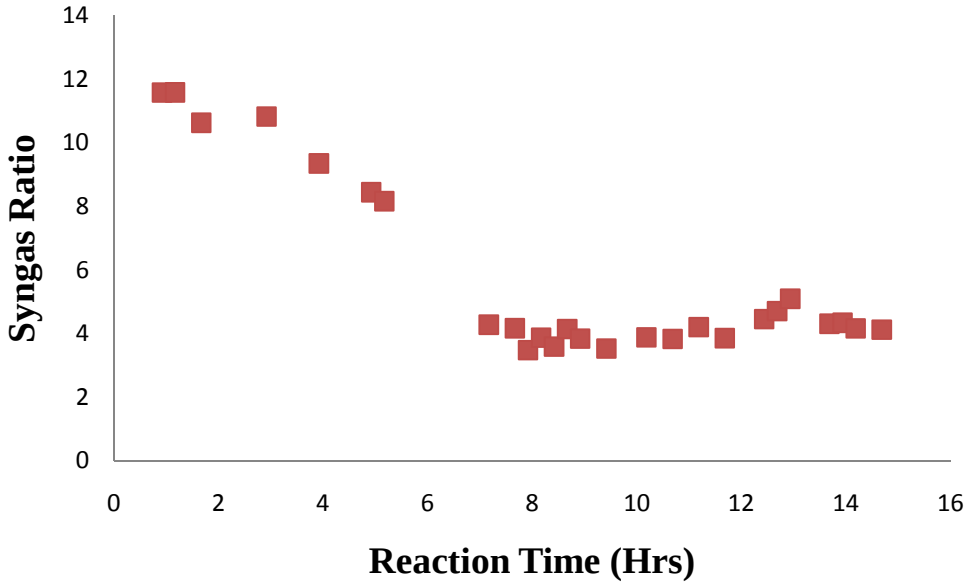

Figure 4.3.3.2d – Product gas syngas ratio for acid-washed glycerol reforming over Ni/MgO

Figure 4.3.3.2e shows the LHV of the product gas versus reaction time. These values ignore the presence of the carrier gas. The LHV of the product gas increases with the increase of methane production.

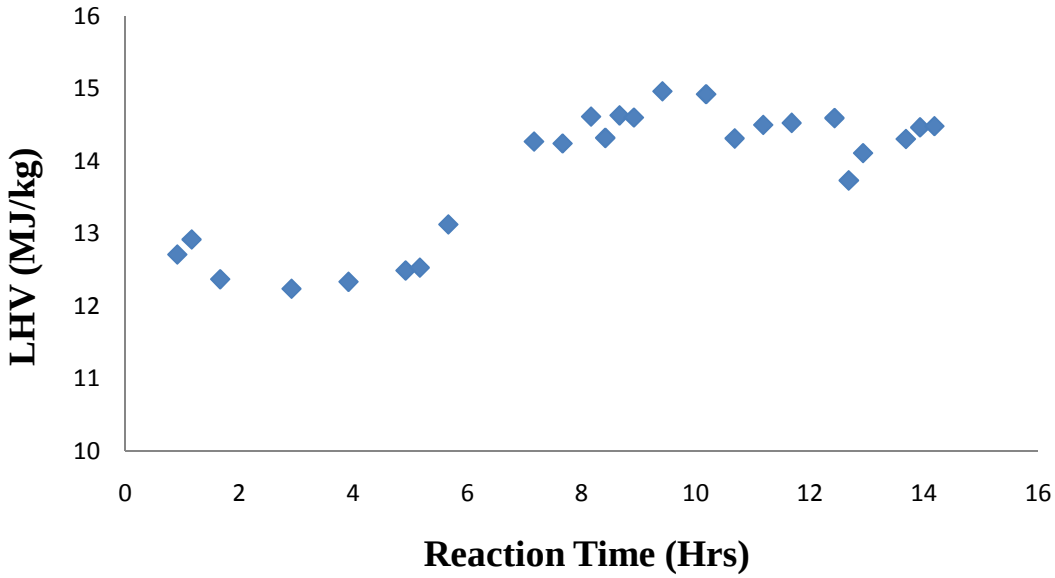

Figure 4.3.3.2e – Product gas LHV for acid-washed glycerol reforming over Ni/MgO

4.4 Comparison

It is important to compare the data between the runs to understand the differences between pure, crude, and acid-washed glycerol reforming. Also, it is important to compare the results to gain a greater understanding in the differences in performance. A final comparison will be made between the experimental results and the estimated thermodynamic equilibrium for each reaction.

First, it must be noted that the amount of glycerol in each of the runs was not constant. Although, each reactant mixture was mixed at approximately 69 volume % H_2O and 31 volume % reactant (which comes to a 9:1 H_2O:glycerol molar ratio and a 3:1 steam to carbon atom ratio for pure glycerol), the actual composition of the reactant mixture was not constant between reactions. A volume basis was used because the instrumentation required to determine soap and unreacted triglycerides was not available. Therefore, consistency between the runs was maintained on a volume basis. Table 4.4a shows the approximate composition of each reactant by volume. The percent glycerol component includes all components besides water and methanol.

Table 4.4a - Reactant composition for each run

Run	% Glycerol	% Methanol	% Water	WRR	S/C
Pure Glycerin	31.1	0.0	68.9	9.0	3.0
Crude Glycerin	27.3	5.6	67.1	7.3	3.0
Ni/γ-Al_2O_3 Acid-Washed Glycerin	20.0	8.0	72.0	8.5	3.9
Ni/MgO Acid-Washed Glycerin	17.0	7.4	75.6	10.1	4.8

It has been shown previously that crude glycerol reforming can perform on par with or better than pure glycerol reforming over a Ni/γ-Al_2O_3 commercial catalyst [39]. This has proven

to be the case in this study as well. Figure 4.4a shows the percent hydrogen for each of the runs over Ni/γ-Al_2O_3 (pure, crude, and acid-washed). This graph shows significant deactivation of the catalyst during pure glycerol reforming. The deactivation can be seen by the drop in hydrogen purity in the product gas after four hours of reaction. It also shows the catalytic stability for the crude and acid-washed glycerol runs. There is no significant catalytic deactivation for these runs. The acid-wash, in particular, has significantly increased the productivity and efficiency of the catalytic reforming.

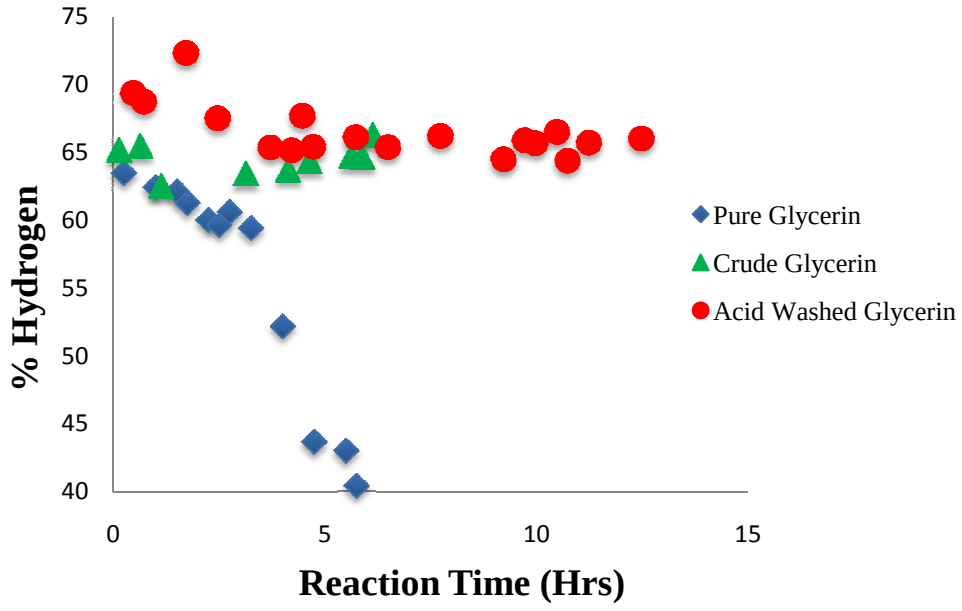

Figure 4.4b shows the syngas ratio over time for pure, crude, and acid-washed glycerol reforming over Ni/γ-Al_2O_3. The syngas ratios for pure and crude glycerol start around four. The pure glycerol syngas ratio drops over time in conjunction with the deactivation of the catalyst. The crude glycerol stays around four for the entirety of its run. Acid-washed glycerol has a syngas ratio that is initially twice as high as the ratio for pure and crude glycerol. After two hours, the acid-washed glycerol syngas ratio starts to drop. After four hours, the syngas ratio

stays around six for the rest of the reaction. The syngas ratio for acid-washed glycerol is at least 1.5 times higher than the crude glycerol syngas ratio for the entirety of the run.

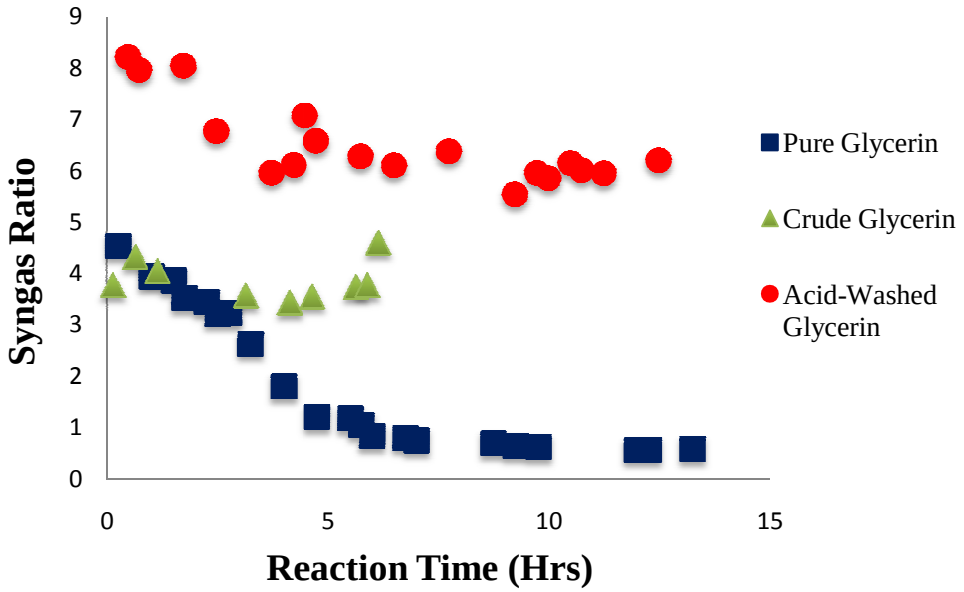

This is due to two factors. The main factor is that the liquid reactant used in acid-washed glycerol reforming has a higher steam to carbon atom ratio. The steam to carbon atom ratio is 3.9 for acid-washed glycerol reforming compared to 3.0 for pure and crude glycerol reforming. Thermodynamics have shown that the higher the water to carbon ratio the more CO_2 and H_2 is produced by the water-gas shift reaction [53, 76]. The second factor plays a lesser role. It is the increased amount of methanol in the reactant. Compared to glycerol, methanol steam reforming will produce one-third the amount of carbon atoms but three-sevenths to one-half the amount of hydrogen compounds. This means that methanol will produce more hydrogen per carbon compound than glycerol. This yields a higher syngas ratio for crude and acid-washed glycerol.

As stated previously in the literature background, nickel promotes dehydration and metal sintering which leads to catalyst deactivation. The acidic nature of γ-Al_2O_3 encourages dehydration which increases coking as well. This is why the pure glycerol run quickly deactivates. The metal active-sites are gradually covered with coke and eventually prevent the reactants from bonding to the metal. Also, the number of nickel active sites decreases due to sintering as the reaction progresses. This creates a situation where the catalyst is deactivated after five hours.

One simple way to increase the catalyst life may be to increase the reduction temperature. For this study, Ni/γ-Al_2O_3 was reduced at 600 °C but TPR analysis showed a significant peak at 820 °C. Therefore, it's possible that Ni/γ-Al_2O_3 was not completely reduced and ready for the reaction. The reduction temperature used in this project was based off of TPR findings in literature [37, 77] and a TPR of a 5% Ni/γ-Al_2O_3 prepared via the incipient wetness impregnation method made before catalytic tests. The commercial catalyst used in this study must have been prepared under conditions that changed the location of the reduction peaks. Literature has shown that catalyst preparation methods of Ni/γ-Al_2O_3 can influence the Ni form in Ni/γAl_2O_3. Song et al. [78] show that 14%-Ni/Al_2O_3 prepared by the wetness impregnation method provides three reduction peaks at 400, 700, and 810 °C but Ni/γ-Al_2O_3 prepared by the sol-gel or a modified sol-gel method provides one reduction peak at 815 °C. They say this is because the sol-gel and modified sol-gel preparation methods favorably enhance the uniformity of Ni in Al_2O_3, where nickel species mainly existed in the form of $NiAl_2O_4$ spinel. It is likely that the commercial nickel catalyst had a similar composition of nickel and that a different reduction temperature (than 600 °C) would be more applicable. Still, increasing the reduction temperature would not solve the problems caused by metal sintering and catalyst coking.

Crude and acid-washed glycerol did not show the same signs of deactivation, which shows that reduction temperature was not the main factor in deactivation. This is most likely due to the large presence of potassium in the crude and acid-washed glycerol. Potassium, as shown in the literature background, helps to promote gasification, which helps prevent catalyst coking. This keeps the active sites open and available for reaction. It is hard to prove this conclusively because it is difficult to tell if there is potassium on the catalyst. For crude glycerol reforming, deposits of potassium can be seen visually in the heating zone of the reactor, but deposits are not visible on the catalyst. Further testing and analysis needs to be performed on the catalyst and liquid product to discover where the potassium is deposited.

Figure 4.4c shows the hydrogen production for pure, crude, and acid-washed steam reforming over Ni/MgO. All three runs show very similar behavior. Each run has a gradual decrease in hydrogen purity of the product gas over time. Hydrogen content decreases from 66 mol % to 60 mol % for pure glycerol over 12 hours. The crude glycerol run only lasted five hours due to reactor blockage caused by tar and coke formation in the heating zone of the reactor. Still, over that time, hydrogen content drops from 66 mol % to 64 mol %. Acid-washed glycerol reforming has the largest drop in hydrogen purity. Over a 15 hour reaction, hydrogen content of the product gas dropped from 71 mol % to 61 mol %. Even though, there is a greater decrease in hydrogen purity for acid-washed glycerol, it produces a higher purity of hydrogen than pure glycerol at similar points in time throughout the reaction. The higher hydrogen content is to be expected because the acid-washed glycerol reactant had a higher steam to carbon ratio (as shown in Table 4.4a). Still, this data shows that acid-washed glycerol steam reforming is as effective as (or better than) pure glycerol reforming for producing high purity hydrogen over a Ni/MgO catalyst.

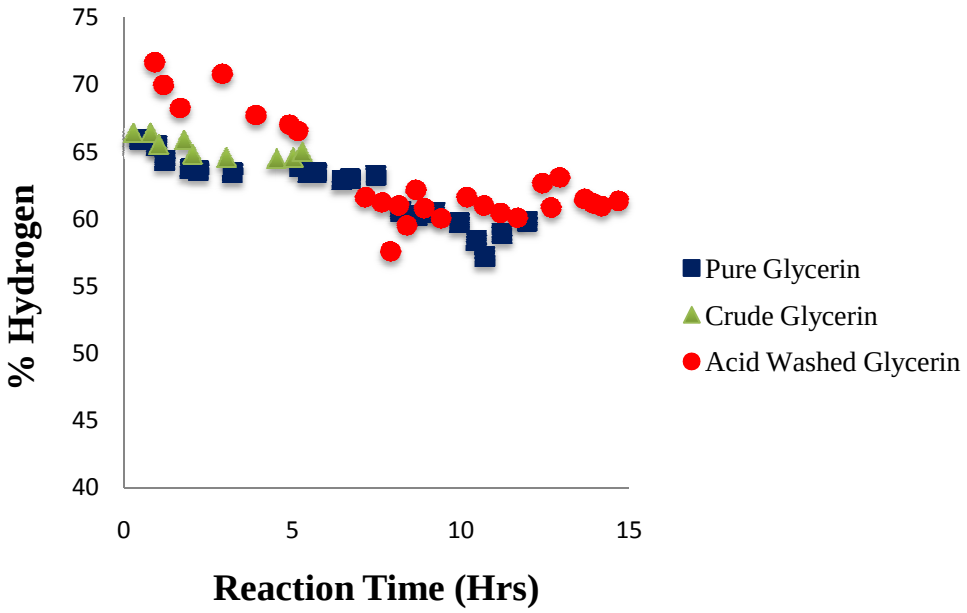

The syngas ratios for pure, crude, and acid-washed glycerol steam reforming followed a similar pattern of decrease, as shown in Fig. 4.4d. This is to be expected because hydrogen production and the synthesis gas ratio are linearly correlated. The pure glycerol syngas ratio drops from seven to three. For crude glycerol reforming, the syngas ratio drops from 4.5 to 4.0 throughout the reaction. Acid-washed glycerol reforming initially produces syngas ratios of almost 12. These ratios decrease quickly over the next six hours until they are around four, where they hold for the last eight hours of the reaction. The reasons the acid-washed glycerol produces higher syngas ratios are the same as they were for the reactions using Ni/γ-Al_2O_3: more water, more methanol and less glycerol in the reactant.

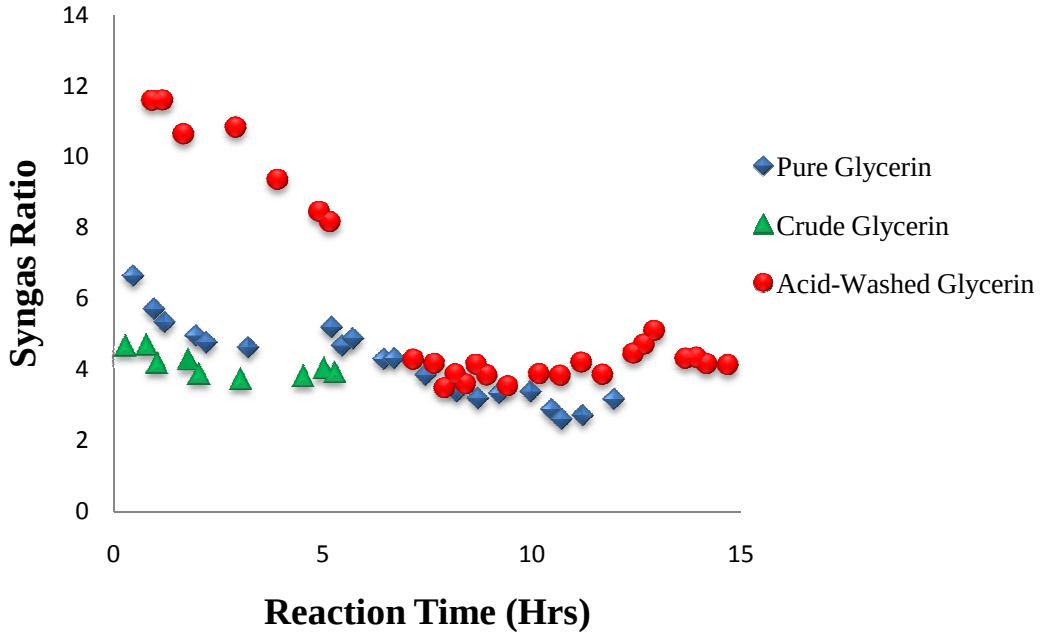

Although it was not the goal of this project, some comparisons can be made between the two catalysts. For pure glycerol reforming, Ni/MgO is clearly more successful at reforming pure glycerol than Ni/γ-Al_2O_3 at these operating conditions. Ni/MgO remained catalytically active throughout the reaction. The quality of the product changed over time but the change was small (less than 10%). Ni/γ-Al_2O_3 quickly lost its activity. After six hours of reaction time, the product gas was similar to a non-catalyzed product gas. The MgO support was better, as stated in the literature review, because of its ability to inhibit coke formation. This kept the active sites open and available throughout the reaction. In contrast for the acid washed experiments, it seems that Ni/γ-Al_2O_3 performed better than Ni/MgO at maintaining a constant composition. Figure 4.4e shows the hydrogen content over time for each catalyst. Figure 4.4f shows the syngas ratio produced over time for each catalyst.

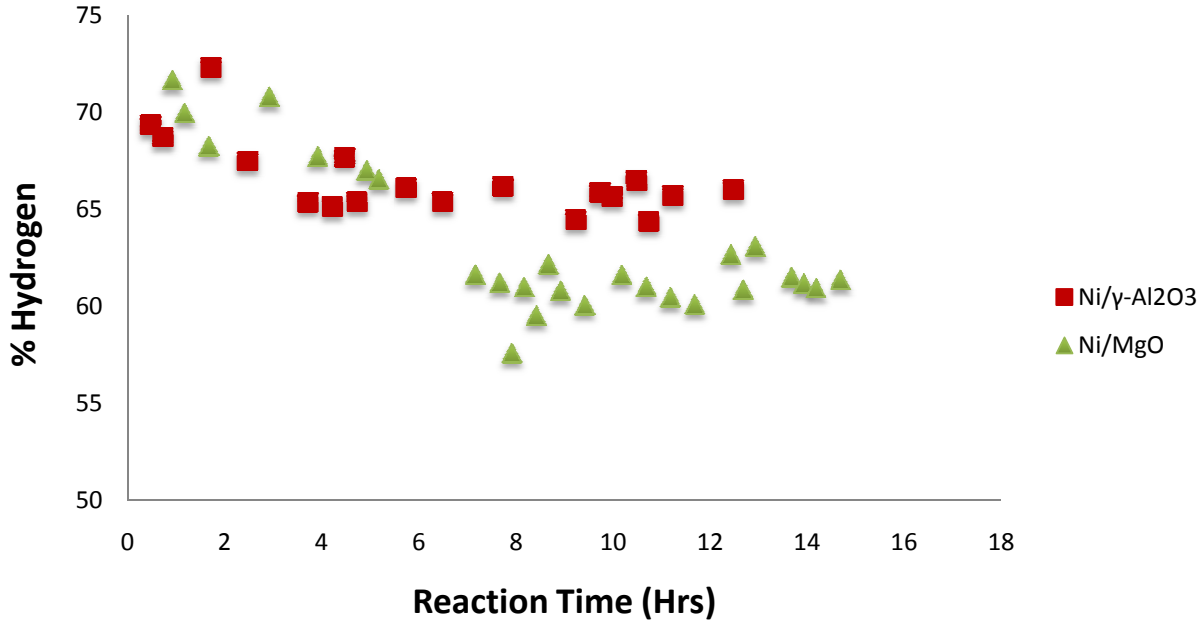

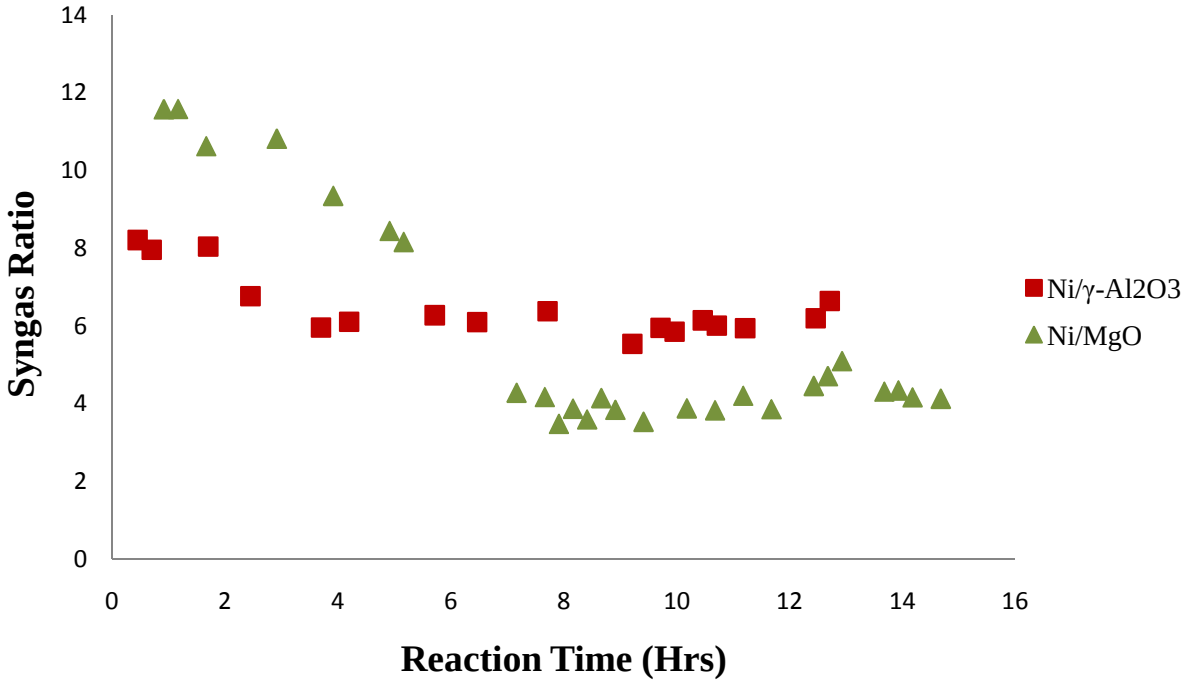

Although Ni/MgO initially produces higher values for hydrogen content and syngas ratios (probably due to the higher steam to carbon ratio of the liquid reactant), Ni/γ-Al_2O_3 holds

its values better throughout the length of the reaction. This happens for a couple of reasons. First, the major reason for Ni/γ-Al_2O_3 deactivation, coking, is inhibited by the presence of K^+ particles in the reactant. Second, Ni/γ-Al_2O_3 has 3.8 times more active sites than Ni/MgO due to catalyst loading and surface area. Since nickel sintering still occurs as the reaction progresses at high temperatures, the larger number of active sites on a larger surface area may slow down the effect of sintering helping Ni/γ-Al_2O_3 to maintain its activity longer.

If you compare the catalysts on a per site basis, the comparison between the catalysts shows that Ni/MgO actually outperforms Ni/γ-Al_2O_3. The rate of hydrogen molecules produced per active site of catalyst for acid-washed glycerol over Ni/γ-Al_2O_3 was 0.83 s^{-1} and for acid-washed glycerol over Ni/MgO it was 2.56 s^{-1}. The turnover frequency (TOF) based on the molecules of reactant fed for Ni/γ-Al_2O_3 was 0.28 s^{-1} and 0.67 s^{-1} for Ni/MgO. This data shows that each active site of Ni/MgO was better at converting glycerol and methanol to hydrogen for these operating conditions and catalyst loadings.

Table 4.4b -TOF and H_2 production for acid-washed glycerol

Catalyst	TOF (s^{-1})	Hydrogen atoms produced per active site (s^{-1})
Ni/MgO	0.67	2.56
Ni/γ-Al_2O_3	0.28	0.83

It is difficult to accurately compare these two catalysts for crude and acid-washed glycerol reforming. Although it appears that Ni/γ-Al_2O_3 is better because it produces a more consistent product, Ni/MgO is producing more hydrogen per active site by a significant margin. The rate of hydrogen of Ni/MgO is over three times higher than Ni/γ-Al_2O_3. It is likely that with similar metal loadings that Ni/MgO would be able to maintain a consistent product as well as

Ni/γ-Al_2O_3. Also, since Ni/MgO significantly outperforms Ni/γ-Al_2O_3 for pure glycerol reforming, it appears that Ni/MgO shows more promise as a glycerol reforming catalyst.

Further testing, at a variety of operating conditions, is needed to fully determine the effectiveness of these catalysts. Regardless, the data provided in this paper shows that both catalysts have an aptitude for successfully producing hydrogen from crude and acid-washed glycerol.

Thermodynamic Comparison

The final comparison that needs to be made is between the thermodynamically predicted equilibrium of each reaction and the experimental results. Also, thermodynamics can help address the impact of methanol on equilibrium. ChemCad was used to determine the effect of methanol on glycerol steam reforming and to estimate the thermodynamic equilibrium of the crude and acid-washed glycerol used in this study.

First, to determine the effect of methanol, equilibrium values were obtained for pure glycerol steam reforming and for four different methanol concentrations (1.0, 2.5, 3.5, and 5.0 mol %) from 450 °C to 1100 °C. From this data, the thermodynamic hydrogen yield and hydrogen product gas composition was determined. Figure 4.4g displays the results for the thermodynamic hydrogen yield versus reaction temperature. Figure 4.4h displays the results for the thermodynamic hydrogen purity versus temperature.

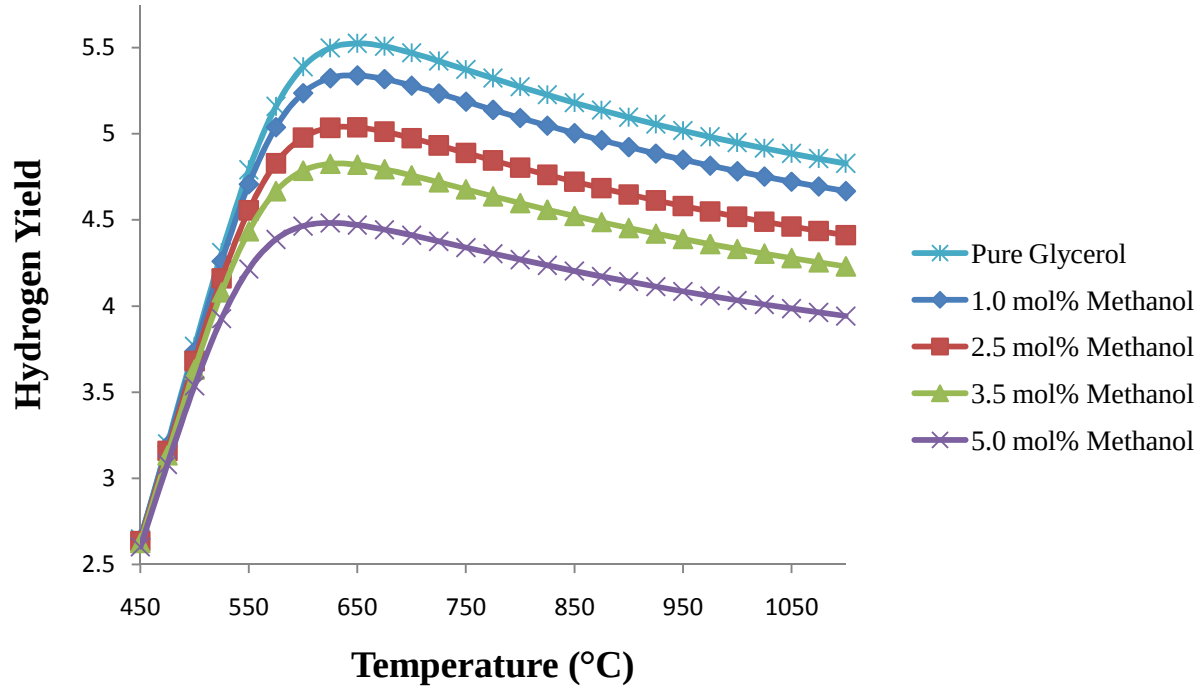

Figure 4.4g – Thermodynamic hydrogen yield for a 9:1 (water:reactant) molar ratio with various amounts of methanol

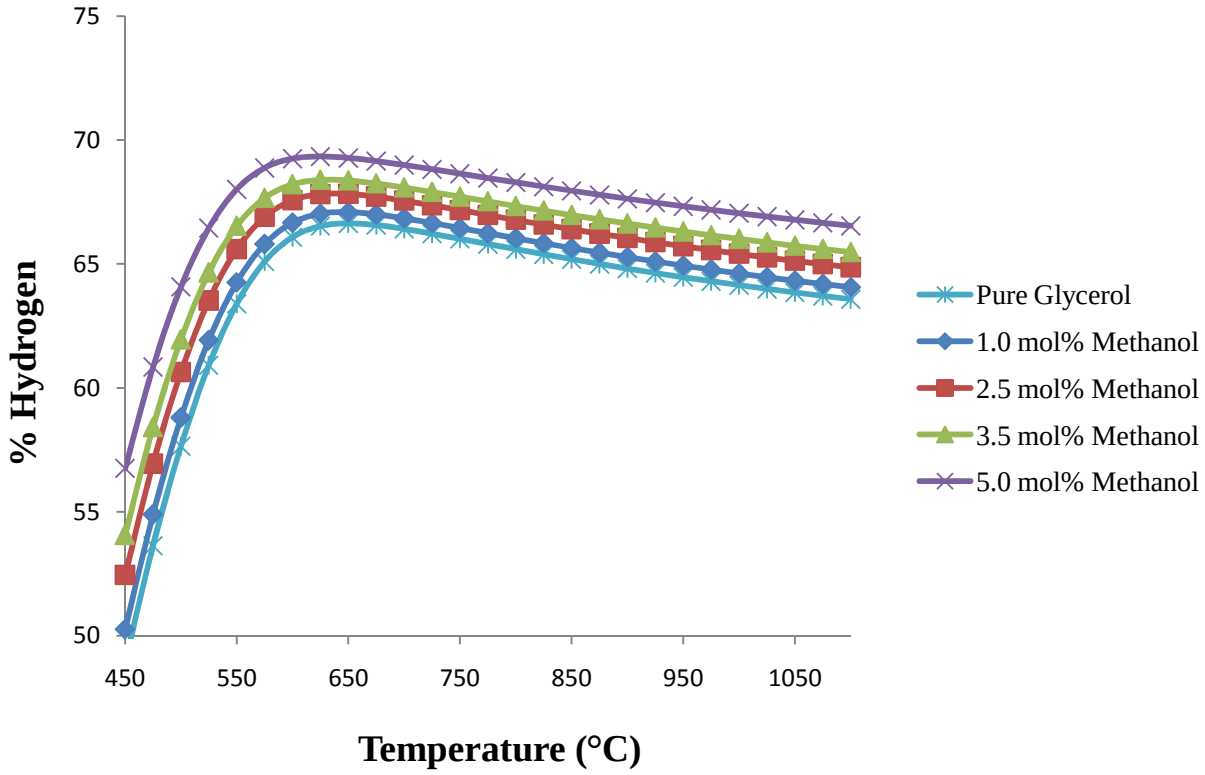

Figure 4.4h – Percent hydrogen of product gas

These figures show that methanol increases hydrogen purity in the product gas but lowers the overall hydrogen yield. As methanol content increases, the thermodynamic hydrogen purity at 725 °C rises from 66.2% for pure glycerol to 68.8% for 5.0 mol% methanol, but the thermodynamic hydrogen yield drops from 5.42 for pure glycerol to 4.37 for 5.0 mol% methanol. The drop in hydrogen yield occurs because each mole of glycerol can theoretically produce up to seven moles of hydrogen during glycerol steam reforming, whereas, each mole of methanol is only able to theoretically produce three moles of hydrogen during methanol steam reforming. Therefore, as methanol replaces glycerol in the reactant there is less available hydrogen to produce. This data shows that if a high purity hydrogen product is desired the addition of methanol in the feed can help.

The reason this occurs can be discovered by looking at what happens to the composition of the reactant when methanol is introduced. For reference sake, Table 3.2a is provided again to show the composition used in each simulation.

Table 3.2a - Molar composition of feeds used in thermodynamic equilibrium analysis

Run	% Glycerol	% Methanol	% Water	WRR	S/C
Pure Glycerin (0 mol % methanol)	10.0	0.0	90.0	9.0	3.0
1.0 mol % methanol	9.0	1.0	90.0	9.0	3.2
2.5 mol % methanol	7.5	2.5	90.0	9.0	3.6
3.5 mol % methanol	6.5	3.5	90.0	9.0	3.9
5.0 mol % methanol	5.0	5.0	90.0	9.0	4.5
Crude Glycerol	8.8	3.3	87.9	7.3	3.0
Ni/MgO acid-washed run	5.0	4.0	91.0	10.1	4.8
Ni/γ-Al_2O_3 acid-washed run	6.1	4.4	89.4	8.5	3.9

This table shows that the S/C ratio increases with the replacement of glycerol with methanol. This occurs even though the WRR stays the same. Therefore, even though the molar

ratio between water and the reactant stays the same, the ratio between the molecules of water and the number of carbon atoms is changing.

The initial reforming of glycerol and methanol produces hydrogen and carbon monoxide. Therefore, hydrogen, carbon monoxide, and steam will be in the system regardless of the water-gas shift reaction. Carbon dioxide, on the other hand, is produced mainly through the water-gas shift reaction. Since methanol will produce less carbon monoxide than glycerol, the amount of excess steam compared to carbon monoxide increases with the introduction of methanol. This means that increasing the methanol content in the reactant will shift the equilibrium of the water-gas shift reaction towards the production of hydrogen and carbon dioxide. This will provide an equilibrium product that has a higher hydrogen purity.

Another way methanol impacts the thermodynamic equilibrium is that it causes the optimum temperature for the theoretical hydrogen yield to shift. As methanol content increases, the optimum temperature for hydrogen yield and hydrogen purity shifts from approximately 650 °C for pure glycerol to approximately 625 °C for 5.0 mol% methanol. Although the actual difference in optimum temperature may be less than 25 °C, this shows that an additional advantage of having methanol in the system is that it helps lower required reaction temperatures and the heat duty required for optimum results.

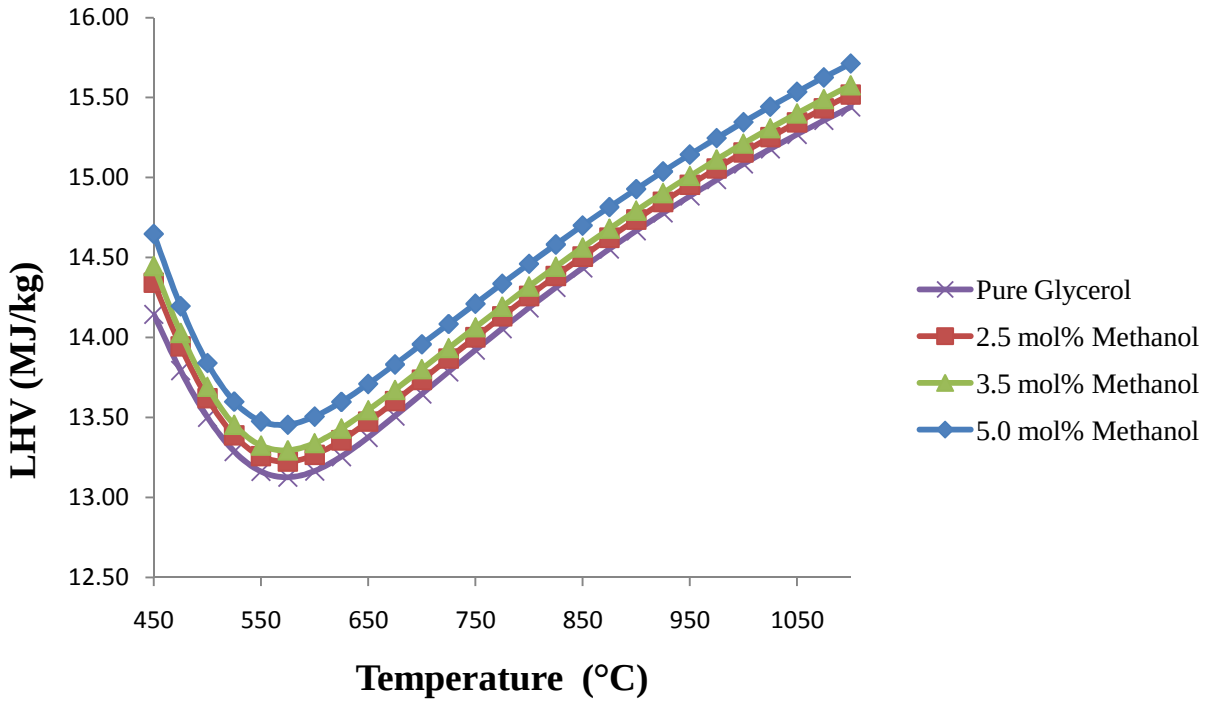

Figure 4.4i – LHV of product gas for different methanol concentrations

In addition to the impact of methanol on hydrogen yield and purity, its impact on the lower heating value (LHV) of the product gas was analyzed. The results of the thermodynamic analysis on the LHV are shown in Figure 4.4i. These results show that there is a direct correlation between methanol content in the reactant and the LHV of the product gas. As the methanol content in the reactant increases, the LHV increases. Still, the difference between pure glycerol and 5.0 mol % methanol reforming in LHV is small. At 625 °C, the LHV for 5.0 mol% is less than a 0.35 MJ/kg increase compared to pure glycerol. This is an approximate 2.5% increase in energy content. This increase decreases slightly as the reaction temperature continues to rise (e.g. at 1000 °C the LHV difference is 0.26 MJ/kg, which is a 1.7% increase). This data shows that methanol has a slight positive impact on LHV but the impact is smaller than the influence of reaction temperature. For example, pure glycerol reforming from 625 °C to 1000 °C has a LHV increase of over 1.8 MJ/kg (approximately 13.7%).

The other goal of the thermodynamic analysis was to determine the thermodynamic equilibrium data for each of the crude and acid-washed glycerol runs used in this project and compare these results to the experimental data. First, figures 4.4j, k, and l show the thermodynamic equilibrium for the crude and acid-washed glycerol runs from 450 °C to 1000 °C. The reactant composition for each of these graphs is based directly off of the compositions used in the actual experimental reactions. From this data, the actual thermodynamic equilibrium was estimated for 725 °C and compared to the experimental data collected at the same temperature. The results of this comparison are listed in Table 4.4c. The experimental results used in this table are the range of the results over the first five hours of each reaction.

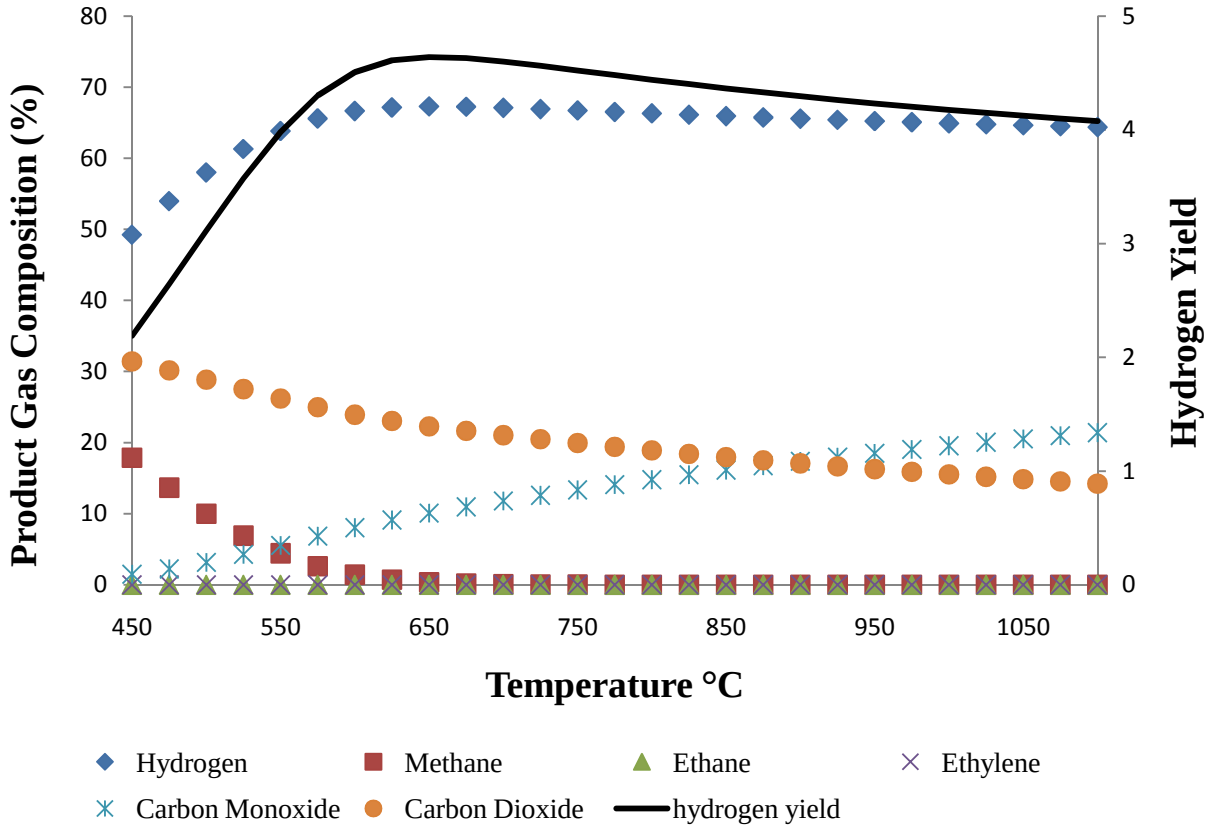

Figure 4.4j – Crude glycerol thermodynamic equilibrium data

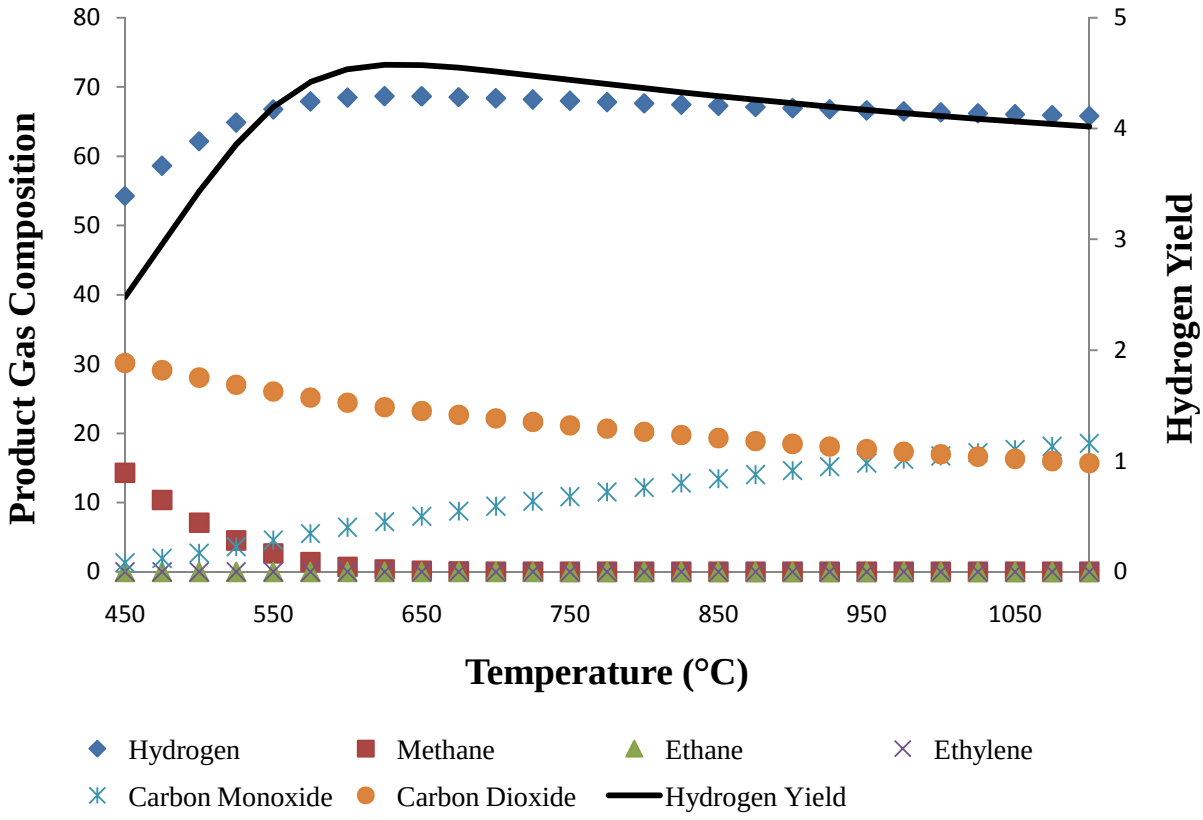

Figure 4.4k – Ni/γ-Al_2O_3 acid-washed glycerol thermodynamic equilibrium data

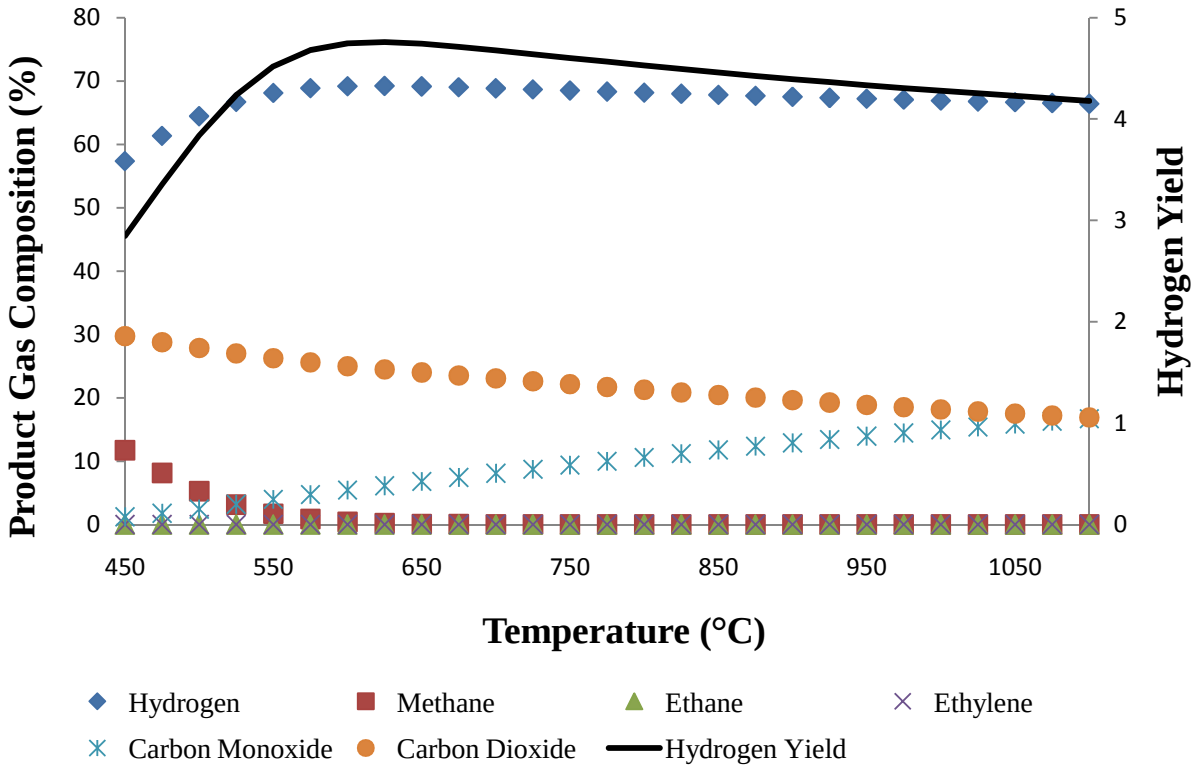

Figure 4.4l – Ni/MgO acid-washed glycerol thermodynamic equilibrium data

Table 4.4c - Comparison between thermodynamic analysis and experimental results

	Crude Glycerol			$Ni/\gamma\text{-}Al_2O_3$ Acid-washed Glycerol		Ni/MgO Acid-washed Glycerol	
	Therm.	$Ni/\gamma\text{-}Al_2O_3$ exp.	Ni/MgO exp.	Therm.	Exp.	Therm.	Exp.
% H_2	66.90	64-66	64-66	68.16	65-69	68.68	67-70
% CH_4	0.05	.2-1	0-1	0.02	0-0.2	0.01	0-0.1
% C_2H_6	0.00	0.00	0.00	0.00	0.00	0.00	0.00
% C_2H_4	0.00	0.00	0.00	0.00	0.00	0.00	0.00
% CO	12.59	16-19	14-16	10.18	8-11	8.72	6-8
% CO_2	20.47	17-19	17-19	21.64	22-25	22.59	22-25
H_2 Yield	4.56	4-4.75	3.9-4.1	4.48	3-4.5	4.64	3-5
Syngas Ratio	5.32	3.7-4	4-4.5	6.70	>6	7.87	8-12
LHV (MJ/kg)	14.24	15-16	15-16	14.10	13-14	13.86	12-13

Table 4.4c shows that for crude glycerol the experimental results were similar to the thermodynamic results in terms of hydrogen production. The main difference between the experimental data and the thermodynamic prediction is the amount of CO and CO_2 produced. More CO and less CO_2 were produced than the thermodynamic model predicted. Therefore, it

can be concluded that the water-gas shift reaction did not progress as far during the reaction as the thermodynamic predictions suggested.

Thermodynamic and experimental results were consistent for acid-washed glycerol reforming over both catalysts. For the reaction temperature and WRR used in the acid-washed glycerol reactions, Ni/γ-Al_2O_3 and Ni/MgO were able to match the thermodynamic predictions over a five hour period. This is promising news. It shows that acid-washed glycerol reforming can match thermodynamic predictions. Also, it shows that Ni/MgO and Ni/γ-Al_2O_3 approach thermodynamic equilibrium and can produce optimum results under these conditions.

Chapter 5
Conclusions and Recommendations

5.1 Conclusions

There were two main goals for this study. The first goal was to discover the effect of impurities commonly found in crude glycerol on catalytic life and activity during glycerol steam reforming. The second goal was predicative on the first. If the impurities, or some of the impurities, negatively affected the reaction or catalysts, a simple acid-wash was to be performed in an attempt to remove the impurities and improve performance. These goals were accomplished by analyzing the performance of Ni/γ-Al_2O_3 and Ni/MgO catalysts for pure, crude, and acid-washed glycerol steam reforming. For Ni/γ-Al_2O_3, it was found that crude and acid-washed glycerol reforming outperformed pure glycerol reforming in terms of catalytic life and activity. Pure glycerol reforming showed significant deactivation after four hours of reaction time. On the other hand, acid-washed glycerol reforming held and maintained its activity for 15 hours and gave a syngas ratio of over six. This was due to the presence of K^+ in the crude and acid-washed glycerol, which promotes gasification and helps limit catalytic coking.

Another factor that played a role in the increased activity of the acid-washed glycerol reaction is the increase in the steam/carbon ratio. The steam/carbon ratio used in this reaction was 3.9 compared to 3.0 (for pure glycerol reforming). The higher steam/carbon ratio helped push the water gas shift reaction to produce more hydrogen and carbon dioxide. This was the main reason for the increase in the syngas ratio of the product gas.

For Ni/MgO, it was found that pure and crude glycerol reforming can produce gases with similar compositions. Unfortunately, crude glycerol could not match the overall performance of the pure glycerol. This was because the impurities in the crude glycerol caused tar and coke

formation in the heating zone of the reactor. After five hours, the gas flow through the reactor was impeded and the reaction stalled. After using acetic acid to remove the unreacted biodiesel components in crude glycerol, the performance of the reaction increased dramatically. Acid-washed glycerol reforming produced a product gas with more H_2 and little deactivation over a 14 hour period. Signs of blockage in the reactor did not appear until after 14 hours. By this time for the pure glycerol reforming, the reaction had been stopped due to a drop in activity.

The acid-washed glycerol reaction for Ni/MgO also had a higher steam/carbon ratio. The steam/carbon ratio used in the acid-washed glycerol reaction was 4.8 instead of 3.0 (for pure glycerol reforming). This steam/carbon ratio enabled the product gas to attain syngas ratios between eight and twelve.

A thermodynamic analysis was performed to help determine the effect of methanol and to compare the experimental results with the thermodynamically predicted equilibrium. The thermodynamic analysis showed that the replacement of glycerol with methanol increases the hydrogen purity of the product gas but decreases the overall hydrogen yield. Also, the presence of methanol has an effect on the optimum reaction temperature. A rise of methanol content from 0 mol% to 5 mol% can decrease the optimum reaction temperature by approximately 25 °C. Finally, methanol has a small impact on the LHV of the product gas but its impact is minimal compared to the effect of temperature.

Another goal of the thermodynamic analysis was to compare the experimental results with the thermodynamic predictions. This comparison showed that the experimental results for crude and acid-washed glycerol reforming were similar to the thermodynamically predicted equilibrium. This shows that Ni/MgO and Ni/γ-Al_2O_3 successfully reform crude glycerol and acid-washed glycerol under these operating conditions.

5.2 Recommendations

The impurities found in crude glycerol prevent it from being a viable choice as a feedstock for steam reforming. After a few hours of reaction, the free fatty acids, potassium, and other impurities in crude glycerol polymerize and start to create significant blockage problems in the heating zone of the reactor. Even though Ni/γ-Al_2O_3 and Ni/MgO do not deactivate significantly with crude glycerol, this benefit is drastically outweighed by the downsides. It is possible that the addition of an atomizer to the heating zone of the reactor may help prevent tar and coke formation. The heating method used in this project may have encouraged polymerization of crude glycerol because it prevented uninhibited evaporation of the reactant. An atomizer would help the crude (or acid-washed) glycerol to evaporate more smoothly. Still, if steam reforming is to be used to address the abundance of crude glycerol on the market, it would help to remove most of these impurities.

Performing an acid-wash on crude glycerol to remove the unreacted triglycerides, takes care of this issue. Acid-washed glycerol steam reforming is a significant improvement over crude glycerol reforming. Signs of reactor blockage do not appear until after 13-15 hours of reaction. Also, acid-washed glycerol reforming maintains its activity and performs similarly to or better than pure glycerol reforming. Improvements to the acid-wash, by improving the removal of impurities, and new methods of delivering the liquid reactant to the reactor heating zone (e.g. atomizer) will further increase the effectiveness and efficiency of acid-washed glycerol reforming. Also, further ICP analysis needs to be performed to fully determine the effectiveness of the acid-wash. It was believed that the acid-wash would remove the majority of the potassium present in the reactant but initial ICP results were contradictory.

Methods need to be developed to determine where the potassium fed to the reactor end up. ICP analysis on the liquid product could determine how much makes it through the entire reactor. More likely, the potassium stays in the heating zone or the reaction zone of the reactor.

Also, a new, novel catalyst could drastically improve bio-diesel derived glycerol reforming. Even though the nickel catalysts used in this study were able to meet the thermodynamic predictions, they struggled with nickel sintering and a gradual loss of activity over time. Rh catalysts would avoid this problem and have shown good activity in pure glycerol reforming [42, 57].

If used in future work, the proper reduction temperature for Ni/γ-Al_2O_3 needs to be used. The 600 °C reduction temperature used in this paper was not appropriate for this catalyst based off of the TPR results. A new reduction temperature should be chosen based off the TPR results provided in the experimental section. The results indicate a reduction temperature of 820 °C would be suitable. Since Ni/γ-Al_2O_3 did not show signs of deactivation for acid-washed glycerol reforming and was able to match thermodynamic predictions, it is debatable how much a new reduction temperature would help.

In this project, the methanol and water content of the crude and acid-washed glycerol reactant was not calculated until after reactions were run and data collected. This caused the composition used in each reaction to vary. Since the goal of this work was to demonstrate the viability of crude (or acid-washed) glycerol reforming and not necessarily compare catalysts or operating conditions, this was not drastically important. Future work should ensure that operating conditions between reactions are as similar as possible. Since the viability of the process has been demonstrated, future work should focus on the role different components (methanol, potassium, etc.), operating conditions (WRR, temperature, flowrate), or catalysts

play. Depending on the goal of the study, the operating conditions should be the same for all reactions. For example, if future work wanted to compare the effectiveness of Ni/MgO, Ni/γ-Al_2O_3, and Rh/CeO_2/γ-Al_2O_3 at acid-washed glycerol reforming, the reactant composition, reaction temperature, GHSV, and other operating conditions should be constant.

References

1. Adhikari, S., S.D. Fernando, and A. Haryanto, *Hydrogen production from glycerol: An update*. Energy Conversion and Management, 2009. **50**(10): p. 2600-2604.
2. Stelmachowski, M., *Utilization of Glycerol, a By-Product of the Transestrification Process of Vegetable Oils: A Review*. Ecological Chemistry and Engineering, 2011. **18**(1): p. 9-30.
3. Spath, P.L.a.D., D.C., *Preliminary Screening - Technical and Economic Assessment of Synthesis Gas to Fuels and Chemicals with Emphasis on the Potential for Biomass-Derived Syngas*, N.R.E. Laboratory, Editor 2003: http://www.ntis.gov/ordering.htm.
4. Gui, M.M., K.T. Lee, and S. Bhatia, *Feasibility of edible oil vs. non-edible oil vs. waste edible oil as biodiesel feedstock.* Energy, 2008. **33**(11): p. 1646-1653.
5. Ahmad, S., D. Papadias, *Hydrogen from Glycerol: A feasibility Study*, U.S.D.o. Energy, Editor 2010: http://www.hydrogen.energy.gov/pdfs/review10/pd003_ahmed_2010_o_web.pdf.
6. Vlysidis, A., et al., *A techno-economic analysis of biodiesel biorefineries: Assessment of integrated designs for the co-production of fuels and chemicals.* Energy, 2011. **36**(8): p. 4671-4683.
7. Xu, Y., et al., *Integrated production for biodiesel and 1,3-propanediol with lipase-catalyzed transesterification and fermentation.* Biotechnol Lett, 2009. **31**(9): p. 1335-41.
8. Hiremath, A., M. Kannabiran, and V. Rangaswamy, *1,3-Propanediol production from crude glycerol from Jatropha biodiesel process.* N Biotechnol, 2011. **28**(1): p. 19-23.
9. Lin, L., et al., *Opportunities and challenges for biodiesel fuel.* Applied Energy, 2011. **88**(4): p. 1020-1031.
10. Yusuf, N.N.A.N., S.K. Kamarudin, and Z. Yaakub, *Overview on the current trends in biodiesel production.* Energy Conversion and Management, 2011. **52**(7): p. 2741-2751.
11. *Regulation of Fuels and Fuel Additives: Changes to Renewable Fuel Standard Program; Final Rule*, E.P. Agency, Editor March 26, 2010, Federal Register. p. 14669-15320.
12. Thompson, J.C. and B.B. He, *Characterization of crude glycerol from biodiesel production from multiple feedstocks.* Applied Engineering in Agriculture, 2006. **22**(2): p. 261-265.
13. Janaun, J. and N. Ellis, *Perspectives on biodiesel as a sustainable fuel.* Renewable & Sustainable Energy Reviews, 2010. **14**(4): p. 1312-1320.
14. Scott, S.A., et al., *Biodiesel from algae: challenges and prospects.* Current Opinion in Biotechnology, 2010. **21**(3): p. 277-286.
15. Chisti, Y., *Biodiesel from microalgae.* Biotechnology Advances, 2007. **25**(3): p. 294-306.
16. Subhadra, B.G. and M. Edwards, *Coproduct market analysis and water footprint of simulated commercial algal biorefineries.* Applied Energy, 2011. **88**(10): p. 3515-3523.
17. Sturm, B.S.M. and S.L. Lamer, *An energy evaluation of coupling nutrient removal from wastewater with algal biomass production.* Applied Energy, 2011. **88**(10): p. 3499-3506.
18. Smith, V.H., et al., *The ecology of algal biodiesel production.* Trends in Ecology & Evolution, 2010. **25**(5): p. 301-309.
19. Shilton, A.N., et al., *Solar-powered aeration and disinfection, anaerobic co-digestion, biological CO(2) scrubbing and biofuel production: the energy and carbon management opportunities of waste stabilisation ponds.* Water Science and Technology, 2008. **58**(1): p. 253-258.

20. Dismukes, G.C., et al., *Aquatic phototrophs: efficient alternatives to land-based crops for biofuels.* Current Opinion in Biotechnology, 2008. **19**(3): p. 235-240.
21. Hara, M., *Environmentally Benign Production of Biodiesel Using Heterogeneous Catalysts.* Chemsuschem, 2009. **2**(2): p. 129-135.
22. Lotero, E., et al., *Synthesis of biodiesel via acid catalysis.* Industrial & Engineering Chemistry Research, 2005. **44**(14): p. 5353-5363.
23. Gallagher, B.J., *The economics of producing biodiesel from algae.* Renewable Energy, 2011. **36**(1): p. 158-162.
24. Dave, C.D. and K.K. Pant, *Renewable hydrogen generation by steam reforming of glycerol over zirconia promoted ceria supported catalyst.* Renewable Energy, 2011. **36**(11): p. 3195-3202.
25. Werpy, T., Petersen, G., Aden, A., Bozell, J, Holladay, J, White, J., Manheim, Amy, Elliot, D., Lasure, L. Jones, S., Gerber, M., Ibsen, K., Lumberg, L., and Kelley, S., *Top Value Added Chemicals from Biomass: Volume 1 - Results of Screening for Potential Candidates from Sugars and Synthesis Gas*, U.S.D.o.E.E.E.a.R. Energy, Editor 2004.
26. Agency, I.E., *Montly Oil Survey*, OECD/IEA, Editor 2011.
27. Chiu, C.-W., et al., *Removal of Residual Catalyst from Simulated Biodiesel's Crude Glycerol for Glycerol Hydrogenolysis to Propylene Glycol.* Industrial & Engineering Chemistry Research, 2005. **45**(2): p. 791-795.
28. Meyer, P., Pankaew, S.,Boonsawang, P.,Tongurai C., *Anaerobic Fermentation of Crude Glycerol to Produce Value-added Products.* Applied Engineering in Agriculture, 2011. **27**(4): p. 655-662.
29. Johnson, D.T. and K.A. Taconi, *The glycerin glut: Options for the value-added conversion of crude glycerol resulting from biodiesel production.* Environmental Progress, 2007. **26**(4): p. 338-348.
30. Clomburg, J.M. and R. Gonzalez, *Metabolic engineering of Escherichia coli for the production of 1,2-propanediol from glycerol.* Biotechnology and Bioengineering, 2011. **108**(4): p. 867-879.
31. Oh, B.-R., et al., *Efficient production of ethanol from crude glycerol by a Klebsiella pneumoniae mutant strain.* Bioresource Technology, 2011. **102**(4): p. 3918-3922.
32. Garcia, R., M. Besson, and P. Gallezot, *CHEMOSELECTIVE CATALYTIC-OXIDATION OF GLYCEROL WITH AIR ON PLATINUM METALS.* Applied Catalysis a-General, 1995. **127**(1-2): p. 165-176.
33. Bühler, W., et al., *Ionic reactions and pyrolysis of glycerol as competing reaction pathways in near- and supercritical water.* The Journal of Supercritical Fluids, 2002. **22**(1): p. 37-53.
34. Onwudili, J.A. and P.T. Williams, *Hydrothermal reforming of bio-diesel plant waste: Products distribution and characterization.* Fuel, 2010. **89**(2): p. 501-509.
35. Kraus, G., *Synthetic Methods of Preparing 1,3-propanediol.* Clean: soil, air, water, 2008. **36**(8): p. 648-651.
36. van Bennekom, J.G., et al., *Reforming of methanol and glycerol in supercritical water.* The Journal of Supercritical Fluids, 2011. **58**(1): p. 99-113.
37. Iriondo, A., et al., *Influence of La(2)O(3) modified support and Ni and Pt active phases on glycerol steam reforming to produce hydrogen.* Catalysis Communications, 2009. **10**(8): p. 1275-1278.

38. Pompeo, F., G. Santori, and N.N. Nichio, *Hydrogen and/or syngas from steam reforming of glycerol. Study of platinum catalysts.* International Journal of Hydrogen Energy, 2010. **35**(17): p. 8912-8920.
39. Valliyappan, T., et al., *Production of Hydrogen and Syngas via Steam Gasification of Glycerol in a Fixed-Bed Reactor.* Topics in Catalysis, 2008. **49**(1): p. 59-67.
40. Huber, G.W., S. Iborra, and A. Corma, *Synthesis of transportation fuels from biomass: Chemistry, catalysts, and engineering.* Chemical Reviews, 2006. **106**(9): p. 4044-4098.
41. Ortiz, F.J.G., et al., *Thermodynamic study of the supercritical water reforming of glycerol.* International Journal of Hydrogen Energy, 2011. **36**(15): p. 8994-9013.
42. Adhikari, S., S. Fernando, and A. Haryanto, *Production of hydrogen by steam reforming of glycerin over alumina-supported metal catalysts.* Catalysis Today, 2007. **129**(3-4): p. 355-364.
43. Pairojpiriyakul, T., et al., *Effect of mode of operation on hydrogen production from glycerol at thermal neutral conditions: Thermodynamic analysis.* International Journal of Hydrogen Energy, 2010. **35**(19): p. 10257-10270.
44. Luo, N.J., et al., *Glycerol aqueous phase reforming for hydrogen generation over Pt catalyst - Effect of catalyst composition and reaction conditions.* Fuel, 2008. **87**(17-18): p. 3483-3489.
45. Wenju, W., *Thermodynamic analysis of glycerol partial oxidation for hydrogen production.* Fuel Processing Technology, 2010. **91**(11): p. 1401-1408.
46. Swami, S.M. and M.A. Abraham, *Integrated Catalytic Process for Conversion of Biomass to Hydrogen.* Energy & Fuels, 2006. **20**(6): p. 2616-2622.
47. Dauenhauer, P.J., J.R. Salge, and L.D. Schmidt, *Renewable hydrogen by autothermal steam reforming of volatile carbohydrates.* Journal of Catalysis, 2006. **244**(2): p. 238-247.
48. Byrd, A.J., K.K. Pant, and R.B. Gupta, *Hydrogen production from glycerol by reforming in supercritical water over Ru/Al2O3 catalyst.* Fuel, 2008. **87**(13-14): p. 2956-2960.
49. Cui, Y., et al., *Steam reforming of glycerol: The experimental activity of La(1-x)Ce(x)NiO(3) catalyst in comparison to the thermodynamic reaction equilibrium.* Applied Catalysis B-Environmental, 2009. **90**(1-2): p. 29-37.
50. Slinn, M., et al., *Steam reforming of biodiesel by-product to make renewable hydrogen.* Bioresource Technology, 2008. **99**(13): p. 5851-5858.
51. Czernik, S., et al., *Hydrogen by catalytic steam reforming of liquid byproducts from biomass thermoconversion processes.* Industrial & Engineering Chemistry Research, 2002. **41**(17): p. 4209-4215.
52. Dou, B., et al., *Thermogravimetric kinetics of crude glycerol.* Bioresource Technology, 2009. **100**(9): p. 2613-2620.
53. Adhikari, S., S. Fernando, and A. Haryanto, *A comparative thermodynamic and experimental analysis on hydrogen production by steam reforming of glycerin.* Energy & Fuels, 2007. **21**(4): p. 2306-2310.
54. Chen, H.S., et al., *A comparative study on hydrogen production from steam-glycerol reforming: thermodynamics and experimental.* Renewable Energy, 2011. **36**(2): p. 779-788.
55. Li, Y.H., et al., *Thermodynamic analysis of hydrogen production via glycerol steam reforming with CO(2) adsorption.* International Journal of Hydrogen Energy, 2010. **35**(15): p. 7768-7777.

56. Wang, X.D., et al., *Hydrogen production by glycerol steam reforming with/without calcium oxide sorbent A comparative study of thermodynamic and experimental work.* Fuel Processing Technology, 2010. **91**(12): p. 1812-1818.
57. Chiodo, V., et al., *Catalytic features of Rh and Ni supported catalysts in the steam reforming of glycerol to produce hydrogen.* Applied Catalysis a-General, 2010. **381**(1-2): p. 1-7.
58. Vaidya, P.D. and A.E. Rodrigues, *Glycerol Reforming for Hydrogen Production: A Review.* Chemical Engineering & Technology, 2009. **32**(10): p. 1463-1469.
59. Hirai, T., et al., *Production of Hydrogen by Steam Reforming of Glycerin on Ruthenium Catalyst.* Energy & Fuels, 2005. **19**(4): p. 1761-1762.
60. Ni, M., D.Y.C. Leung, and M.K.H. Leung, *A review on reforming bio-ethanol for hydrogen production.* International Journal of Hydrogen Energy, 2007. **32**(15): p. 3238-3247.
61. Alberton, A.L., M. Souza, and M. Schmal, *Carbon formation and its influence on ethanol steam reforming over Ni/Al2O3 catalysts.* Catalysis Today, 2007. **123**(1-4): p. 257-264.
62. Dou, B., et al., *Steam reforming of crude glycerol with in situ CO2 sorption.* Bioresource Technology, 2010. **101**(7): p. 2436-2442.
63. Buffoni, I.N., et al., *Nickel catalysts applied in steam reforming of glycerol for hydrogen production.* Catalysis Communications, 2009. **10**(13): p. 1656-1660.
64. Lee, Y.J., S.-I. Hong, and D.J. Moon, *Studies on the steam and CO2 reforming of methane for GTL-FPSO applications.* Catalysis Today, 2011. **174**(1): p. 31-36.
65. Wang, H.T., Z.H. Li, and S.X. Tian, *Effect of promoters on the catalytic performance of Ni/Al2O3 catalyst for partial oxidation of methane to syngas.* Reaction Kinetics and Catalysis Letters, 2004. **83**(2): p. 245-252.
66. Shang, S., et al., *Research on Ni/γ-Al2O3 catalyst for CO2 reforming of CH4 prepared by atmospheric pressure glow discharge plasma jet.* Catalysis Today, 2009. **148**(3-4): p. 268-274.
67. Furusawa, T. and A. Tsutsumi, *Comparison of Co/MgO and Ni/MgO catalysts for the steam reforming of naphthalene as a model compound of tar derived from biomass gasification.* Applied Catalysis A: General, 2005. **278**(2): p. 207-212.
68. Li, C.S., D. Hirabayashi, and K. Suzuki, *Steam reforming of biomass tar producing H(2)-rich gases over Ni/MgO(x)/CaO(1-x) catalyst.* Bioresource Technology, 2010. **101**: p. S97-S100.
69. Hua, W., et al., *Preparation of Ni/MgO catalyst for CO2 reforming of methane by dielectric-barrier discharge plasma.* Catalysis Communications, 2010. **11**(11): p. 968-972.
70. Li, C.P. and Y.W. Chen, *TEMPERATURE-PROGRAMMED-REDUCTION STUDIES OF NICKEL-OXIDE ALUMINA CATALYSTS - EFFECTS OF THE PREPARATION METHOD.* Thermochimica Acta, 1995. **256**(2): p. 457-465.
71. Choi, Y., et al., *Effect of N2O-mediated calcination on nickel species and the catalytic activity of nickel catalysts supported on γ-Al2O3 in the steam reforming of glycerol.* International Journal of Hydrogen Energy, 2011. **36**(6): p. 3844-3852.
72. Tang, S., J. Lin, and K. Tan, *Partial oxidation of methane to syngas over Ni/MgO, Ni/CaO and Ni/CeO<sub>2</sub&gt.* Catalysis Letters, 1998. **51**(3): p. 169-175.

73. Wang, Y.-H., H.-M. Liu, and B.-Q. Xu, *Durable Ni/MgO catalysts for CO2 reforming of methane: Activity and metal–support interaction.* Journal of Molecular Catalysis A: Chemical, 2009. **299**(1-2): p. 44-52.
74. Sánchez, E.A., M.A. D'Angelo, and R.A. Comelli, *Hydrogen production from glycerol on Ni/Al2O3 catalyst.* International Journal of Hydrogen Energy, 2010. **35**(11): p. 5902-5907.
75. Fernández, Y., et al., *Comparative study of conventional and microwave-assisted pyrolysis, steam and dry reforming of glycerol for syngas production, using a carbonaceous catalyst.* Journal of Analytical and Applied Pyrolysis, 2010. **88**(2): p. 155-159.
76. Wang, X.D., et al., *Thermodynamic Analysis of Glycerin Steam Reforming.* Energy & Fuels, 2008. **22**(6): p. 4285-4291.
77. Juan-Juan, J., M.C. Román-Martínez, and M.J. Illán-Gómez, *Catalytic activity and characterization of Ni/Al2O3 and NiK/Al2O3 catalysts for CO2 methane reforming.* Applied Catalysis A: General, 2004. **264**(2): p. 169-174.
78. Song, Y.Q., et al., *Partial Oxidation of Methane to Syngas over Ni/Al(2)O(3) Catalysts Prepared by a Modified Sol-Gel Method.* Energy & Fuels, 2009. **23**: p. 1925-1930.

Appendix

Appendix A - Acid Wash Experiment

Materials: A38C-212 acetic acid, glacial; distilled H_2O; crude glycerol from biodiesel lab; glassware; pipet

Procedure:

1. Make 5 M solution of Acetic Acid.

2. Collect crude glycerol.

3. Fill each container with 20 mL of crude glycerol and number from 1-6.

4. Put 1.0, 1.5, 2.0, 2.5, 3.0, 3.5 mL of 5 M acetic acid into each container respectively (e.g. container 1 gets 1.0 mL of acid, container 2 gets 1.5 mL of acid, etc.).

5. Cap containers. Shake well for 1 minute and let sit overnight.

6. Next day, check for phase separation and clarity of bottom layer.

7. Check pH of each container.

Appendix B - 5 M Acetic Acid Preparation

Materials: A38C-212 acetic acid, glacial; distilled H_2O; glassware; funnel; fume hood

Procedure:

1. Clean glassware with soap and DI water.
2. Get glacial Acetic Acid.
3. Find appropriate volumetric flask for desired amount of 5 M acetic acid.
4. Fill volumetric flask ½ full with DI water.
5. Take glassware and materials to a fume hood.
6. Inside of the fume hood, measure the appropriate volume of glacial in a graduated cylinder (5 M acetic acid requires 28.6 mL of glacial acetic acid per 100 mL of solution).
7. Use a funnel and pour glacial acetic acid slowly into the volumetric flask.
8. Mix thoroughly.
9. Fill the remainder of the volumetric flask with DI water up to the fill line.
10. Cap off the volumetric flask and mix thoroughly.
11. Accurately label volumetric flask with type and molarity of acid, date of preparation, and the preparer's name.
12. 5 M acetic acid is prepared and ready to be used.

Appendix C – Steam Reforming Start-up Procedure

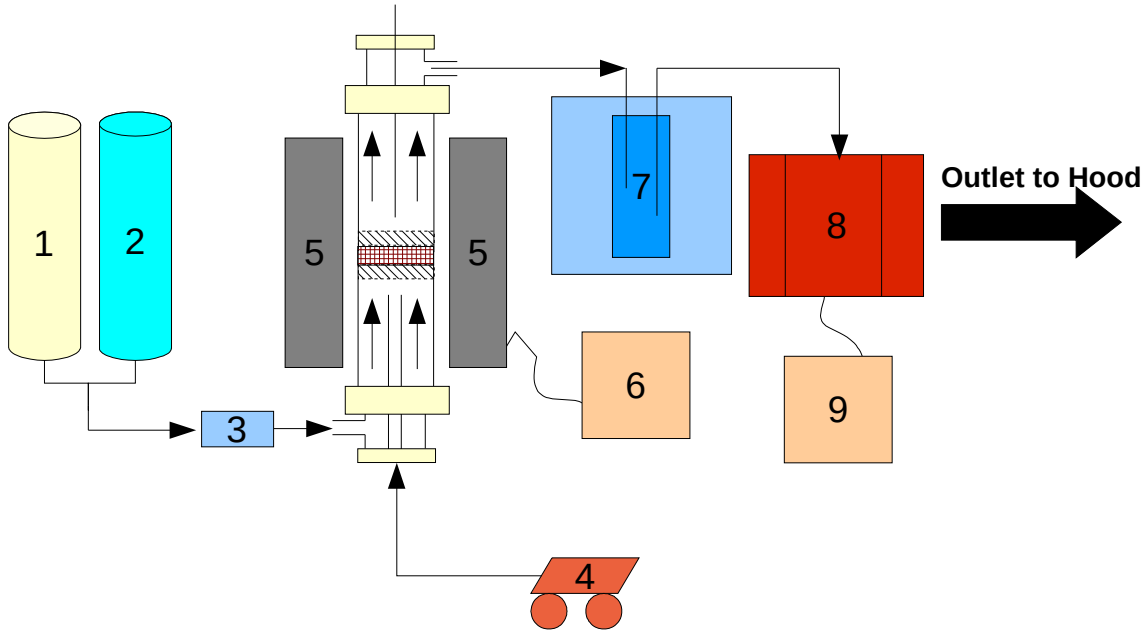

Appendix C Figure 1 - Overall schematic diagram of the small scale reformer. (1) 5% nitrogen/argon cylinder; (2) 5% hydrogen/argon cylinder; (3) mass flow controller for inlet gases; (4) Inlet pump for liquid water-glycerol mix; (5) Reactor Oven; (6) Computer (temperature control); (7) Ice Bath and Liquid Product Collection; (8) SRI 8610 Gas Chromatograph;(9) Computer (GC control);

Materials:

Procedure:

8. Prepare ice bath.

9. Use syringe to push air through feed line to remove any liquid. Then use syringe to rinse feed line with distilled water 3 times. Remove water from lines with syringe after each wash.

10. Clean syringe and fill feed lines with reactant. Fill lines up to the bottom of the oven in the inner quartz tube.

11. Load quartz reactor tube as dictated in quartz tube SOP.

12. Hook up the condenser, ice bath, and stainless steel tubing from the reactor to the GC. Tighten all fittings.

13. Set carrier gas (5% N_2/Ar) flow rate to 50 ml/min. (Mass flow controller set point = 6.7, actual flow is approximately 48 mL/min).

14. Check for leaks by using leak solution and checking flow rate in the hood (should be between 46-51 mL/min.

15. Put quartz wool above and below reactor.

16. Reduce catalyst for 1.5 hours. Check reduction SOP for procedure.

17. Switch gas flow to carrier gas (~ 100 mL/min).

18. Use Labview to ramp oven to reaction temperature.

19. During ramp, run GC calibration, refer to calibration SOP.

20. Let gas flow until hydrogen is removed from system. Check hydrogen content with Peaksimple and GC using H_2 settings.

21. Fill a beaker with liquid reactant. Measure and record volume.

22. Lower flow rate to 50 mL/min and check reactor temperature.

23. Change settings in Peaksimple to reaction settings and start GC data collection. Record file name. First sample is a blank. N_2 area should be between fifty and sixty. If not, perform another blank.

24. Once flow rate and reactor temperature reach desired values, start glycerol flow by setting flow rate on pump to 0.15 mL/min (or the desired flow rate) and press enter. Record time, reaction temp, and mass flow controller setpoint.

25. It should take 30 minutes to 1 hour for system to reach equilibrium.

26. If leaving system for more than two hours, make sure glass condenser knob is open (turned vertically). Otherwise, system will overflow.

27. Add ice to ice bath as needed.

Appendix D – Steam Reforming Shutdown Procedure

Materials:

Procedure:

1. Stop flow of reactant from pump. Record time. Record remaining volume in reactant beaker. Calculate the total amount of reactant fed to reactor.

2. Let Peaksimple finish current chromatograph. Once a stopping point is reached, change settings to prevent future data from being collected.

3. Let carrier gas run for 15-20 minutes before shutting down oven.

4. Shut down oven by switching Labview control to manual and setting power to 0%.

5. Run another GC calibration, refer to calibration SOP.

6. Allow system to cool.

7. Once cool, stop Labview program and carrier gas flow. Take apart system.

8. Weigh reactor tube and calculate added weight.

9. Measure and collect liquid product. Record this value and describe appearance of product (e.g. clear, cloudy, faint yellow, or oil layer on top).

10. Clean fittings and tubing with distilled water. Replace any tubing, fittings, etc. that need to be replaced.

11. Check to see if product is pure water by using the index refractometer and by distillation. Refer to SOP.

12. Analyze GC chromatographs to determine product gas composition versus time.

Appendix E – Quartz Reactor Tube Loading Procedure

Materials: 10 mm O.D. (6 mm I.D.) quartz tubing; quartz wool; catalyst; silica fragments; digital scale; marker

Procedure:

13. Load quartz tubing into reactor and mark locations of thermocouple and inner quartz tube with marker.

14. Insert approximately 3/8” of quartz wool into the quartz tube below the thermocouple mark.

15. Place quartz tube on digital scale and tare to zero.

16. Add approximately 0.05 g of catalyst onto the quartz wool inside the quartz tubing. Make sure the catalyst is loaded on the correct side of the quartz wool (the opposite side of the marking).

17. Weigh quartz tube and record weight of catalyst added. Tare the instrument.

18. Add approximately 0.08 g of silica to the quartz tube and mix the catalyst and silica together.

19. Weigh quartz tube and record weight of silica added. Tare the instrument.

20. Repeat process until approximately 0.2 g of catalyst is loaded.

21. Record total weight of catalyst and silica.

22. Insert approximately 3/8” of quartz wool into the quartz tube, so that the catalyst is located securely inside the tubing.

23. Weigh and record total weight of quartz tube and packing.

24. Load quartz tubing into the reactor.

Appendix F – Catalyst Reduction Procedure

Materials:

Procedure:

1. Perform up to step 8 of Steam Reforming Set-up Procedure.
2. Start Labview program. Power should be on manual and set for 0%.
3. Switch gas flow to 5% H_2/Ar at 50 mL/min (setpoint = 9.5).
4. Set power to 75%, record time.
5. Once temperature approaches reduction temperature set PID temp to reduction temperature, switch to PID control.
6. Record starting time.
7. Hold at this temperature for at least 1.5 hours.
8. After 1.5 hours, stop hydrogen flow and switch to carrier gas. Record time.
9. If performing a reaction, proceed to step 10 of Steam Reforming Set-up Procedure.
10. If reducing only, switch Labview power control back to manual. Set to 0% power.
11. Once cool, turn off carrier gas flow and end Labview program.
12. Remove quartz reactor from set-up and collect catalyst.

Appendix G – GC calibration Procedure

Materials:

Procedure:

1. Unhook product tubing from GC inlet.

2. Attach tubing from calibration gas to the GC inlet.

3. Check to make sure GC has H_2 and Ar pressure. Turn GC on. Carrier and hydrogen lights should be lit.

4. Open Peaksimple and set temperature ramp to reaction profile, create new save file name.

5. Record filename.

6. Ignite FID flame.

7. Start calibration gas flow.

8. Wait 1 minute and start injection of sample (Press 'spacebar' in Peaksimple).

9. After GC chromatograph is collected calculate H_2/CO, H_2/CH_4, H_2/CO_2, CO/CO_2, CO/CH_4, CO/C_2H_4, and CO/C_2H_6 response factors (H_2 response factors are based off TCD signal, the rest are based off of FID signal). TCD based response factors should be within 10% of the calculated value. FID based should be within 5%.

10. If response factors fall within the appropriate ranges, proceed with steam reforming procedure.

11. After reaction, calculate product gas composition based off of response factors and data collected from this procedure. The values should be similar.

12. If data does not fit, collect another chromatograph. If response factors do not converge, try restarting the GC.

Appendix H – Response Factor Calculation

Materials:

Procedure:

1. Before and after a set of reactions, response factors should be checked and calculated to ensure their accuracy.

2. To do this, connect both feed lines (carrier gas and reduction gas lines) directly into the GC inlet.

3. Unhook reduction gas cylinder and connect calibration gas cylinder to mass flow controller 1.

4. Check to make sure GC has H_2 and Ar pressure. Turn GC on. Carrier and hydrogen lights should be lit.

5. Open Peaksimple and set temperature ramp to reaction profile, create new save file name.

6. Set mass flow controller 2 set point to 6.8 (5% N_2/Ar). Set mas flow controller 1 set point to 18.7 (Calibration gas). Total flow rate should be approximately 100 mL/min.

7. Inject sample into GC and collect a chromatograph.

8. Repeat step 7 until 5 chromatographs are collected.

9. Calculate average response factors between each gas.

10. Previously calculated response factors are shown below.

Appendix H Table 1a - Response factors

TCD		FID	
H2/N2 Respons Factor	11.46	CO/CH4 Response Factor	0.95
CO/N2 Respons Factor	0.97	CO/CO2 Response Factor	0.89
CH4/N2 Respons Factor	3.37	CO/Ethane Response Factor	0.48
CO2/N2 Respons Factor	1.10	CO/Ethylene Response Factor	0.46
H2/CO Response Factor	11.87		
H2/CH4 Response Factor	3.42		
H2/CO2 Response Factor	10.50		
H2/Ethane Response Factor	3.23		
H2/Ethylene Response Factor	2.53		